Assessing the Effects of Climate Change in a Semiarid Basin Utilizing a Fully Distributed Hydrologic Model: A Case Study of Beaver Creek, Arizona.

by

Gretchen Hawkins

A Thesis Presented in Partial Fulfillment
of the Requirements for the Degree
Master of Science

Approved July 2012 by the
Graduate Supervisory Committee:

Enrique R. Vivoni, Chair
Steven Semken
Larry W. Mays

ARIZONA STATE UNIVERSITY

August 2012

ABSTRACT

The North American Monsoon (NAM) is characterized by high inter- and intra-seasonal variability, and potential climate change effects have been forecasted to increase this variability. The potential effects of climate change to the hydrology of the southwestern U.S. is of interest as they could have consequences to water resources, floods, and land management. I applied a distributed watershed model, the Triangulated Irregular Network (TIN)-based Real-time Integrated Basin Simulator (tRIBS), to the Beaver Creek basin in Arizona. This sub-basin of the Verde River is representative of the regional topography, land cover, and soils distribution. As such, it can serve to illustrate the utility of distributed models for change assessment studies. Model calibration was performed utilizing radar-based NEXRAD data, and comparisons were done to two additional sources of precipitation data: ground-based stations and the North American Land Data Assimilation System (NLDAS). Comparisons focus on the spatiotemporal distributions of precipitation and stream discharge. Utilizing the calibrated model, I applied scenarios from the HadCM3 General Circulation Model (GCM) which was dynamically downscaled by the Weather Research and Forecast (WRF) model, to refine the representation of Arizona's regional climate. Two time periods were examined, a historical 1990-2000 and a future 2031-2040, to evaluate the hydrologic consequence in the form of differences and similarities between the decadal averages for temperature, precipitation, stream discharge and evapotranspiration. Results indicate an increase in mean air temperature over the basin by 1.2 ºC. The average decadal precipitation amounts increased between the two time periods by 2.4 times that of the historical period and had an increase in variability that was 3 times the historical period. For the future period, modeled streamflow discharge in the summer increased by a factor of 3. There

was no significant change in the average evapotranspiration (ET). Overall trends of increase precipitation and variability for future climate scenarios have a more significant effect on the hydrologic response than temperature increases in the system during NAM in this study basin. The results from this study suggest that water management in the Beaver Creek will need to adapt to higher summer streamflow amounts.

ACKNOWLEDGEMENTS

I would like to give my deepest appreciation to my advisor Enrique Vivoni; he has made getting my master's degree possible. I am grateful that he accepted me as a masters student, helped guide me through the process of how to conduct research, and lead me to complete this degree.

I would like to give a big warm thank you to Agustin Robles-Morua for all of his assistance. He has always been such a support and has never wavered in his openness to help. Your door was always open and you always made me feel like a fellow colleague. Thank you for your guidance with Matlab, processing forcing, and being my triathlon partner.

I am grateful to the support and friendship of my fellow researchers. Long hours and constant frustrations made bearable with you who also walk the road. Thank you Taufique Mahmood, Luis Mendez Barroso, Hernan Moreno, Ryan Templeton, Alex Baish, Nolie Pierini, Tiantian Xiang, Tom Volo, Cody Anderson, and Danny Che.

Gratitude goes out to the Decision Center for a Desert City (DCDC) for funding me and this project. Margaret (Peggy) Nelson, Dave White, and Liz Marquez have a tremendous group of researcher and tirelessly work to bring the science community and policy making agencies together.

Dr. Francina Dominguez and Erick Rivera Fernandez have a special place in this body of work as they provided the WRF Climate Change weather forcing. Their work is an invaluable part of the results of this work I am incredible grateful and appreciative.

This body of work would not be possible without the support and encouragement of my family. My family is my constant companion, there would be no way to stand as tall or work as long without knowing their love is there for me.

TABLE OF CONTENTS

Page

Page

LIST OF TABLES

Page

LIST OF FIGURES

Page

Page

Page

Page

1 INTRODUCTION

Evidence has suggested, and it is the general consensus of the scientific community, that the Earth's climate is changing, with a general trend towards warmer temperatures and changing precipitation patterns. The Intergovernmental Panel on Climate Change (IPCC) is an international organization established by the United Nations Environmental Program and the World Meteorological Organization, whose main purpose is to assess climate change possibilities and scientific statements on its potential impact to the environment. In the Fourth Assessment Report (AR4), the IPCC states that warming of the climate is now evident from observed increases in global average air and ocean temperatures (IPCC, 2007). Probable impacts associated with climate change have previously been documented (Arnell and Reynard 1996; Strzepek and Yates 1997; Leung and Wigmosta 1999; Pfister, et al. 2004). Changes to the frequency and intensity of extreme events are expected to have significant impacts on natural as well as human systems (Aerts & Droogers, 2004). Thus, determining the possible effects that climate change has on a regional basis to watersheds would be important to resource and infrastructure planning.

Although the system as a whole will change, the effects of climate change will vary substantially across different regions (Dessai & Hulme, 2007). There are several different models that are utilized in climate change analysis and the degree of change as well as what to expect in certain areas of the Earth are not always similar from model to model. However, the IPCC projections for the western United States are reasonably consistent among projection models (Tarlock, et al. 2009). As a result, hydrological responses to changes in temperature and precipitation amounts and variability have been

documented for the region, in particular under wintertime conditions (Hidalgo & Dracup, 2009).

The Southwester U.S. vulnerability to climate change is of particular interest as it is historically characterized by climate variability, aridity, and population growth. Dramatic increases in any of the above would lead to a decreased reliability in the current water supply system as well as a re-examination of infrastructure needs. Under climate change, the region is expected to experience higher temperatures, diminishing snow packs, lower snow water content, earlier snow melt, and change in timing of streamflow (Saunders & Maxwell, 2005). Christensen et al. (2004) found that climate change would greatly degrade the hydrologic system of the Colorado River basin.

Although climate models show a trend towards more arid conditions, these statements do not typically capture the bimodal precipitation regime of the southwestern U.S. Many reports predict that climate change will impact winter precipitation and runoff with earlier snow melt, which affects streamflow seasonality (Christensen, et al. 2004; Diffenbaugh, et al. 2008). Although much has been studied and forecasted for the winter precipitation season, there still remains the question about the impact of climate change to the runoff response with regards to the summer precipitation, typically referred to as the North American Monsoon (NAM).

The summer monsoonal precipitation is very different from winter systems and is characterized by convective storm bursts that are localized and higher in intensity, and which have a large degree of spatial heterogeneity (Wheater 2008; Martinez-Mena, et al. 1998; Pilgrim, et al. 1988). Diffenbaugh (2005) branded the southwestern as a ‘hotspot’ for climate change activity due to impacts on precipitation variability to the region.

Increases in variability for the U.S. southwestern are predicted to be a factor in the future outlook such as water resource availability for the region and is inclined towards changes in precipitation characteristics such as shift in precipitation timing and amounts (Christensen, et al. 2004; Kim 2005; Seager, et al. 2007).

Increases in temperature increases the moisture holding capacity of the air, and in turn will increase rates of precipitation and the number and intensity of convective storm events. Increases in these rates at a global and at a regional scale have been documented by various studies (Fowler and Kilsby 2003b; Zwiers and Kharin 1998; Frich, et al. 2002, Bengtsson and Semenov 2002; Fowler and Kilsby 2003b). For example, a study done by Buonomo (2007) showed that extreme and short duration events are projected to increase in precipitation intensity. It is of interest to understand how climate change may affect the hydrologic response in a semiarid basin as the monsoon season brings with it many concerns; flood risk to wild fire are all concerns during this time of year. Devastation due to wildfires has become a typical tale in the southwestern and the monsoon is an important combatant in the fight against such tragedies; the start of the monsoon is typically the onset to the end of the fire season (Ray, et al., 2007).

Changes in the climate systems may lead to a more dramatic hydrological cycle than we have been exposed to. Past precedents are what are relied on for in emergency planning and water management. Due to the discrepancy with predicted future events to historical records, design criteria for water resources that are based on past probability distributions, will need to be re-examined to meet future conditions (Milley, et al., 2007).

Climate change conclusions are typically drawn by using General Circulation Models (GCMs) which are numerical models that represent the atmosphere, ocean,

cryosphere, and land surface physical processes. GCMs have been used to evaluate environmental impacts on the climate with increasing greenhouse gas emissions (Chiew, et al. 1995; Cameron, et al. 2000; Bergstrom, et al. 2001; Li, et al. 2008).

However, GCMs generally do not always realistically represent precipitation well enough due to their coarse spatial resolution in complex terrain (Dominguez, et al. 2012); (Lee, et al., 2007). There are several GCMs that use a number of methods to discern the global circulation. Model resolution ranges from 250 to 600 km; this coarse resolution, in part, is accountable for some inaccuracies of GCM to model climate at the regional scale (Brazel, et al. 1993).

Current GCMs do not always capture interactions between surface forcing and large scale atmospheric dynamics, which organize terrain-induced convective rainfall. (Castro, et al. 2007b). However, the role of terrain is only half the picture of the NAM system. Moisture that feeds the southwestern U.S. is supplied, in part, by moisture from the Gulf of California (also commonly referred to as the Sea of Cortez) (Adams & Comrie, 1997). Surface heating of moist air and orographic lifting generates frequent convective precipitation events (Jones Jr., 2007). The Gulf of California is not a significant body of water, on a global scale, and the coarseness of GCMs tend to mute out, if not completely negate, this.

Higher temperatures and greater precipitation variability trends implicated by GCM models over the southwestern U.S. have been shown to dampen extreme events, due to coarse pixel resolution that masks the localized summer monsoon storms (Rind, et al. 1989; Cubasch, et al. 1995). For this reason, methods to downscale GCMs to the regional scale, has been an area of interest to the scientific community to produce climate

effects on a localized scale. Downscaling improves the analysis and accuracy of such models (Kim 2005; Mearns, et al. 1995). It is this downscaling that makes capturing monsoonal effects more available for evaluation. It is also anticipated that subsequent use of high-resolution general circulation models (GCMs) or regional climate models (RCMs), will be able to generate long-term simulations resolved enough to represent the NAM as a salient feature. Current GCMs cannot capture interactions between surface forcing and large-scale atmospheric dynamics, which organize terrain-induced convective rainfall (Castro et al., 2007b).

This study uses the HadCM3 General Circulation Model (GCM) that was dynamically downscaled using the Weather Research and Forecast (WRF) model to refine the representation of climate in areas of the U.S. southwestern. In collaboration with Dr. Francina Dominguez and Erick Rivera Fernandez, the RCM employed for this study was applied at the University of Arizona. Their work is specific to the regions encompassed by Arizona and Sonora Mexico and in capturing summer convective storms using RCMs.

This study investigates the impacts of climate change on the hydrologic system of a semiarid basin in the U.S. southwestern during the summer monsoonal period. This was done by using a RCM and appling it to a physically based distributed model to detect changes in average streamflow as well as evapotranspiration (ET). Hydrologic models are valuable tools and can be essential in evaluating changes due to physical phenomenon that we are unable to presently measure, such as climate change. Modeling approaches have a wide range of applications and data needs, from lumped models (Rango and Kock

1990; Kite 1993) to distributed models (Christensen, et al. 2004) and (Liuzzo, et al. 2010).

In this study, the physically based TIN-based Real-time Integrated Basin Simulated (tRIBS) hydrologic model is applied to the Beaver Creek (BC) watershed in central Arizona. Beaver Creek was chosen for several reasons; size, physical characteristics, and data availability. This watershed is just over 1000 km^2 and is varied in its topographic relief and landscape regimes; it is a good representation of the central regional of Arizona. Its size is not excessively large to impose large computation demands within the modeling context. The watershed is characterized as having two stretches of significant stream paths, Wet and Dry Beaver Creek, which both have available USGS stream gauge historical data that correlate to available precipitation products. The first portion of this study is to develop the model and examine its representation of streamflow events for the summers of 2005, 2006, and 2007. Following model calibration and validation, a series of GCM climate change scenarios are applied to the model and an analysis was conducted to evaluate changes to the hydrologic response of the basin by comparing and contrasting a historical GCM scenario to a future projected scenario.

The distributed physically based models such as tRIBS not only allows for streamflow response to be quantified, but also capture the spatial distribution of hydroclimatic elements of the basin such as ET.

The objective of this thesis is to illustrate the hydrologic process in a large semiarid basin through the utility of a distributed hydrologic model, accounting for spatial and temporal variations in precipitation forcing during the summer monsoonal

precipitation period. Model calibration establishes confidence in the model's ability to capture the physical characteristics of the basin. Once the model is found to represent the basin within acceptable limits, hydrologic impacts due to future climate changes are assessed through the use of GCMs. Hydrologic variable such as precipitation, stream response and evapotranspiration are examined for differences between historical and future simulations.

This study is laid out in the following manner:

- Chapter 2 discusses the study area and its characteristics including model inputs and the physical processes captured in the numerical model.
- Chapter 3 discusses the results of model calibration and climate change scenarios simulated from the calibration parameters.
- Chapter 4 presents conclusion and possible future avenues of research.

2 METHODS

2.1 STUDY AREA DESCRIPTION

The Beaver Creek watershed is located approximately 80 km (50 miles) south of Flagstaff, Arizona. The basin is approximately 1100 km^2 (275,000 acres) contains pinyon-juniper, Ponderosa Pine, and semi-desert shrub; and empties into the Verde River (Baker M. B., 1986). The elevation of Beaver Creek Watershed ranges from 900 to 2,400 m (3,000 to 8,000 ft) above sea level (Baker M. B.). Winter precipitation accounts for approximately 60% of the annual precipitation which ranges from about 550 to 785 mm. The remaining 40% precipitation falls during the months of July, August, and September (Baker, 1986). Mean temperatures at Beaver Creek range from -2.2˚C in January to 17.8˚C in July. There are two major stream systems within the watershed, the Dry Beaver Creek with an ephemeral stream that flows mainly after a significant precipitation event, and there is the Wet Beaver Creek which flows throughout the year and is fed from groundwater draining from Mogollon Rim aquifers. Figure 1 depicts each USGS stream gauge site that tabulates these flows, along with the outlet gauge station site just up-stream of where the streamflows into the Verde River, the 10 Yavapai Flood Control Districts rain gauge stations, and where the basin is situated within the Verde River watershed.

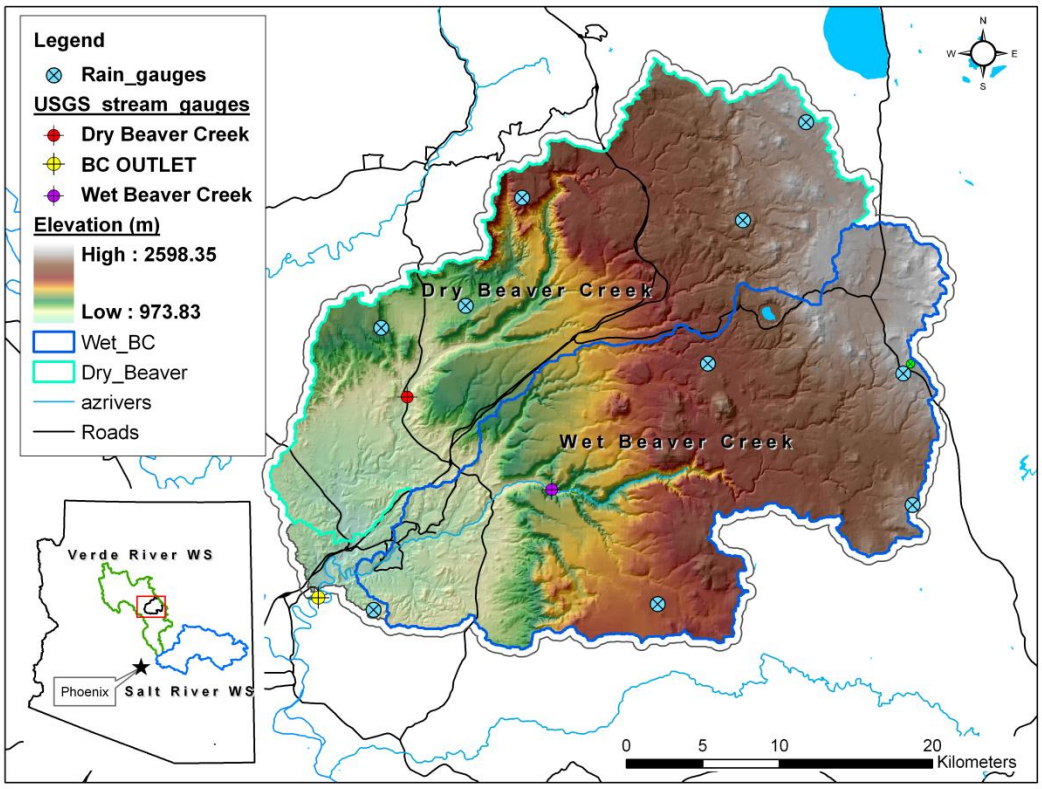

Figure 1: Beaver Creek site map including USGS stream gauge, rain gauge sites, and elevation gradient

The hydrologic model used in this study is a physically based distributed model, and therefore the physical inputs of the model and their level of accuracy are highly important to model results. The advantages of distributed models are their spatially distributed nature of their inputs and the use of physically based parameters (Beven K. , 1985). The development of spatially distributed hydrologic models provides a means to interpret the spatial response to ground and remote sensing data which provides information on the state variables of fundamental importance to watershed hydrology (Grayson & Bloeschl, 2000) . Several governmental organizations generate spatially distributed data sets that are utilized in this model, and are easily interpreted in a Geographical Information System (GIS) format, or can be converted to a format that can

be read by the model. Such data sets include topographic data, soil, land cover, and precipitation.

2.1.1 Topographic Data

The United States Geological Survey (USGS) has developed several topographic datasets at differing resolution. Data are available as a National Elevation Dataset (NED) in the form of a Digital Elevation Model (DEM), which is a digital representation of cartographic information. The spatial resolutions that are available through NED include 1 arc-second (~30 meters), 1/3 arc-second (~10 meters) and in limited areas 1/9 arc-second (~3 meters). Although there has been much improvement in 1/3 arc-second NED elevation artifacts still occur and lead to unrealistic parallel overland flow direction and therefor the 1 arc-second dataset was selected. The vertical accuracy of the 1 arc-second dataset is ± 7 to 15 meters depending on the source of the DEM (USGS, 2011).

The DEM obtained from www.seamless.usgs.gov was used to delineate the watershed initially using an area much larger than the actual watershed. To process the raw elevation data into a readable format for the model, the ArcHydro tools in ArcMap was utilized. The first step in processing the DEM grid is to fill any sinks within the dataset. Sinks are cells that are surrounded in all directions by higher cells and thereby any water cannot drain from that cell. Sinks can be errors in the dataset, sampling routines, or elevation values rounding to the nearest integer. If sinks are not raised to the height of their pour point, the derived drainage network may be discontinuous (ESRI, 1995-2011).

The filled DEM is processed for flow directions, flow accumulation, stream definition, catchment grid delineation, catchment polygon processing, and drainage line.

A stream network is produced using a stream threshold that reproduces the stream network density to that of the USGS published network. The threshold is the minimum number of cells that drain to a particular cell to be considered as part of the stream network. The stream networks produced by different thresholds were compared to the accepted hydrography of the basin, and a threshold of 750 grid cells or 0.6 km^2 was determined to best fit this criteria.

The filled DEM, flow direction, and flow accumulation are required to make the Triangular Irregular Network (TIN) generation. Using these files, the TIN was created in a program called TIN-Index Analysis Package (TIAP), which is a set of ArcInfo aml scripts that generate a series of files (*.pnt and *.lin). Further discussion on TINs and their role in the modeling process will be elaborated on in the next section.

These *.pnt and *.lin files are fed into the model during an initial model run; from this run tRIBS produces a file (*.point) that describes the properties of the TIN vertices. This points file contains the x and y coordinates, elevation, and type of node and can be seen in Figure 2. The different node types are: boundary nodes, interior nodes, stream nodes, and an outlet. The points are used to construct the polygon mesh where all calculations take place.

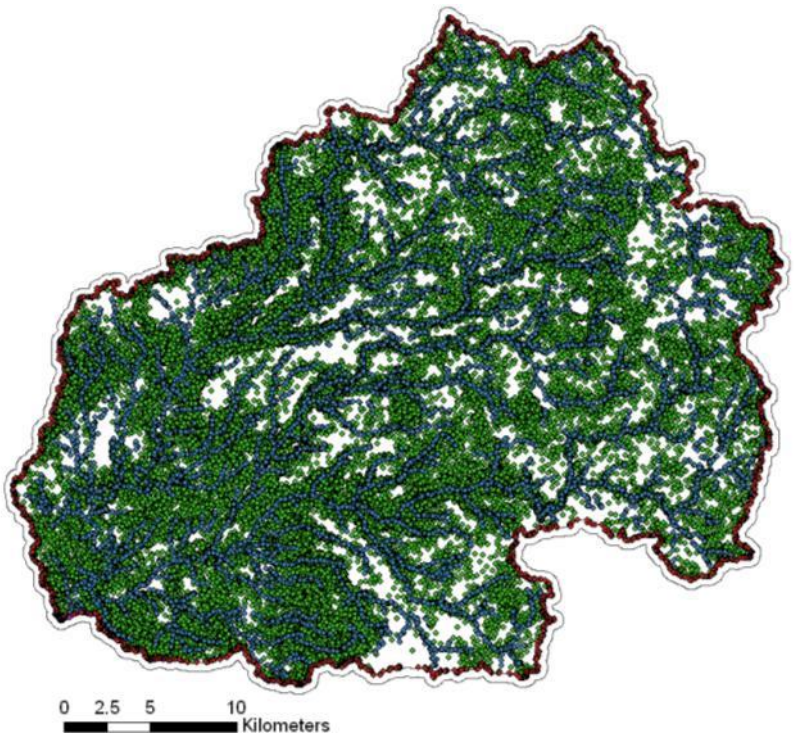

Figure 2: Points file for the Beaver Creek, ~76,624. Stream nodes – blue, interior nodes – green, boundary nodes – red, outlet node – pink.

2.1.2 Soil Data

Spatial distribution of soil texture was obtained from the National Resources Conservation Service (NRCS) Soil Survey Geographic (SSURGO) Database. The soil survey for the Beaver Creek watershed is divided into 73 different classes as seen in Table 1. This table as calls out, using color, that many of these classes are very similar in nature. In order to limit the complexity of model inputs any map units that includes the description of cobbly, gravelly, or stony were reduced to the base texture type. For example RrC—Retriever very stony loam, 0 to 20 percent slopes was classified as loam (NRCS).

Table 1: SSURGO soil classification and simplified aggregated classification used in model setup.

SSURGO Classification	Texture Classification
An—Anthony fine sandy loam	Sandy loam
Ba—Basalt rock land	bedrock
Bg—Bridge gravelly sandy loam	sandy loam
Bl—Bridge stony loam	loam
Bm—Brolliar gravelly clay loam	clay loam
Bn—Brolliar silt loam, deep	silt loam
BoB—Brolliar stony clay loam, 0 to 10 percent slopes	clay loam
BoC—Brolliar stony clay loam, 10 to 20 percent slopes	clay loam
BoD—Brolliar stony clay loam, 20 to 30 percent slopes	clay loam
Bp—Brolliar very rocky complex	clay loam
BrB—Brolliar very stony loam, 0 to 10 percent slopes	loam
BrC—Brolliar very stony loam, 10 to 20 percent slopes	loam
BrD—Brolliar very stony loam, 20 to 30 percent slopes	loam
Bu—Brolliar clay loam and alluvial land	clay loam
Bv—Brolliar cobbly loam and alluvial land	loam
Ca—Cabezon very stony loam	loam
Cc—Cabezon stony clay loam, dark variant	clay loam
Cd—Cornville fine sandy loam	sandy loam
Cg—Cornville gravelly sandy loam, thin solum variant	sandy loam
Ch—Courthouse gravelly fine sandy loam	sandy loam
Cs—Courthouse stony fine sandy loam	sandy loam
Fk—Friana clay, black variant	clay
Fn—Friana soils	clay loam
Gm—Gem clay loam	clay loam
Gn—Gem-Springerville complex	clay loam
Gs—Gila very fine sandy loam, reddish variant	sandy loam
Gt—Glendale silt loam	silt loam
Gu—Guest clay	clay
Ha—Hantz silty clay	clay
Hg—Hogg stony silt loam	silt loam
Hm—House Mountain stony loam	loam
Ja—Jacks fine sandy loam	sandy loam
Jc—Jacks very rocky fine sandy loam	sandy loam
Ka—Karro and laveen fine sandy loams	sandy loam
La—Laveen gravelly sandy loam	sanndy loam
Ln—Lynx silt loam	silt loam
Ly—Lynx silt loam, heavy subsoil variant	silt loam
Ms—Mescal fine sandy loam	sandy loam
Pc—Penthouse cobbly clay loam	clay loam
Ph—Penthouse stony loam	loam
Re—Retriever loam	loam
RrC—Retriever very stony loam, 0 to 20 percent slopes	loam
RrD—Retriever very stony loam, 20 to 40 percent slopes	loam
Rw—Riverwash	sand
Rx—Rock land-Springerville complex	clay
Ry—Rough broken and stony land, limestone	bedrock
Sa—Sandstone outcrop	bedrock
Sd—Sandstone rock land	bedrock
Se—Schnebly very stony clay loam	clay loam
Sf—Siesta silt loam, deep	silt loam
Sg—Siesta stony silt loam	silt loam
ShC—Sponseller stony silt loam, 5 to 15 percent slopes	silt loam
ShD—Sponseller stony silt loam, 15 to 40 percent slopes	silt loam
Sk—Springerville clay	clay
Sl—Springerville clay, red phase	clay
Sm—Springerville cobbly clay	clay
SnB—Springerville very stony clay, 0 to 10 percent slopes	clay
SnC—Springerville very stony clay, 10 to 20 percent slopes	clay
SnD—Springerville very stony clay, 20 to 30 percent slopes	clay
So—Stagecoach cobbly sandy loam	sandy loam
Sr—Stony hilly land, ash and tuff	bedrock
Ss—Stony rough land, basalt and cinders	bedrock
St—Stony rough land, sandstone	bedrock
Su—Stony steep land, basalt	bedrock
Sv—Stony very steep land, basalt	bedrock
Tb—Tobler fine sandy loam	sandy loam
Tg—Tobler gravelly fine sandy loam, brown variant	sandy loam
To—Toquop loamy fine sand	sandy loam
Tx—Toquop-Carrizo complex	sandy loam
W—Water	water
Wa—Waldroup loam, brownish variant	clay loam
Wc—Waldroup clay loam, deep	clay loam
Wg—Waldroup gravelly loam, moderately deep	loam

The SSURGO database contains vast amounts of data for each map unit. This database includes information on such characteristics as saturated hydraulic conductivity, percent sand silt, and clay, percent organic matter, and moisture bulk density. This data set is for surface and sub-surface characteristics; depending on the map unit data is available for as much as 1.0 meter below the surface. Figure 3 provides soil map units for the aggregated soil classes used as input into the mode1 (A) and for the raw SSURGO map units (B).

The main soil types as seen in Table 2 and inferred from the above figure are clay, clay loam, and bedrock; and to a lesser degree, loam and silt loam. The three most dominant soil types were the main focus of soil parameters calibration.

Table 2: Soil texture area coverage

Soil Texture	Area (km^2)	Basin Coverage (%)
Bedrock	226	18.58
Clay	343	28.24
Clay loam	234	19.22
Loam	175	14.35
Loamy Sand	1	0.08
Sand	11	0.91
Sandy Loam	82	6.73
Silt Loam	139	11.41
Silty Clay Loam	5	0.41
Water	1	0.06

Soil units are manipulated in GIS and initially are downloaded in the format of a *.shp file. To be able to be read into the model the reclassified aggregated map was converted from *.shp to raster and then to ASCII format.

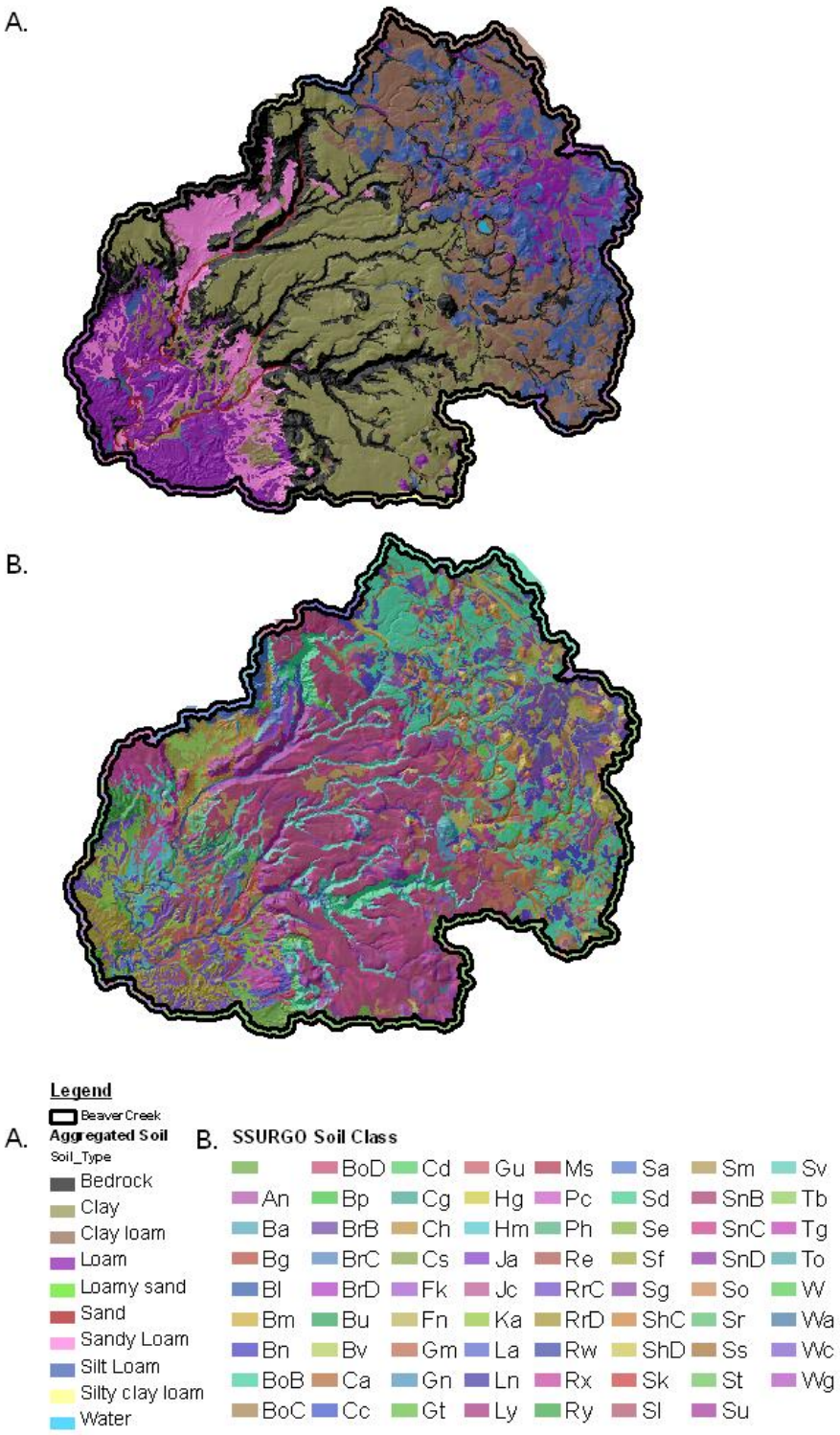

Figure 3: (A) Aggregated soil based on similar texture types (B) Raw SSURGO soil map

2.1.3 Land Cover Data

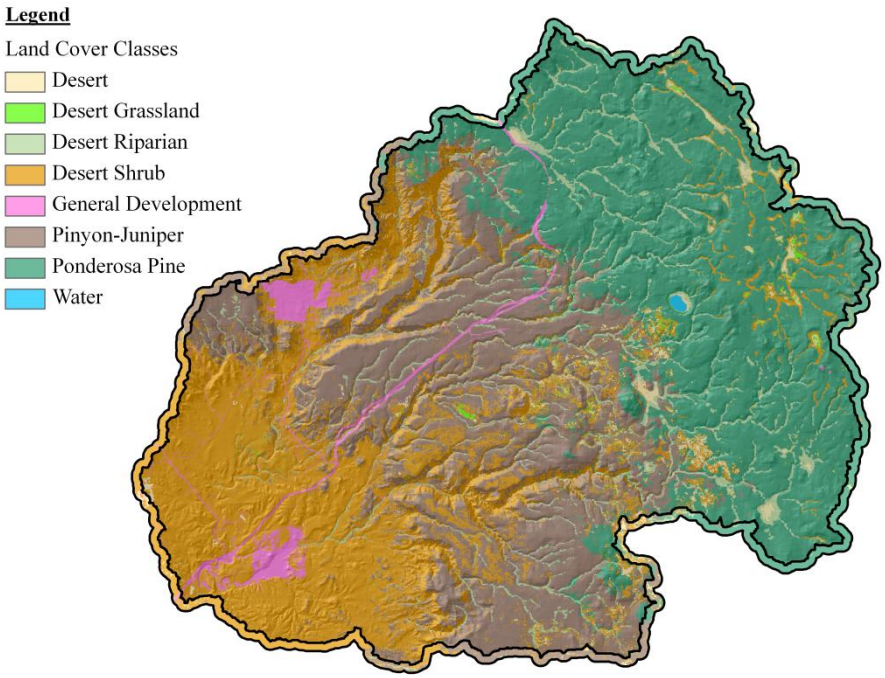

Figure 4: Land cover map obtained from the Department of Agriculture Forest Services.

The land cover spatial map was obtained from www.LANDFIRE.gov and depicts the wildlife habitat, vegetation or canopy characteristics, and landscape features of the continental U.S. This dataset is a service of the US Department of Agriculture Forest Service and the US Department of the Interior. The dataset has a vast amount of different data in 10 meter resolution raster-based format. The data are based on peer reviewed science and obtained by procedures including relational databases, geo-referenced land-based plots and polygons representing field conditions, satellite-enabled remote sensing, systems ecology, gradient analysis, predictive landscape modeling, and vegetation and disturbance dynamics (USDA). Figure 4 displays the land cover map used for Beaver Creek.

The main land cover classification types Table 3 and inferred from Figure 4 are desert shrub, pinyon-juniper and Ponderosa pine. The three most dominant land cover types were the main focus of calibration parameters adjustment.

Table 3: Land cover type area coverage

Land Cover Type	Area (km^2)	Basin Coverage (%)
Desert	17	1.38
Desert Grassland	4	0.35
Desert Riparian	61	5.01
Desert Shrub	345	28.37
General Development	27	2.25
Pinyon-Juniper	335	27.57
Ponderosa Pine	410	33.73
Water	1	0.06

2.1.4 Depth to Bedrock

The depth to bedrock in the model can be represented as a uniform distance from the land surface for the entire domain or variable and set up in grid ASCII format. In tRIBS, bedrock is a representation of an impermeable boundary condition beyond which vertical soil moisture fluxes do not extend. The SSURGO data obtained have a good deal of depth to bedrock information. However, no measurements were taken beyond approximately the first ~2. Only the dominant classes of soil types were evaluated for depth to bedrock.

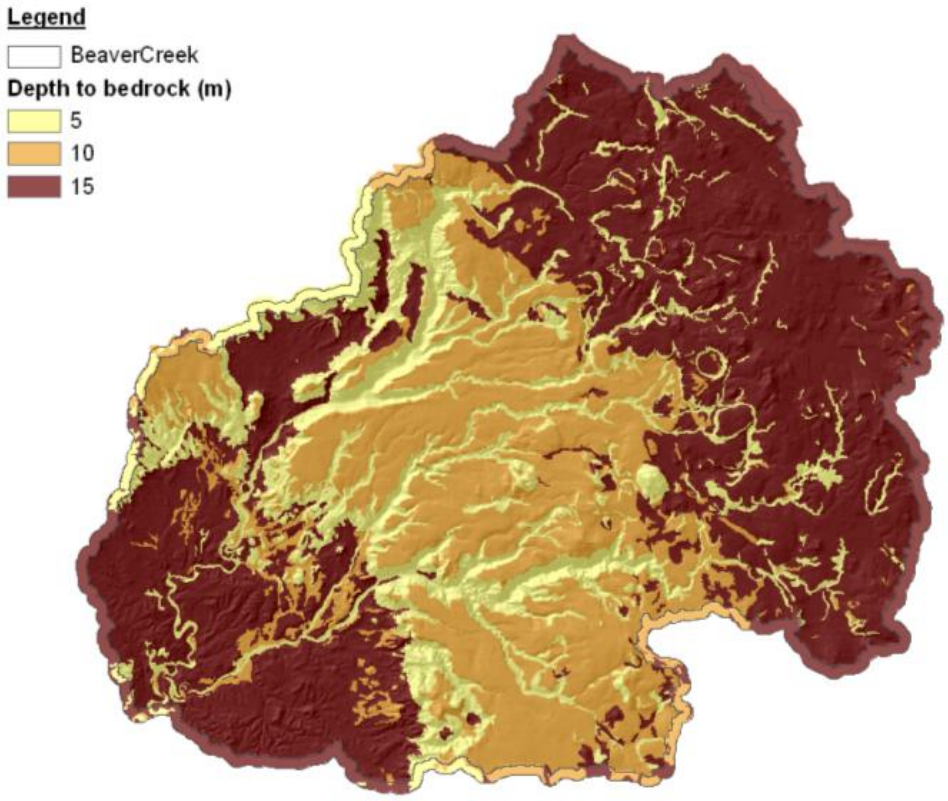

Figure 5: Depth to bedrock based on SSURGO data

In much of the channel network of Beaver Creek, bedrock outcrops are present at the land-atmosphere interface. To put the depth to bedrock at the surface would prevent infiltration into any of this soil class, which is not representative of what occurs. tRIBS has limited capability to model infiltration in regions of low permeability due to exposed bedrock. Due to this limitation, any class that had a depth to bedrock at the surface (e.g. exposed bedrock) was lowered 5 meters to account for subsurface moisture flux. Consequently, all other types were lowered as well to maintain differing levels in relation to the bedrock soil class and to give adequate room for wetting front movement.

Clay soil classes were reported as varying in depth to bedrock, but on average, were in the range of just under a meter from the surface. To correctly relate this to the bedrock class, clay was lowered to 10 meters.

Silty loam and clay loam were both reported, on average, around 1.6-1.7 meters from the surface and are likely the result of measurement limitation. Therefore, as with clay, were extended to 15 meters for the same reasons. Figure 5 represents the depth to bedrock configuration utilized in the model.

2.1.1 Precipitation Data

In this study, three types of precipitation forcing will be reviewed: a network of 10 ground based rain gauge stations, and two remote sensing products, one from radar and the other from satellite. The following describes advantages and disadvantages of each product, cites the sources they were obtained from, and describes the data collection process.

Historically, rain gauges have been the chosen method to drive hydrologic models. Rain gauge stations, however, are only point sources and when used in hydrologic models they represent a large extensive area from that point. A rain gauge network, of fine spatial scale necessary to capture the spatial variability of rainfall in an area, is often only available in experimental or research watersheds (Moon, et al.2004). Although there is uncertainty in the remote sensing product, rain gauge data have their own set of inaccuracies. Systematic effects such as wind, splashing, evaporation and mechanical and electrical malfunction result in errors in the data. Other uncertainties possibly results from differences in sampling areas of remote sensing and gauge points or

point area difference (Neary, et al. 2004). As more advance methods become available and refined there are alternatives to rain gauge precipitation inputs.

Next Generation Weather Radar System (NEXRAD) Stage IV data were obtained from the Colorado Basin River Forecasting Center (CBRFC) of the National Weather Service (NWS). The CBRFC hourly digital precipitation (HDP) system is made up of 15 stations located in various cities in New Mexico, Colorado, Nevada, Utah, Idaho, Wyoming, and Arizona. The HDP is then corrected based on available rain gauge data and presented in 4x4 km grid format. Radar is a viable alternative to gauge, but it has its own uncertainties and errors including beam attenuation, terrain blockage, range and scale angle limitations, and mixed-phase hydrometeor effects. Another type of uncertainty is that surface rainfall has to be deduced from radar measurements sampled at certain heights above the ground. Variability in the vertical profile of precipitation fields can cause significant over/underestimation of the true surface precipitation (Neary, et al. 2004). These issues can be further magnified during warm season convective events in mountainous terrain (Delrieu, et al. 2000) and (Grassotti, Hoffman, Vivoni, & Entekhabi, 2003).

North American Land Data Assimilation System (NLDAS) data were obtained from the National Center for Environmental Prediction Climate Prediction Center (NCEP CPC) using daily gauge-based precipitation data (Nan, Wang, Liang, & Adams, 2010). These data were interpolated from daily adjusted Parameter-Elevation Regression on Independent Slope Model (PRISM) (Daly, et al. 1994) to NLDAS $1/8^{th}$ grid using least square distance weighting scheme and then disaggregating from daily to hourly amounts based on hourly temporal weights (Cosgrove, et al., 2003). These data corresponds to a

pixel size of 12 x 12 km, much larger than the NEXRAD. As with the other two forcing types NLDAS precipitation field uncertainty has been documented in many studies (Luo, et al., 2003), (Robles-Morua, et al. 2012).

Precipitation forcing for all types had to be organized and/or converted in some way to make the data into a viable format for the model. Rain gauge data were obtained from the Yavapai County Flood Control District and were organized in a simple text following a column format of year, month, day, hour, precipitation amount (mm). The other two precipitation types required a much more complex process to get them into a format that is model friendly. NEXRAD data come in binary format with the time stamp of Greenwich Mean Time (GMT) and were converted to ASCII using a FORTRAN code. The next step was to convert the ASCII files from the latitude-longitude coordinate system to Universal Transverse Mercator (UTM), convert the time from GMT to the Arizona UTM zone 12 (-7 hours from GMT), and clip the files to area of interest for this study as the original NEXRAD data was supplied for the entire US. This secondary step was done using an R code program. NLDAS was supplied in Gridded Binary (GRIB) format and was converted to ASCII, and much like NEXRAD was modified to UTM, time corrected, and clipped, this was done using a MATLAB code. All ASCII files were renamed to be readable in tRIBS in the form of *mmddyyyyhh.txt.

Each precipitation forcing has a different spatial resolution from another, which invariably has a marked effect on the modeled basin response. The following figure is a visual representation of the comparison of the NEXRAD 4 x 4 km cell, the NLDAS 12 X 12 km cell and the rain gauge distribution in the basin. Rain gauge area of influence over the basin is based on Thiessen polygons and is created using a weighted area average.

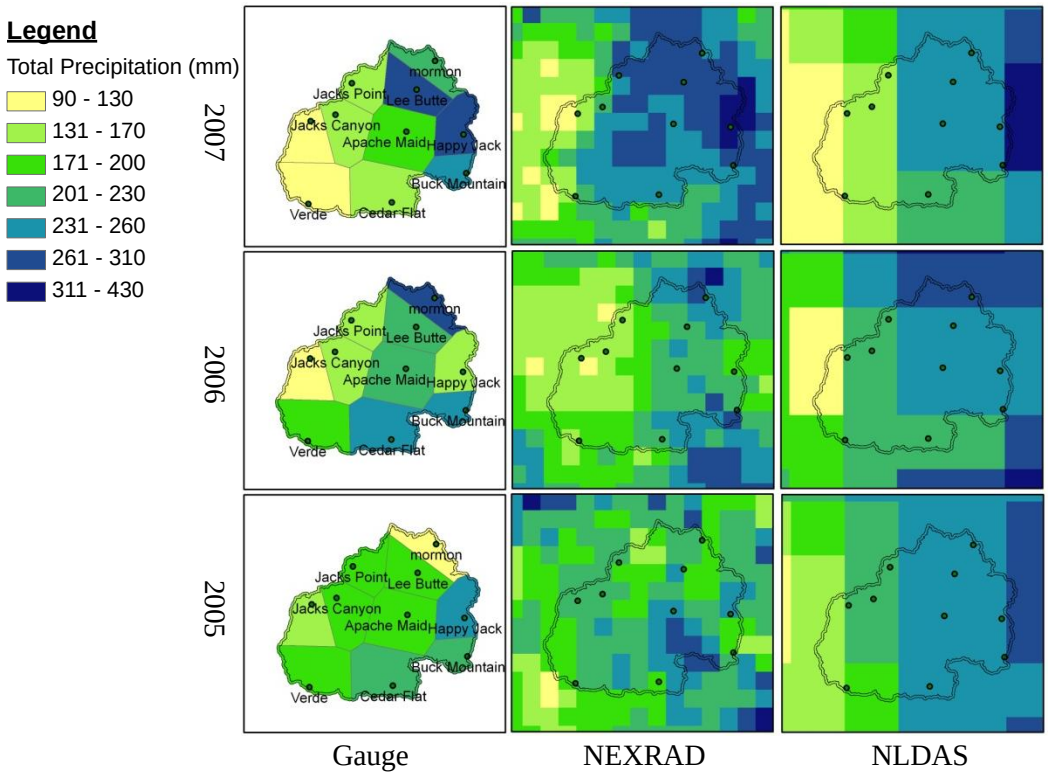

Figure 6: Summer precipitation totals for 2005, 2006, and 2007 for Rain Gauge Thiessen polygons, NEXRAD, and NLDAS pixels.

Figure 6 is the summation of the summer precipitation for all summers examined in this study for all three precipitation types. Further comparison analysis will be detailed in the next section and will include statistical comparisons at individual pixel sites, basin wide totals, and model output evaluation.

2.1.2 Comparison of Precipitation Forcing

The accuracy of hydrologic model results depends heavily on the accuracy of model inputs, especially rainfall, which is the driving function in the hydrologic process (Moon, et al. 2004). Precipitation is difficult to measure accurately over a basin as it is variable in time and space. The timing and intensity of precipitation affect the basin

response, and needs to be considered carefully when choosing a precipitation type. Precipitation is one of the major limitations to hydrologic predictability (Entekhabi, 2002).

Rain gauge forcing has been the principal historical forcing for hydrologic models, and therefore, a statistical comparison was between the 10 gauge station sites to the corresponding pixels of both the NEXRAD and NLDAS products. Table 4 is the correlation coefficient, the closer to 1 the higher the correlation, and Root Mean Square Err (RMSE), the lower the number the better the agreement, calculated from the daily totals for the 2007 summer of observations. Figure 7 on the following page represents each pixel and compares how close the remote sensing products come to the one-to-one line of the rain gauges daily rain totals.

Table 4: Statistical analysis of daily precipitation for NEXRAD and NLDAS pixels using the corresponding 9 rain gauge observation stations.

	Correlation Coefficient		RMSE (mm/day)	
	NEXRAD	NLDAS	NEXRAD	NLDAS
Apache Maid	0.84	0.60	3.0	4.0
Cedar Flat	0.81	0.70	4.9	5.3
Happy Jack	0.90	0.78	2.3	3.4
House Mountain	0.61	0.57	4.5	4.5
Jacks Canyon	0.80	0.43	2.8	4.8
Jacks Point	0.66	0.45	3.8	4.8
Lee Butte	0.55	0.63	4.5	3.9
Mormon	0.73	0.54	3.9	4.8
Buck Mountain	0.66	0.59	4.1	4.1
Verde	0.49	0.59	4.4	3.2

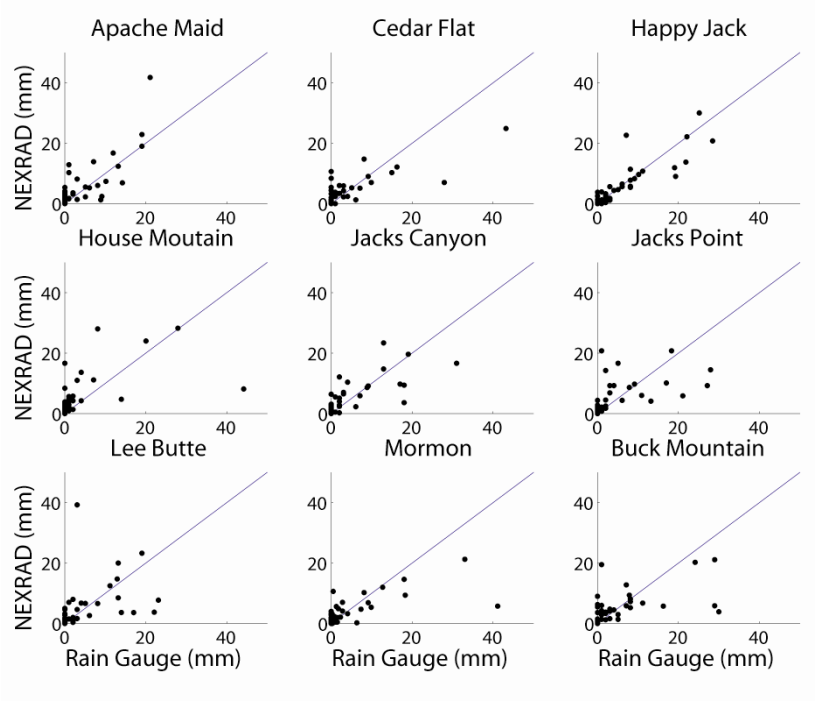

(a)

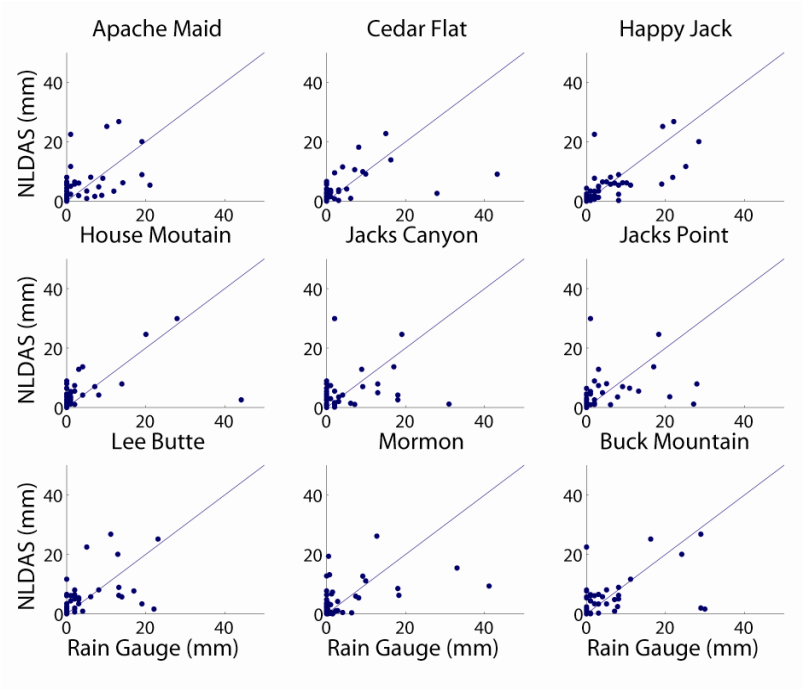

(b)

Figure 7: Scatter plots of daily precipitation totals for 2007 for 9 rain gauge station sites and the corresponding pixel cells for both remote sensing products (a) NEXRAD (b) NLDAS.

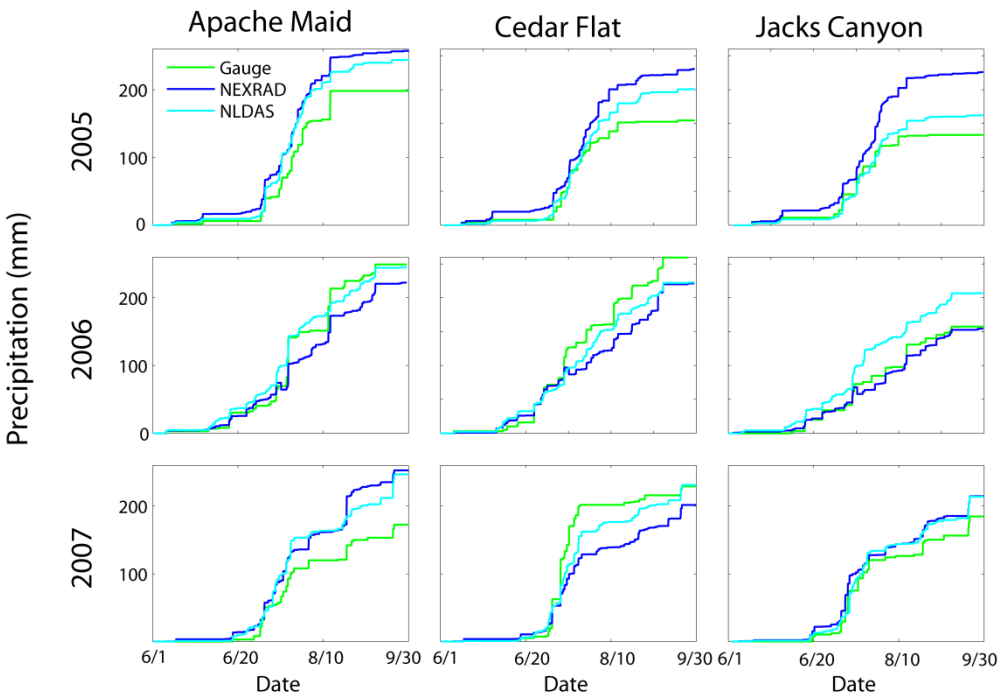

Figure 8: Summer simulation cumulative rainfall totals for three key pixel locations in the basin for summers 2005, 2006, and 2007 using rain gauge, NEXRAD and NLDAS forcing.

For both remote sensing products the Happy Jack site is the closest to the rain gauge stations, whereas Jacks Canyon shows good correlation to the gauge station site using NEXRAD and poorer correlation using NLDAS. However, as the scatter plot Figure 7 shows, the Jacks Canyon site has a large number of smaller events that correspond well the gauge measurements.

In Figure 8, cumulative precipitation total for all three forcing types tells the story about how each one varies over the course of the summer. These three gauge site locations were chosen due to their influence on the model during simulations using gauge forcing, and thereby other forcing as well. The Thiessen polygons at Apache Maid and Cedar Flat cover a wide breadth of Wet Beaver Creek over most of the clay soil type and

Jacks Canyon covers much of Dry Beaver Creek. This point is important to model parameterization and model calibration as the forcing type greatly influences soil parameter values. The higher the intensity of rain over an area, the more a parameter needs to be adjusted to match observed streamflow records.

By evaluating individual sites, the complexities of how the products differ are illuminated. As discussed above, the Apache Maid and the Cedar Flat rain gauge stations are important to Wet Beaver Creek. When comparing all precipitation products for the calibration summer, the remote sensing products vary to that of the rain gauges. The rain gauge underestimates when compared to NEXRAD and NLDAS for the Apache Main pixel, and overestimates for the Cedar Flat pixel. It is important to point out that this cumulative comparison of the products does not fully characterize the variation between products for individual storm events'; further assessment of this point will be discussed below.

A further analysis of this point is made in the results section of this report and will provided model streamflow output in comparison to all precipitation forcing products for all summers examined in this study.

In table 5 the conditional mean is calculated to examine rainfall event totals at certain location in the basin for all three forcing. The conditional mean (CM) is given by:

$$CM = \frac{Total\ Rainfall}{\#\ of\ Events} \qquad \text{Equation 1}$$

Each pixel location evaluated corresponds to the equivalent NEXRAD and NLDAS pixel for three different rain gauge sites; Apache Maid, Cedar Flat, and Jacks Canyon.

Table 5: Number of rainfall events, totals, and conditional mean for the summer of 2007 (calibration summer) at three strategic locations in the basin.

Apache Maid

	# of events	Total Rainfall (mm)	Conditional Mean (mm/event)
Gauge	25	172.5	6.9
NEXRAD	56	251.8	4.5
NLDAS	59	245.1	4.2

Cedar Flat

	# of events	Total Rainfall (mm)	Conditional Mean (mm/event)
Gauge	23	228	9.9
NEXRAD	48	199	4.1
NLDAS	53	228	4.3

Jacks Canyon

	# of events	Total Rainfall (mm)	Conditional Mean (mm/event)
Gauge	22	185	8.4
NEXRAD	48	210	4.4
NLDAS	48	211	4.4

Events were chosen if the total precipitation was over 0.1mm for four hours, meaning that for one hour total accumulation was 0.1 mm or greater or for four consecutive hours there was at least 0.025 mm/hr of precipitation. This point is important

when considering the NLDAS forcing, and to a much lesser degree, the NEXRAD forcing. NLDAS tended to record events over many hours over the same events recorded in NEXRAD or gauge. NEXRAD would span 4-5 hours and NLDAS would span 7-10 hours. In the case where gauge events aligned with these products, the gauge only registered 1-2 hours. NEXRAD and NLDAS had several cases that recorded events with very little volume, too low for gauge measurements to accurately read anything. There were several events that NEXRAD and NLDAS had very similar totals but very different time patterns. Gauge events happening only at higher intensities and for a few hours are seen in the higher conditional mean for all three sites.

2.2 MODEL INTRODUCTION AND DESCRIPTION

The model utilized here is the TIN-based Real-time Integrated Basin Simulator (tRIBS). The model's heritage lies in the Real-time Integrated Basin Simulator (RIBS) (Garrote & Bras, 1995) and the Channel-Hillslope Integrated Landscape Development (CHILD) models (Tucker, et al. 2001a). The tRIBS model is a physically based, distributed hydrologic model capable of simulating detailed surface-subsurface dynamics and the lateral redistribution of moisture within a system (Vivoni, et al. 2005). It does this by coupling a moving infiltration front with variable groundwater to capture soil moisture transfers between surface and subsurface. Topographic representation is accounted for using a Triangular Irregular Network (TIN) that offers substantial computational savings that can be significantly seen in watersheds greater than 1000 km^2. In each individual cell tRIBS simulates physical hydrologic processes such as canopy interception, evapotranspiration, infiltration, soil moisture redistribution, runoff, and channel flow. The following section describes the model in a semi-detailed format to assist the reader in understanding parameters that are essential to this study. A further

detailed description of the model can be found in Ivanov (2002) and Ivanov et al. (2004a).

2.2.1 Model Topography

Correct topographic representation is the first step in building a hydrologic model as it is a controlling factor in the basin hydrologic response. Readily available are high resolution elevation datasets that will facilitate detailed domain. These datasets, however, can become cumbersome in large domain watersheds (> 1000 km^2), and a more efficient manner in representing these data sets is needed.

This need is driven by computational efficiency. Large model domains, utilizing high-resolution grids require a means by which to reduce data or coarsening to obtain reasonable computational performance (Wigmosta, et al. 1994; Vazquez, et al. 2002; Vivoni, et al. 2005). There is a tradeoff, however, in efficiency to proper topographic aggregation of the terrain to represent the watershed well enough. In aggregating the original DEM cell structure to a coarser resolution (as much as an order of magnitude) there is a level of error introduced into the structure. However, the ability to capture important topographic features and save computation effort by aggregation is possible, and has been examined in several studies (Vivoni, et al. 2005). In determining the means by which to aggregate the DEM, the overall objectives should be following:

- Representation of topographic variation
- Linear features such as stream networks and ridge lines
- Appropriately represent basin area and boundary

An alternative to the DEM grid cell is to model the TINs as a method of aggregation. The TIN based network resampling of the DEM is done using criteria that represents a measure of topographic and hydrologic significance, and at the same time preserves the distribution of the topographic slope and curvature (Vivoni, et al. 2005).

Triangular irregular networks (TIN) are a piecewise linear representation of a surface defined by triangular elements of varying sizes (Vivoni, et al. 2005). TINs possess the distinct advantage of representing terrain variability at multiple resolutions through non-uniform distribution of triangle vertices (Nelson, et al. 1999) and (Vivoni, et al. 2004). In areas of low terrain, the need for a large number of elements is unnecessary. However, in areas of complex and rugged terrain, a fine resolution network is best to capture the topography. This can be seen in the Figure 9, where areas of higher relief, as characterized by the tightly spaced contour lines, are heavy in TIN population and areas of lower relief have a sparser number of TIN cells.

To select the TIN node cells from the original DEM, an algorithm that is developed from criteria fitting the needs of the hydrologic model is necessary. Vivoni et al. (2005) developed a hydrographic TIN method for capturing topographic variability and basin morphometry. This method, known as the drop heuristic (DH) method, uses a criterion based on preserving the topographic slope. The DH method selects nodes for the TIN from the DEM by using a metric of Z_r, which is a measure of tolerance.

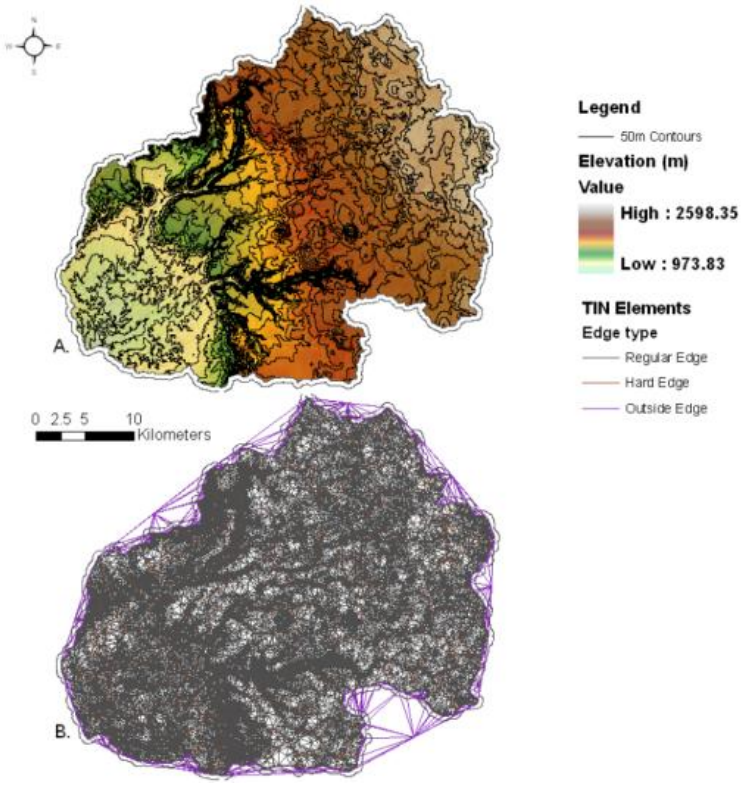

Figure 9: Aggregation of DEM grid network to TIN. (A.) USGE 30 m DEM overlaid with 50 m contour lines. (B.) TIN network derived from DEM using a Zr of 8 m.

This means that elevation nodes are removed with a resulting network of TIN exceeding the tolerance value (Lee 1991). This resulting TIN network can be significantly leaner than the original DEM. To capture this reduction and accurately compare the two, the following metric is introduced:

$$d = \frac{n_t}{n_g} \qquad \text{Equation 2}$$

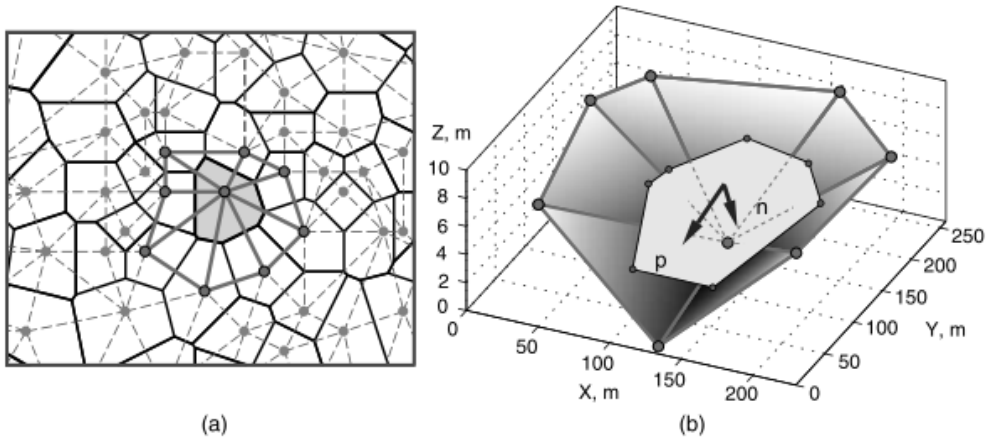

Figure 10: (a) Voronoi polygon created from TIN network (b) single Voronoi cell representing directional flow and flux lines. From (Ivanov, et al., 2004a)

In this equation, n_t is the number of TIN nodes and n_g is the number of DEM grid cells. As the ratio becomes closer to 1, the number of TIN cells converges onto the number of DEM cells. Conversely, as the ratio approaches zero, the aggregation is increased and the TIN resolution becomes coarser.

The TIN mesh nodes describe the control volume in which the computational geometric elements are defined. Each control volume around the mesh nodes is used to estimate the state variables; these volumes are Voronoi polygons (or Thiessen polygons) and are created from connecting the perpendicular bisector of each TIN. They define a boundary around a TIN node where all the space inside the boundary is closer to that node than any other node. Voronoi polygons defined around a TIN node are exemplified in Figure 10. Fluxes between cells follow the parallel *p* axis of a polygon and follow the (Tucker, et al. 2001a) method of flow being routed along the steepest edge, constraining the flow along the edge rather than the surface (Ivanov., et al. 2004a). One-dimensional equations conserve mass in the normal direction *n*.

The following sections describe the physically based mathematical equations the model solves in each Voronoi polygon to evaluate the hydrological processes in a basin.

2.2.2 Rainfall Interception, Energy Balance, and Evapotranspiration.

Rainfall interception is a hydrological process that redistributes the rainfall captured by vegetation. The water is held temporarily by the surface tension and finally evaporates back into the atmosphere or reaches the ground surface as canopy drainage or stem flow (Lu, 2011). The tRIBS model utilizes the canopy storage model as described below in the form as outlined in (Rutter et al, 1971) and (Rutter et al, 1975). This canopy water balance model appropriates a portion of rainfall *R* as the input using the free throughfall coefficient *p* and delegates output into two lumps, the canopy drainage *D* and the potential evaporation rate $E_{p.}$ The evapotranspiration rate is based on the fraction of canopy storage *C* to the canopy capacity S.

$$\frac{dC}{dt} = (1 - \mathrm{p})\mathrm{R} - \mathrm{D} - \frac{C}{S}E_p \qquad \text{Equation 3}$$

The canopy drainage *D* identifies the losses from dripping water off of leaves as well as streamflow; it is modeled as the following:

$$D = Ke^{g(C-S)} \qquad \text{Equation 4}$$

K is the drainage rate coefficient and *g* is the exponential decay parameter (Shutterworth, 1979) and (Ivanov et al. 2004a). The model requires input values for parameters *p*, *S*, *k*, and *g*.

The energy balance of the system is directly linked to soil moisture and evaporation; how much radiation there is available to hydrologic processes states the levels of evaporation moisture loss. Broken down into its basics, radiation has three components; latent λE, ground G, and sensible H heat fluxes.

$$R_n = \lambda E + H + G \qquad \text{Equation 5}$$

Latent Heat flux is calculated at the soil surface using the Penman-Monteith model (Penman, 1948) and (Monteith, 1965).

$$\lambda E = \frac{\Delta(R_n - G) + \gamma \frac{\rho_m \lambda_v \delta q_a}{r_a}}{\Delta + \lambda(1 + \frac{r_s}{r_a})} \qquad \text{Equation 6}$$

Δ is the slope of the Clausius-Clayperson relationship, γ is the psychometric constant, ρ_m is the moist air density, λ_v is the latent heat of vaporization, and δq_a is specific humidity deficit. These variables are calculated from methods outlined in (Rogers & Yau, 1989) and (Bras, 1990). The aerodynamic resistance is symbolized by r_a and r_s is the stomatal resistance as outlined in (Shuttleworth, 1992).

The calculation of latent heat is used as an estimate for actual evaporation E_a which is a component of the potential evaporation equation obtained from (Wigmosta, Vail, & Lettenmaier, 1994):

$$E_p = E_a \frac{\Delta + \gamma \quad 1 + \frac{r_a}{r_s}}{\Delta + \gamma}$$ Equation 7

Evaporation is partitioned into three components; evaporation from bare soil E_s, evaporation from wet canopy E_{wc}, and evaporation from canopy transpiration $E_{dc.}$ Each computational element in the model has a portion of the three evaporation components that contributes to the overall evaporation; the vegetation fraction v determines this apportionment. Evaporation from bare soil is determined from the following equation (Deardorff, 1978).

$$E_s = (1 - v)\beta_e E_p$$ Equation 8

β_e is determined from the soil moisture in the top 100 mm of the soil column θ_{100} and saturated soil moisture θ_s. It is a reduction factor for the near surface portion of the soil column.

$$\beta_e = \min(1, \frac{\theta_{100}}{0.75\theta_s})$$ Equation 9

In the denominator, the 75% of the saturated soil moisture indicated is approximately the field capacity. Field capacity is the amount of water held in soil after excess water has drained away and the rate of downward movement has materially decreased (Veihmeyer & Hendrickson, 1931) .

Evaporation from vegetation can occur in two ways, from the canopy, E_{wc} and from transpiration, E_{dc}. The level of saturation on the plant canopy determines the evaporation rate. If the canopy storage is greater than the canopy capacity then evaporation happens at its potential. If canopy storage is less than the capacity then the evaporation is a fraction of the potential and transpiration occurs.

$$E_{wc} = vE_p,\ E_{dc} = 0, C \geq S \qquad \text{Equation 10}$$

$$E_{wc} = \frac{C}{S} vE_p,\ E_{dc} > 0, 0 \leq C \leq S \qquad \text{Equation 11}$$

Transpiration occurs at the following rate:

$$E_{dc} = \beta_t v(E_p - E_{wc})\ \frac{\Delta + \gamma}{\Delta + \gamma\ \ 1 + \frac{r_a}{r_s}} \qquad \text{Equation 12}$$

β_t in this equation represents the plant's stress due to soil moisture variability and limits root uptake.

$$\beta_t = \min(1, \frac{\theta_{top} - \theta_r}{0.75\theta_s - \theta_r}) \qquad \text{Equation 13}$$

θ_{top} is the soil moisture content in the top meter and θ_r is the residual moisture content (Brooks & Corey, 1964) and (Ivanov, et al. 2004a).

Sensible heat flux is calculated based on the difference between surface T_s and air temperature T_a using an aerodynamic surface resistance approach (Ivanov, et al. 2004a).

$$H = \frac{\rho_m C_p}{r_a}(T_s - T_a) \qquad \text{Equation 14}$$

C_p is the specific heat capacity (all other variables have been previously defined).

Ground heat flux is based on solving the heat diffusion equation between a soil surface layer and a deeper soil profile (Ivanov, et al. 2004a). The ground heat flux *G* is obtained from (Lin, 1980).

$$G = \frac{1}{2} C_s d_1 (\xi \frac{dT_s}{dt} + \omega(T_s - T_a)) \qquad \text{Equation 15}$$

C_s is the soil heat capacity, ω is the daily frequency of oscillation, d_1 is the soil heat wave damping depth and is described as the square root of $2k/\omega$, $k = k_s/C_s$ and is the soil diffusivity, k_s is the soil heat conductivity.

2.2.3 Infiltration Scheme and Runoff

The infiltration model is based on the kinematic approximation and on a simplified mathematical description of soil anisotropy and heterogeneity which allow for analytical treatment of the problem (Cabral, Garrote, Bras, & Entekhabi, 1992). Flow equations are defined by the directions parallel *p* and normal *n* to the surface of the hillslope. An illustration of this dynamic is shown in figure 11.

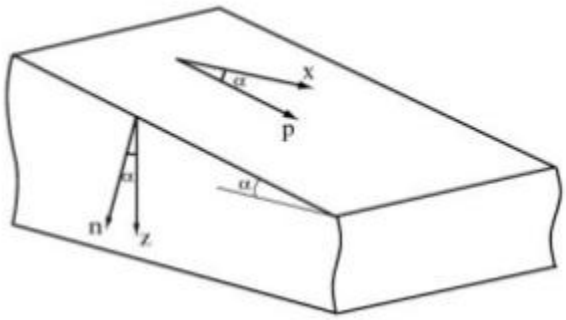

Figure 11: Representation of the coordinate system on a hillslope. Axis p is the component is the direction of greatest slope, n is the component normal to the p and α is the angle between the gravitational component and n.

The assumption in this model is that saturated hydraulic conductivity decays from the surface in the direction normal to the hillslope. This assumption is a common practice in hydrology (Cabral, Garrote, Bras, & Entekhabi, 1992), and was shown to work well with several soil data sets from a variety of watersheds (Beven K. J., 1984). Soil layering is represented by a dimensionless anisotropy coefficient defined as the ration between the saturated conductivities in the parallel direction and in the direction normal to the soil surface (Ivanov, et al. 2004a).

When the rainfall rate is greater than the hydraulic conductivity of a soil ponded infiltration occurs; the standard practice is to model this condition using the Green-Ampt model. The tRIBS model uses a modified version of Green-Ampt equation as outlined in (Childs & Bybordi, 1969) and (Beven K. J., 1984).

$$q_n(N_f) = -K_{eff}\left(\frac{h_f(N_f)}{N_f} - 1\right) \qquad \text{Equation 16}$$

In equation 16, $q_n(N_f)$ is flow perpendicular to the hillslope, N_f is the wetting front depth, K_{eff} is the harmonic mean of conductivities over the saturated depth. From the surface into the soil column the saturated hydraulic conductivity K_{On} decays exponentially at the rate of f, and is determined by the following (Ivanov V. Y., 2002):

$$K_{eff}(N_f) = K_{On}\frac{f(N_f)}{e^{fN_f} - 1} \qquad \text{Equation 17}$$

The pore space below the wetting front is at a pressure that is less than the atmospheric pore pressure. Changes in soil moisture and conductivity with depth of the wetting front is effected by the capillary pressure, $h_f(N_f)$ and expressed as:

$$h_f(N_f) = \Psi_b\frac{1 - S_{ei}^{3+\frac{1}{\lambda\ N_f}}}{3\lambda(N_f) + 1} \qquad \text{Equation 18}$$

Ψ_b is the air entry bubbling pressure, λ is the pore-size distribution index, and S_{ei}, is the effective saturation, described in the following equation.

$$S_{ei} = \frac{\theta(N_f) - \theta_r}{\theta_s - \theta_r} \qquad \text{Equation 19}$$

Here $\theta_i(N_f)$ is the moisture content at the depth N_f, θ_r is the residual soil moisture content and θ_s is the saturated soil moisture content. Porosity of the soil is the combination of θ_r and θ_s.

Using equations 15, 16, and 17; the flux rate of the wetting front is put into terms of the following equation:

$$\Psi_{is}(N_f) = -K_{eff} \quad \frac{h_f(N_f)}{N_f} \qquad \text{Equation 20}$$

On the hillslope the vertical component of the gravitational forces and the component normal to the direction of flow most of the time do not match and therefore it is necessary to derive the normal component to the hillslope represented by α. Thus the modified Green-Ampt equations can be rewritten as:

$$q_n(N_f) = N_{eff}(N_f)\cos\alpha + \Psi_{is}(N_f) \qquad \text{Equation 21}$$

This equation indicates how the model accounts for infiltration when the rainfall rate is higher than or equal to the infiltration rate (Ivanov, et al. 2004a).

An additional condition to consider, other than the fully saturated state, is the unsaturated state that occurs when the rainfall rate is less than the infiltration rate. In this case only infiltration excess runoff is produced (runoff mechanism will be explored in a subsequent section) and wetted unsaturated wedge is produced. If the rainfall rate continues a perched zone may be formed. As discussed above, hydraulic conductivity decays from the surface down into the soil column. In the instance of unsaturated

condition, this decay factor leads to the buildup of saturated conditions below the soil surface. This buildup is the wetting front. The wetting front is the representation of the soil moisture wave into the soil (Ivanov V. Y., 2002). The buildup or formation of the perched layer creates a shock wave that ascends, creating a separate front called the top front.

An equation for this phenomenon is very similar to that of the saturated condition with a few deviations. An equivalent rainfall R_e is needed, which is defined as the value that leads to the same moisture content above the wetting front as from a constant rainfall R_e under equilibrium conditions (Ivanov, et al. 2004a) and (Garrote & Bras, 1995). The reader is referred to Ivanov (2002) for a detailed discussion on how to obtain R_e. The redistribution flux for the unsaturated wetting wedge is described as:

$$q_n(N_f) = R_e \cos\alpha + \Psi_{ie}(N_f) \qquad \text{Equation 22}$$

Ψ_{ie} is the capillary drive across the wetting front in this the unsaturated state. This term is dependent on the initial wetness and the moisture magnitude in the wetted wedge and is defined below:

$$\Psi_{ie}\ (N_f, \theta_i, \theta_e) = -K_{Sn}(N_f)\frac{h_f(N_f, \theta_i, \theta_e)}{N_f} \qquad \text{Equation 23}$$

In equation 23, the term $K_{se}(N_f)$ is the saturated conductivity at depth N_f and $h_f(N_f, \theta_i, \theta_e)$ is the effective unsaturated capillary pressure evaluated for an arbitrary moisture range in soils with decaying saturated conductivities.

$$\mathrm{h}_f\ (N_f, \theta_i, \theta_e) = \psi_b \frac{S_{ee}^{3+\frac{1}{\lambda(N_f)}} - S_{ei}^{3+\frac{1}{\lambda(N_f)}}}{3\lambda\ N_f\ + 1} \qquad \text{Equation 24}$$

$$S_{ee}(N_f) = \frac{(\theta_e(R_e, N_f) - \theta_r)}{(\theta_s - \theta_r)} \qquad \text{Equation 25}$$

For equations 24 and 25, θ_i is the moisture content at depth N_f of the initial moisture profile and θ_e is the maximum moisture value in the wetting wedge (Ivanov V. Y., 2002).

As described above, a perched zone can form if a saturated layer is developed at some depth in the soil column. In this instance similar assumptions to the ponded infiltration case are used as follows:

$$q_n(N_f, N_t) = N_{eff}(N_f, N_t)\cos\alpha + \Psi_{ie}(N_f) \qquad \text{Equation 26}$$

As previously noted, K_{eff} is the harmonic mean of conductivities over the saturated depth, and for this instance is described as:

$$K_{eff}(N_f, N_t) = K_{On}\frac{f(N_f - N_t)}{e^{fN_t} - e^{fN_t}} \qquad \text{Equation 27}$$

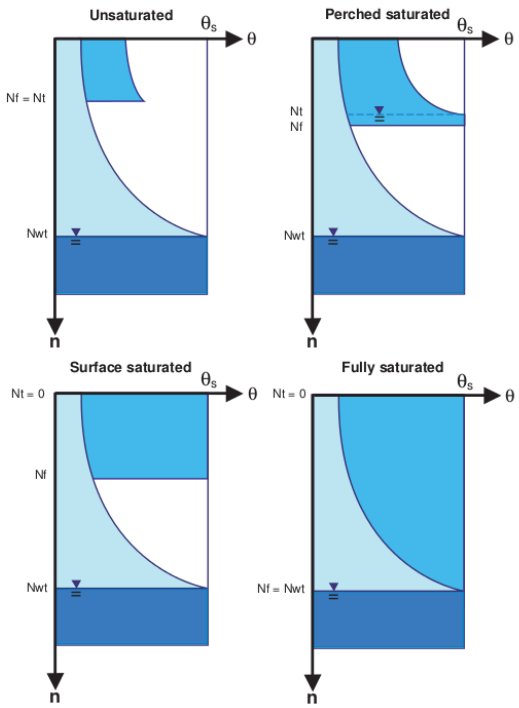

Figure 12: Soil moisture profiles possible in tRIBS leading to differing runoff mechanisms. The figure represents the initial soil moisture profile in light blue, the groundwater table in darkest blue, and the soil moisture development under the four situations for the wetting front and the top front. From (Ivanov V. Y., 2002).

In the previous section, soil moisture distribution in a soil column was described briefly. Each moisture front position: complete saturation, perched saturation, surface saturation, and unsaturated; has the potential to turn into runoff as seen in the Figure 12. The runoff mechanisms that the tRIBS model is capable of accounting for are infiltration excess, saturation excess, perched subsurface storm flow, and groundwater exfiltration (Ivanov V. Y., 2002).

Complete saturation occurs when the wetting front is at the water table, the top front is at the soil surface, and the entire soil column is saturated and so can hold no additional water. This condition can lead to saturation excess runoff. Groundwater exfiltration occurs when an upstream saturated cell contributes water to a downstream

saturated cell. Perched return flow occurs when an up stream unsaturated cell contributes to a downstream saturated cell (Ivanov V. Y., 2002).

Surface saturation occurs when there is a fully defined wetting front above the water table and the top front is at the soil surface. This can happen as the hydraulic conductivity decays and the wetting front moves farther into the soil column. This produces saturation excess runoff. The soil column may also generate return flow if subsurface inflows into the element exceed both outflows and the rate of redistribution of the moisture wave in the normal to the surface direction (Ivanov V. Y., 2002).

As discussed above unsaturated conditions can lead to infiltration excess runoff, also referred to as Hortonian runoff. Infiltration excess runoff is often the main mechanism for overland flow in semiarid environments (Beven K. J., 2002). In the model, runoff is considered to be of infiltration excess type when the redistribution rate of the top saturated layer is lower than the rainfall intensity (Ivanov et al. 2004a).

A re-infiltration scheme is not considered and runoff produced in a cell is assumed to contribute to the streamflow at the catchment outlet (Ivanov et al. 2004a). Once rainfall falls on a cell it must infiltrate there or, once it leaves that cell as runoff it will travel the full length of the basin to the outlet.

2.2.4 Groundwater Model

The model utilizes a quasi three-dimensional groundwater model that routes flow across TIN edges, *j*.

$$\Sigma Q_{Sout_j} = \Sigma(-TW_J \tan \beta_J) \qquad \text{Equation 28}$$

In equation 28, Q_{Soutj} is the out flux from a saturated layer, *W* is its width, and *tanβ* is the local gradient of the water table (Ivanov, et al. 2004a).

The aquifer transmissivity *T* nonlinearly depends on the groundwater depth N_{wt} and bedrock depth η′ due to the exponential decay *f* of the saturated conductivity (Ivanov, et al. 2004a).

$$T = \frac{a_r K_{On}}{f}(e^{-fN_{wt}} - e^{-f\eta'}) \qquad \text{Equation 29}$$

As discussed earlier K_{On} is the surface hydraulic conductivity and a_r is the anisotropy ratio. To account for an influx of groundwater for a given Voronoi cell the model sum the out flux of neighboring cells and the tallies to the depth to groundwater:

$$S_y \frac{dN_{wt}}{dt} = \frac{\Sigma Q_{Sout_j} - \Sigma Q_{Sin_j}}{A} \qquad \text{Equation 30}$$

A is the cell area, Q_{Sin} is the saturated layer influx, and S_y is the specific yield. Due to computationally heavy work with specific yield, the model deals with this based on mass conservation. The reader is directed to (Ivanov V. Y., 2002) for a more detailed account of the groundwater model.

2.2.5 Hydrologic Routing

Runoff on the hillslope follows the TIN edges in the drainage direction and transfers runoff to the channel network. The model assumption is that bulk transport of water is the dominant process in runoff routing. This simplified scheme helps reduce the parameterization and computational complexity that a full or approximated Saint-Venant equation would have on the model. The objective of the adopted solution is to differentiate between the two transport mechanisms that operate in overland and streamflow and to account for some non-linearities in the basin response (Ivanov V. Y., 2002). The hillslope travel time is calculated as:

$$t_\tau = \frac{l_h}{v_h(\tau)} \qquad \text{Equation 31}$$

In equation 31, l_h is the hillslope runoff length and the hillslope velocity varying in space and time, $v_h(\tau)$ is given as the following:

$$v_h\ \tau\ = c_v\ \left(\frac{Q\ \tau}{A_c}\right)^{r} \qquad \text{Equation 32}$$

The discharge at the outlet stream node at time τ is represented as $Q(\tau)$, A_c is the contributing area of the outlet node, and r and cv are parameters for a given basin (Ivanov, et al. 2004a).

2.2.6 Hydraulic Routing

Routing the runoff once it hits the channel is done by way of the kinematic wave equation. The one-dimensional, unsteady free surface flow continuity equation is given as the following:

$$\frac{\partial F}{\partial t} + \frac{\partial Q}{\partial x} = R_b \qquad \text{Equation 33}$$

F is the cross sectional area, Q is the discharge in the x direction, and R_b is the lateral water influx into the channel per unit length. The discharge term is described by Manning's equation, assuming the cross section is approximated as a rectangle.

$$Q = \frac{\sqrt{i_0}}{n_e} H^{5\,3} b \qquad \text{Equation 34}$$

H is the depth, i_0 is the channel slope, n_e is the channel roughness, and b is the channel width (Ivanov, et al. 2004a).

2.2.7 Summary

This section was intended to capture the complexity of the model and outline the physical nature of the equations that are being solved. Further discussion on key parameters in many of the presented equations and their effects on the model simulations will be covered in the calibration section. A large portion of this model discussion relied on the work as laid out in (Ivanov V. Y., 2002) and (Ivanov, et al. 2004a).

3 RESULTS AND DISCUSSION

3.1 MODEL CALIBRATION

A distributed model, such as tRIBS, represents the system in realistic terms. Parameter values can be obtained from literature values based on field measurements. For large to mid-size basins field-tested parameters become an inherent problem due to the exhaustive approach needed to establish all spatial variations. For the purposes of this study, parameter values have been obtained from published values and previous model studies and then adjusted during calibration to approximate observed streamflow. Extensive calibration was done on only certain parameters for which the model is most sensitive.

While most models focus on the catchment outlet, tRIBS has the ability to examine multiple interior points, and thereby the model has the ability to capture the catchment response throughout the basin, as well as realistically simulate hydrologic process. The tRIBS model resolves mass equations at a fine temporal (~4 min) and spatial (~30 m) scales and thus using physically meaningful parameters that have quite narrow plausible ranges (Ivanov V. , et al. 2004b).

The following section describes parameters, their selection, and adjustments made in the calibration phase to match streamflows at the USGS outlet station, as well as at the two interior gauge station sites. The gauge station sites are operated by cooperation among the Salt River Valley Water Users' Association, the Arizona Department of Water Resources, and the USGS. Available data for the outlet stream gauge site just upstream of the junction of Beaver Creek with the Verde River is limited; data are available only

from 2004 to 2008. The 2007 summer was chosen for calibration due to its availability of data as well as other weather station data that will be described in further detail in the single point modeling section. Summers 2005 and 2006 were chosen for validation purposes used to corroborate parameter selection from the 2007 simulation.

3.1.1 Land Cover Parameterization

Land cover characteristics affect the soil water dynamics by means of energy and radiation balances at the land surface-atmosphere interface. The parameters employed in the model determine the necessary energy balance by calculating rainfall interception, bare soil evaporation, and evapotranspiration. The model has the capability to compute rainfall interception in a simplistic manner, or with the more complex Rutter model; the latter is the scheme that is utilized in this study. For a more detailed description of these equations see section 2.2.2. Table 6 provides land cover description and units. The first four parameters are involved in the Rutter model for interception and the proceeding five are involved in various calculations for evapotranspiration.

Table 6: Land cover parameter description

Parameter	Description	Units
P	Free Throughfall coefficient	[ ]
S	Canopy Field Capacity	[mm]
K	Drainage Coefficient	[mm/hr]
g	Drainage Exponential	[mm-1]
Al	Albedo	[ ]
h	Vegetation height	[m]
K_t	Optical Transmission Coefficient	[ ]
R_s	Canopy-avg stomatal Resistance	[s/m]
V	Vegetation Fraction	[ ]
LAI	Leaf Area Index	[ ]

Table 7: Land cover parameter values for Beaver Creek

	P	S	K	g	Al	h	K_t	R_s	V
Desert Shrub	0.85	1	0.1	4.0	0.20	1.0	0.6	150	0.2
Desert Riparian	0.5	1.2	0.12	3.5	0.15	5.0	0.5	175	0.5
Grassland	0.9	1	0.12	4.7	0.14	0.6	0.8	100	0.6
Pinyon-Juniper	0.7	1	0.1	4.0	0.18	2.0	0.5	150	0.5
Developed	0.9	0.5	0.05	3.9	0.23	4.0	0.8	50	0.4
Ponderosa Pine	0.5	1.5	0.12	3.5	0.17	10	0.3	175	0.8
Water	1.0	1	0.01	3.7	0.07	0.0	1.0	0	0.9
Desert	0.9	0.2	0.05	3.7	0.25	0.2	0.9	75	0.3

Table 10 presents the parameters used in model simulations. Field-based parameter values are not available for the study area, so values were obtained previous model studies. Many of the values were obtained from (Vivoni, et al. 2005; Ivanov, et al. 2004a; Vivoni, et al. 2009). The highlighted landcover classes are those that have been altered in the calibration process as they are the three most dominant.

Each parameter is a physical trait of the land cover type. The free throughfall coefficient, *P*, is a measure of how much precipitation is captured by the land cover type; 0 being all precipitation is caught and 1 being all of the rainfall reaches the ground surface. Of the three dominant land cover types Ponderosa pine has the highest percentage of rainfall interception at 50%, followed by 30% in the pinyon-juniper and

15% in desert shrub. Forested areas are typically found to have high interception rates (Bras, 1990).

The canopy field capacity *S* is the measure of storage capacity in the land cover type. Both *K* and *g* deal with drainage and are used in the calculation performed in the Rutter Interception Model; as explained in the model description, these parameters are the drainage coefficient rate and exponential decay; of all the land cover types the grassland has the highest drainage and the Ponderosa Pine and Desert Riparian have the lowest.

The parameters pertaining to evapotranspiration and energy flux are albedo, *Al*, vegetation height, *h*, optical transmission coefficient, K_t, stomatal resistance, R_s, and vegetation fraction, *V*. Surface albedo is the fraction of shortwave radiation or solar energy reflected from the land surface back in to the atmosphere. The lower the albedo, the lower the amount of radiation being reflected out. Water effectively absorbs solar energy and therefore has the lowest value of all the land cover types, whereas the desert land cover type tends to be composed of bare soil and has the highest value. The optical transmission coefficient is another measure of radiation absorbance. A value for K_t of 0 results in plant absorption of all radiation and 1 signify that the canopy leads to no radiation loss. The stomatal resistance of a plant is related to evapotranspiration rates, and range from 0.01 for water, to 175 for Ponderosa pine.

3.1.2 Soil Class Parameters

Soil parameters that are utilized are presented in Table 8. The first nine values in the table affect the calculated vertical infiltration and lateral flow distribution and are

associated to the surface soil texture. The latter two parameters are associated with soil thermal properties calculating the soil heat flux.

Table 8: Soil parameter description

Parameter	Description	Units
K_s	Hydraulic Conductivity	[mm/hr]
θ_s	Saturation Soil Moisture	[ ]
θ_r	Residual Soil Moisture	[ ]
m	Pore Distribution	[ ]
Ψ_b	Air Entry Pressure	[mm]
f	Decay Factor	[mm^{-1}]
A_s	Saturated Anisotropy Ratio	[ ]
A_u	Unsaturated Anisotropy Ratio	[ ]
n	Porosity	[ ]
k_s	Volumetric Heat Conductivity	[J/msK]
C_s	Soil Heat Capacity	[J/m^3K]

Many of the soil parameter values were taken from literature based on soil survey information (Rawls & Brakensiek, 1983) and (Rawls, et al. 1982). Many of these values were obtained from previous studies and used as a base line (Ivanov, et al. 2004a; Vivoni, et al. 2009; Vivoni, et al. 2010).

Beaver Creek drainage system includes an ephemeral stream, Dry Beaver Creek; and a perennial stream, Wet Beaver Creek. These two sections of the basin were treated separately for this study. Soil classes were aggregated to make parameterization manageable, however to account for the slight variation in each sub-basin's characteristics, the three main soil classes within each basin were treated separately, as individually highlighted in the Table 9.

Table 9: Soil parameters for Beaver Creek

	K_s	θ_s	θ_r	m	Ψ_b	f	A_s	A_u	n	k_s	C_s
Silty Loam	32.3	0.42	0.07	0.35	-75	0.001	200	300	0.49	0.7	$14x10^5$
Clay Loam (wet)	14.3	0.39	0.08	0.24	-56	0.001	200	300	0.47	0.7	$14x10^5$
Bedrock (wet)	1.0	0.4	0.1	0.2	-37	0.001	200	300	0.48	0.7	$14x10^5$
Sandy Loam	65	0.41	0.05	0.35	-75	0.0007	200	300	0.46	0.7	$14x10^5$
Clay (wet)	3.0	0.4	0.1	0.2	-37	0.005	200	300	0.48	0.7	$14x10^5$
Water	3.2	0.51	0.10	0.35	-75	0.001	200	300	0.61	0.7	$14x10^5$
Loamy Sand	45.0	0.41	0.05	0.35	-75	0.001	200	300	0.46	0.7	$14x10^5$
Sand	105	0.42	0.02	0.35	-75	0.001	200	300	0.44	0.7	$14x10^5$
Silty Clay Loam	3.2	0.51	0.10	0.35	-75	0.001	200	300	0.61	0.7	$14x10^5$
Clay Loam (dry)	14.3	0.39	0.08	0.24	-56	0.001	200	300	0.47	0.7	$14x10^5$
Clay (dry)	3.0	0.39	0.09	0.16	-37	0.0001	200	300	0.48	0.7	$14x10^5$
Bedrock (dry)	1.0	0.39	0.09	0.16	-37	0.001	200	300	0.48	0.7	$14x10^5$
Loam	10.2	0.43	0.03	0.25	-40	0.001	200	300	0.46	0.7	$14x10^5$

Bedrock, clay, and clay loam are the dominant soil classifications and, as seen from Table 9, are redundant across Wet and Dry Beaver Creek. An example of this is the clay soil type; it is highlight in brown to call out it is significant in calibration. There is a different between the properties in each sub-basin, Dry Beaver Creek is called (dry) and Wet Beaver Creek is (wet).

Primary parameters used for calibration are the saturated hydraulic conductivity, K_s, which regulates infiltration rates; conductivity decay parameter *f*, which is the degree to which K_s degrades in the vertical soil column; and to a lesser extent pore distribution and air entry pressure; which both affect soil moisture and in turn evapotranspiration.

Observing the stream hydrographs from USGS stream gauge station site indicates that stream response time after a precipitation event are relatively quick in summer events, many times within 1-2 hours. Streamflow recession limbs quickly recede after the initial spike, indicating high *f* values. The higher the value of *f*, the larger the chance of infiltration excess runoff to occur. The lower values of *f* result in recession limbs that do not fall as fast (Ivanov, et al. 2004b).

3.1.3 Initialization and Groundwater Table Level

A drainage experiment was set up for the model to determine a spatially distributed groundwater table for the initialization of the simulations (Vivoni, et al. 2005). In this model simulation the water table was set to the land surface and allowed to drain naturally. The simulation was set to an extended period of time: 10 years. This allowed for drainage conditions to converge to observed streamflow conditions. Precipitation and evaporation were effectively turned off, allowing for only soil characteristics and basin topography to control subsurface flow. This process was repeated several times, along with soil parameters, as initialization and soil parameters effect streamflow production. Utilizing the calibrated soil parameters, Figure 13 represents the drainage simulation after a 10 year period for a beginning, middle, and final stage.

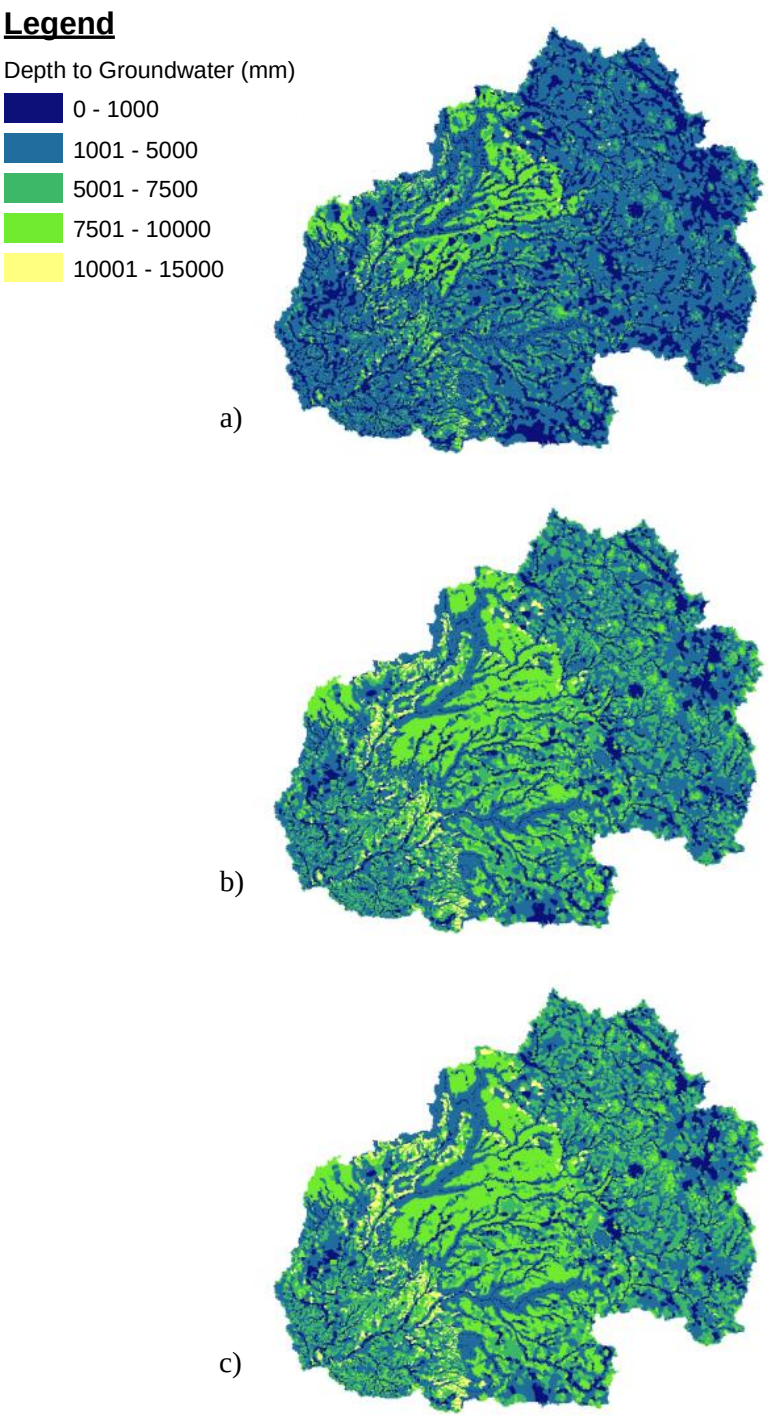

Figure 13: Groundwater depth from the surface for the drainage experiment for hours a) 6000 b) 39000 c) 720000

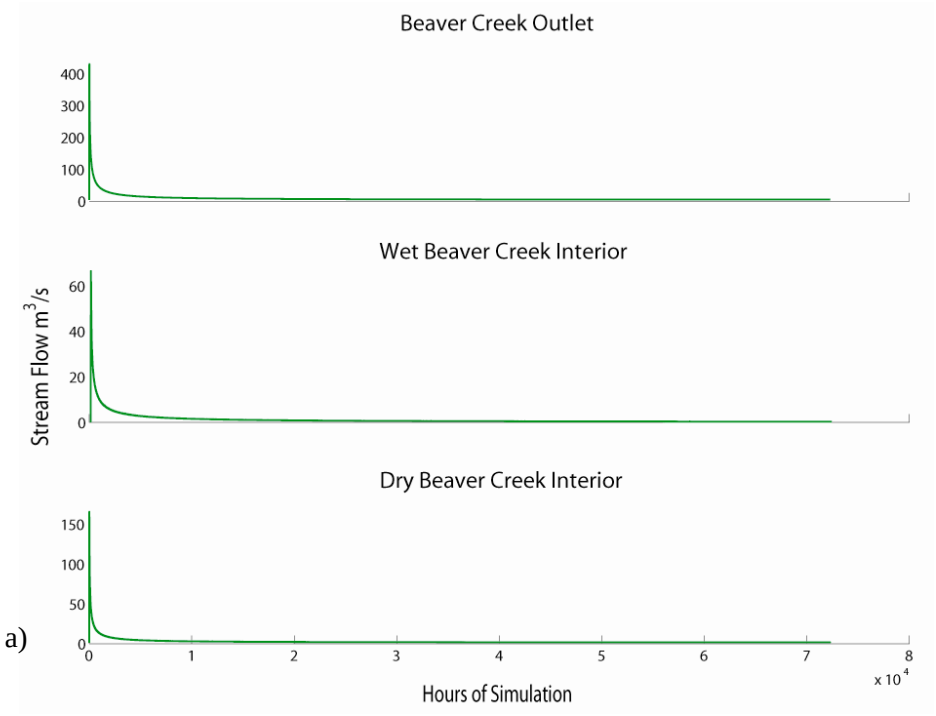

a)

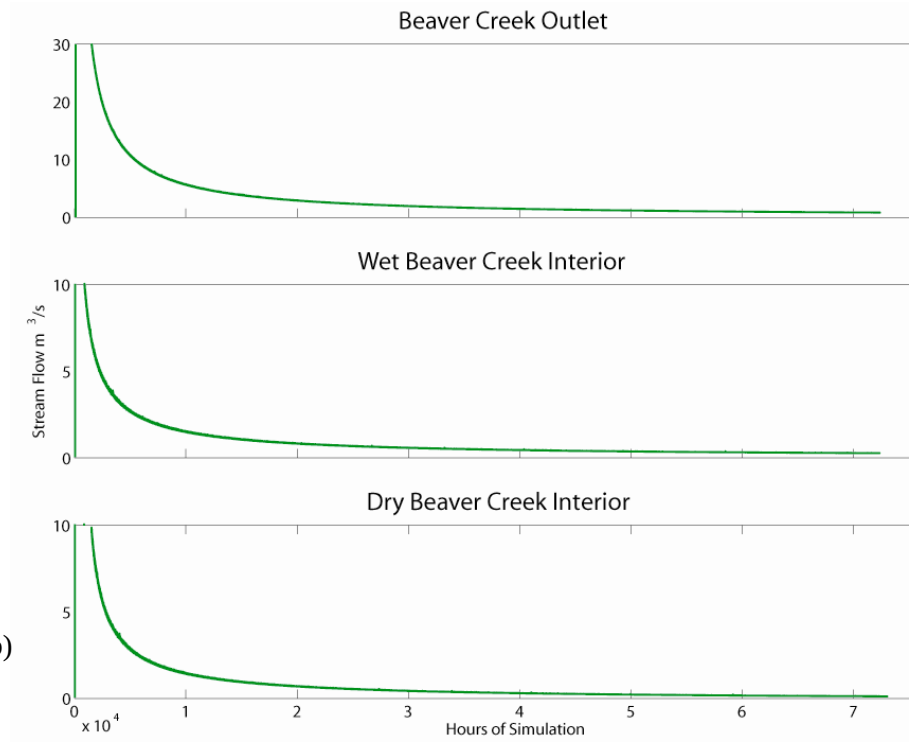

b)

Figure 14: a) Baseflow discharge from drainage experiment for Beaver Creek, Wet Beaver Creek, and Dry Beaver Creek, b) zoomed in version of a)

The resulting streamflow for this simulation typically has a hydrograph-type shape to it; this is due to an initial surge of subsurface moisture from the fully saturated subsurface. As time is extended, the basin responds to the morphometric and soil properties of the basin and begins a recession limb. The water table elevation spatial map was extracted from tRIBS that corresponds to the hour that matched the approximate average stream discharge. This described streamflow can be found in the Figure 14.

3.1.1 Single Point Modeling

tRIBS can be set up to model a single point as well as at the basin scale. The single point model or a point scale model is typically done at research sites where there is a large amount of available data such as an eddy covariance tower (Vivoni, et al. 2010). The point scale model should be situated in an area of the basin to avoid up gradient subsurface fluxes.

To test the response to soil and land cover parameters, a point scale model was set up for the Happy Jack Ranger station where long term weather data were available as well as soil moisture and temperature data (NRCS, 2010-2011). The station is located in the eastern portion of the watershed, at latitude 34° 45 min N and longitude 111° 25 min W. It is located in the Ponderosa pines forest of the basin, located at an elevation of 2326 meters and is illustrated in Figure 15. The model tested parameters for the silty loam soil class and grass land cover type, as the sensors are technically in a grassland clearing of the forested area.

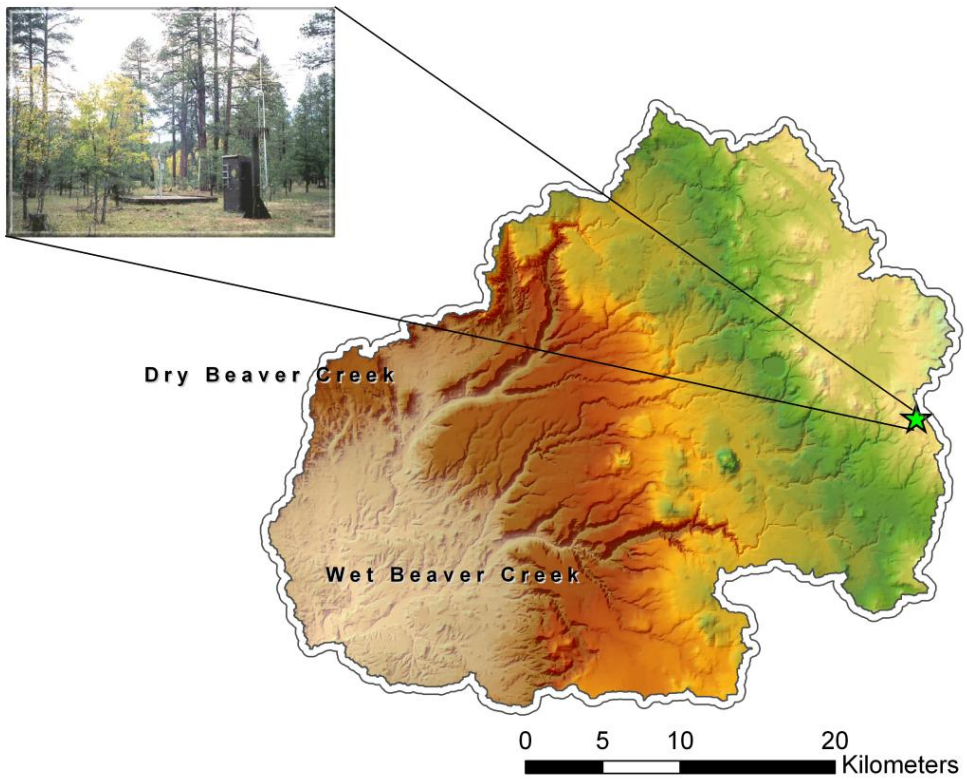

Figure 15: Happy Jack weather station site utilized in point scale modeling observational data available for weather, rain, and soil moisture

The goal of this portion of the study was to more easily distinguish the parameters most sensitive in affecting both evapotranspiration (ET) and soil moisture. These two variables are interlinked, and by adjusting soil parameters the ET is also affected, and vice versa. Adjustments to air entry bubbling pressure were made, which affects the initial soil moisture content. Effects to soil moisture content in this summer simulation also affected ET. Hydraulic conductivity decay parameter, *f*, was also examined in this model as it too effects soil moisture content. ET was also slightly affected by the volumetric heat capacity and the soil heat capacity, these two variables affected the soil temperature, which is an observational data set of this station, see Figure 18.

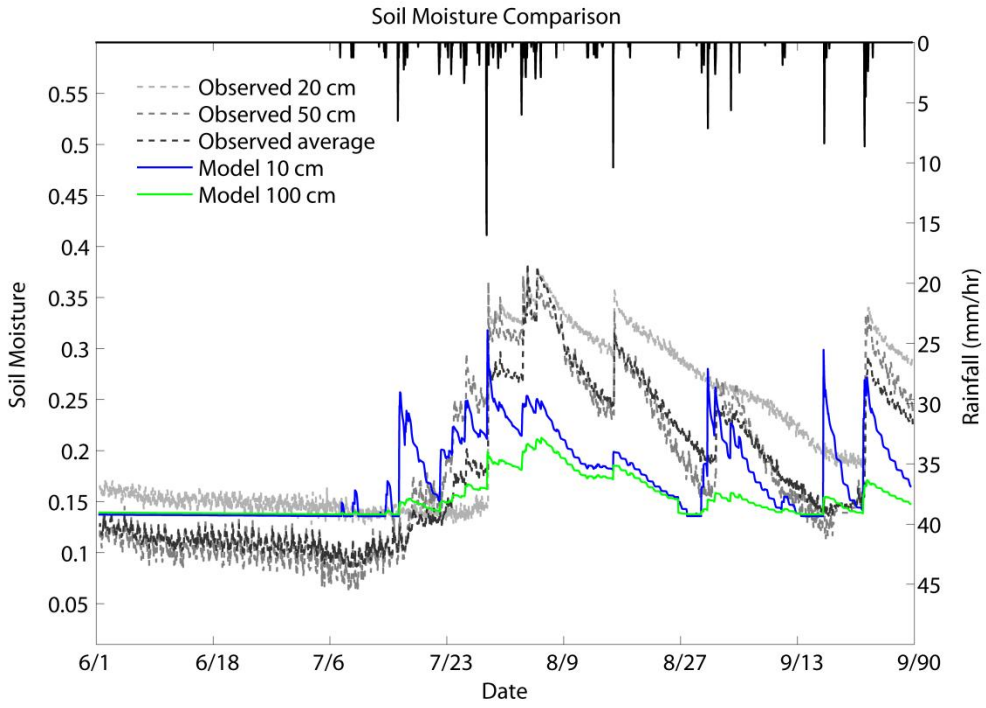

Figure 16: Volumetric soil moisture at the Happy Jack Ranger Station for the summer of 2007 using the single point scale model simulation.

When adjusting the parameters discussed above, the soil moisture at the observable depth, 20 and 50 cm, were compared to model output. The model outputs soil moisture data at 10 and 100 cm depths and therefore a directed comparison to observed measurements is not exact. Trends in soil moisture peaks and the general summer soil moisture pattern were examined between the observed and the modeled when trying to match the two. For the middle part of August, the observable soil moisture was higher than the modeled. The model was unable to capture such a higher degree of soil moisture during this month for any parameters adjusted. The model, however, was able to capture the initial soil moisture peaks as well as the ones in the latter part of August, and September.

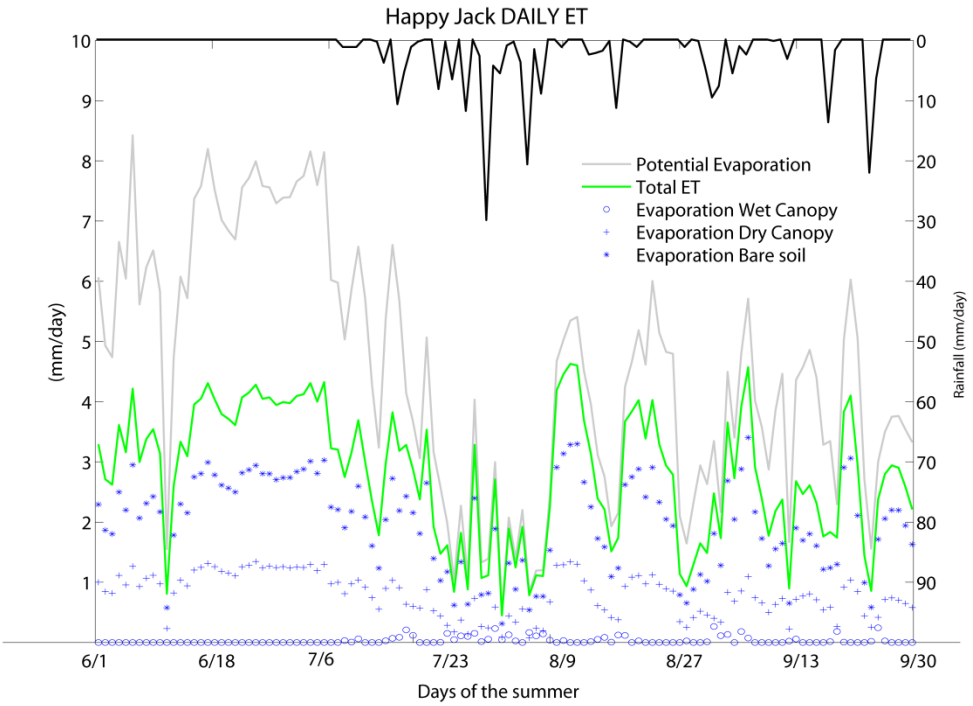

Figure 17: Daily evapotranspiration at the Happy Jack Ranger Station for the summer of 2007 using the single point scale model simulation

In this model, the main goal was to adjust soil and land cover parameters to better match modeled soil moisture to the observed. In doing so, ET was also examined to evaluate it response to these adjustments. Figure 17 displays all ET components; total ET, potential ET (PET) and the ET partitioning from the wet canopy, dry canopy, and bare soil. In the first third of the summer period, potential ET is much higher than actual ET, this corresponds to the drier portion of the period, before the monsoon rain begin. With the onset of the rain, the potential ET is reduced and during the period of high precipitation, July 23rd to August 9th, the total ET very similar to PET. ET partitioning is broken down into three components, with evaporation form bare soil being the greatest. This is due to the modeling being a simulation of the grassland clearing in the Ponderosa Pine.

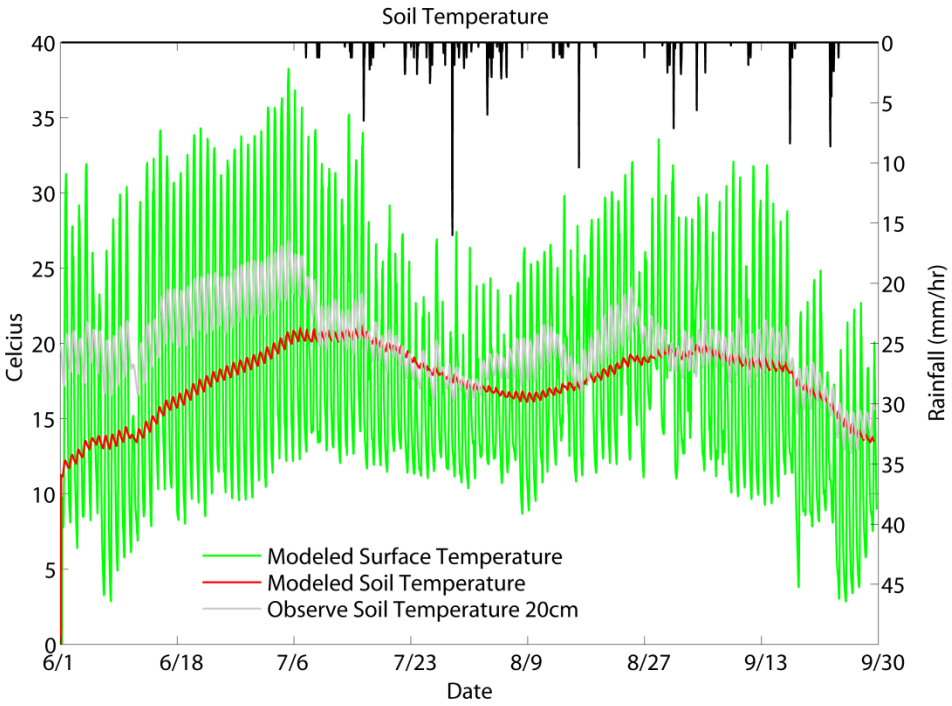

Figure 18: Soil temperature at the Happy Jack Ranger Station for the summer of 2007 determined using the single point scale model simulation.

The grassland land cover type has a free throughfall coefficient of 0.9; much of the precipitation that falls is not captured from the land cover type. This land cover type is also characterized by a vegetation fraction of 60%, meaning that 40% of it is classified as being bare soil.

3.1.2 Basin Scale Modeling

Calibration was performed for the summer of 2007, June 1 to September 30. These dates were chosen to correspond to the monsoonal season in the U.S. southwestern. The monsoon seasons definition was recently changed by the National Weather Service (NWS) to begin on an exact day, June 15, to allow the general public an easier time in determining the start. The old definition, depending on location, was determined by the

first three consecutive days when the average dew point was greater than 55 °F (Ellis, et al. 2004). Model simulations were chosen to contain the core of the monsoon season as well as a preceding dry period, June 1-14.

Model calibration was simulated for a specific summer and then examined in validation summers to determine if parameters were adequate for several sets of observational data. Figures 19 through 22, shows several differences between modeled and observed streamflow; such as magnitude and hydrograph shape. However, general trends are captured and major features are consistent for all summers simulated. Calibration was performed to consider agreement with not only the outlet gauge station site but the two internal sites as well; Wet and Dry Beaver Creek. Figure 19 is the time series comparison for the calibration summer 2007's observed streamflow to the modeled and corresponds to a) summer streamflow b) cumulative stream volume. Validation summers 2005 and 2006 are also presented in figures 21 and 22 for their goodness of fit.

The majority of events for the summer of 2007 occurred between July 22nd and August 11th as seen in Figure 20. In this period there was one large event and several measurable small events. The largest event on July 27th occurred at 4:00pm, of which the model was able to accurately capture the onset of the hydrograph, however the USGS gauge site observed a quickly receding recession limb whereas the model was unable to mimic such a drastic streamflow decline, this is true for both the outlet as well as the Wet Beaver Creek gauge station. Due to this overestimation of the recession limb of the hydrograph, the cumulative streamflow volume for the summer simulation period is overestimated for the outlet as seen in Figure19.

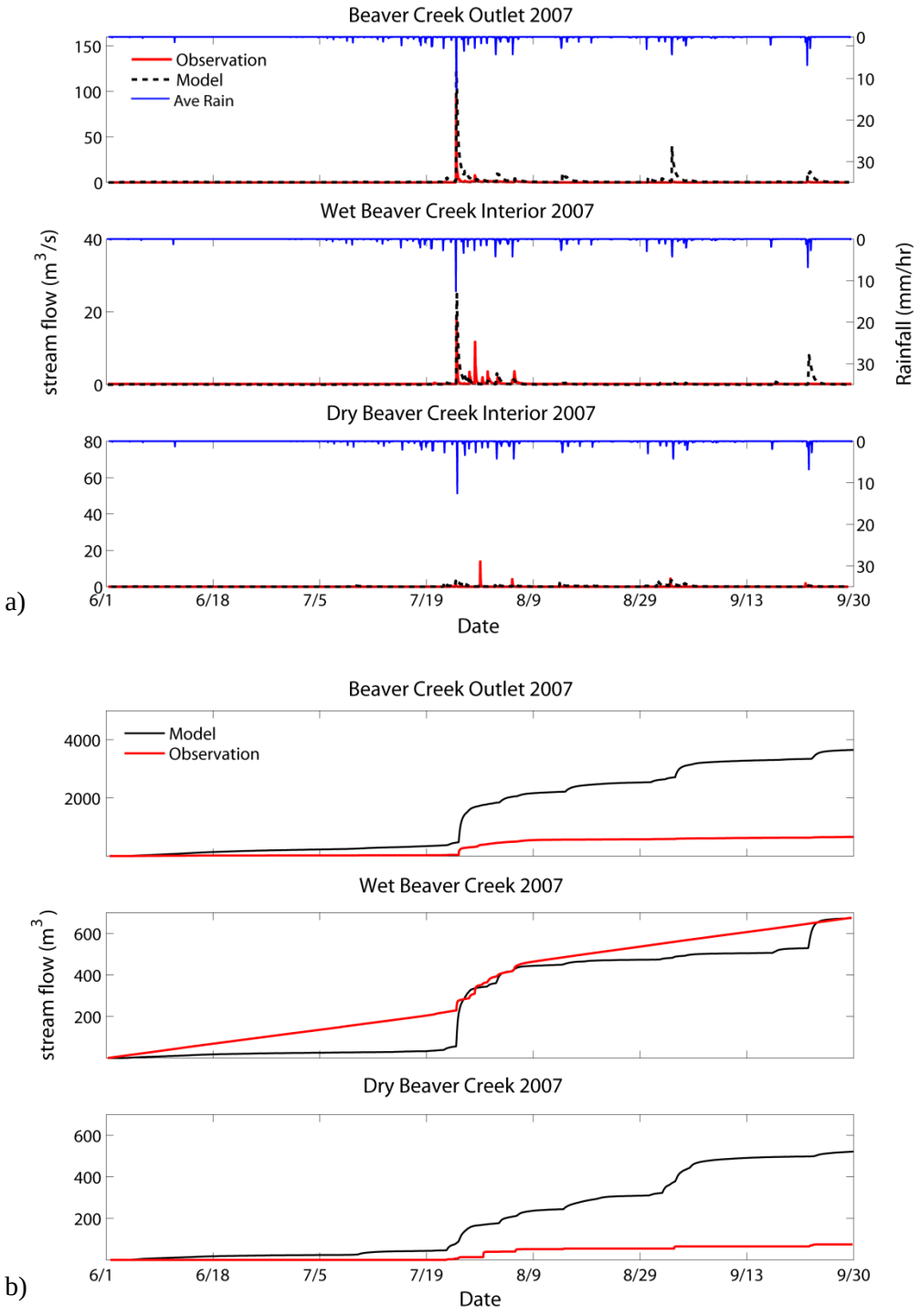

Figure 19: 2007 calibration hydrographs for modeled vs. observed a) the entire summer and b) cumulative stream volume.

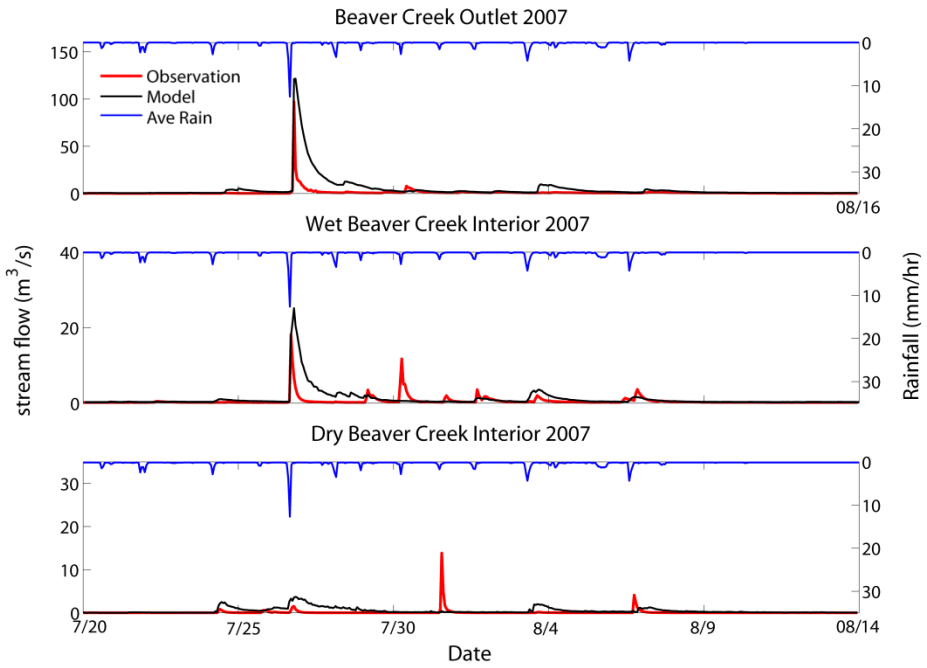

Figure 20: 2007 calibration summer streamflow for time period with the majority of events of interest.

The third event of the simulation took place on July 30th, which occurred in the Wet Beaver Creek drainage and was of a medium magnitude and had a peak flow rate of 11 m^3/s. This event was not detectable in the model results. As discussed in a previous section, several precipitation forcing products were evaluated, resulting in the utilization of NEXRAD for calibration purposes. It should be noted that for the event on July 30th, none of the precipitation products had rainfall totals that could produce the magnitude of the observed streamflow. This particular event, therefore, is considered an anomaly in the data. Estimation for the smaller events in the later part of this period showed greater improvement. Events on June 1st, 3rd, and 6th were simulated fairly well in Wet Beaver Creek based on hydrograph timing, and to a lesser degree the streamflow volume.

During the calibration efforts, parameters were scaled up or down to review the effects on the streamflow hydrographs. It is important to note that these parameters were used for all summers evaluated; when a parameter was changed to affect the streamflow during the 2007 summer, the 2006 summer was also impacted. The point made here is that the goodness of fit for the summer of 2007's streamflow could have a better 'goodness' if not considering two additional summers. For example scaling parameters to more accurately match the event in Dry Beaver Creek for the summer of 2006 would increase the streamflow in 2007, which would not represent the 2007 summer well.

Although the soil classes for each sub-basin are identical the original soil classification was aggregated to make the model manageable. For this reason major soil classes, like clay and bedrock, could be separated by basin to differ slightly in their parameterization; for example the hydraulic conductivity of the Wet Beaver clay soil type was determined to be slightly more permeable then the clay contained in the Dry Beaver Creek. An example of this is the event on July 27th; it is mostly affected by clay soil and increases in its permeability would decrease the modeled hydrograph. However, in doing this the clay is also the driving soil type for the events on June 1st, 3rd, and 6th and raising the permeability would negate any model-observed goodness of fit. There is also consideration of parameters that are realistic. By increasing the conductivity to bring the largest event closer to that of the observed, the parameters start to approach the limits of realistic values.

Dry Beaver Creek discharge for the summer of 2007 was very low; however validation summers have several peaks that are characteristic of this ephemeral creek. As seen from Figure 21, the cumulative streamflow for summer 2007, Dry Beaver Creek is

over estimated. Any further permeability degradation that would capture this summer's extremely low volume would compromise validation summer to suffer greatly in their goodness of fit. As can be seen Figures 21 and 22, 2005 and 2006 cumulative streamflow correspond is fairly satisfactory.

As seen in Figures 19, 21, and 22; model results for all years, in the form of cumulative streamflow amounts, at the outlet overestimate when compared to observations. The possible reasons for the models inability to capture such high stream flows are accounted for in two explanations. In the basin there is urban area, as seen from Figure 4, upstream of the outlet and downstream of Wet and Dry Beaver Creek stream gauge station. This urbanized portion of the basin, Rimrock and Lake Montezuma, utilizes well water for domestic demand. tRIBS does not account for groundwater extractions, and as such may have an effect on streamflows. An additional reason for higher modeled streamflow could be explained with channel losses, which tRIBS does not account for. Channel losses or, transmission losses, is when water infiltrates into steam banks and beds as water flows downstream. This is not seen in either Wet or Dry Beaver Creek, as upstream of the gauge station sites the channels are bedrock lined, stream losses would be low in this situation. However, downstream of these gauge stations and upstream of the outlet, the soil is classified as loam, a soil type that is quite permeable and would incur channel losses.

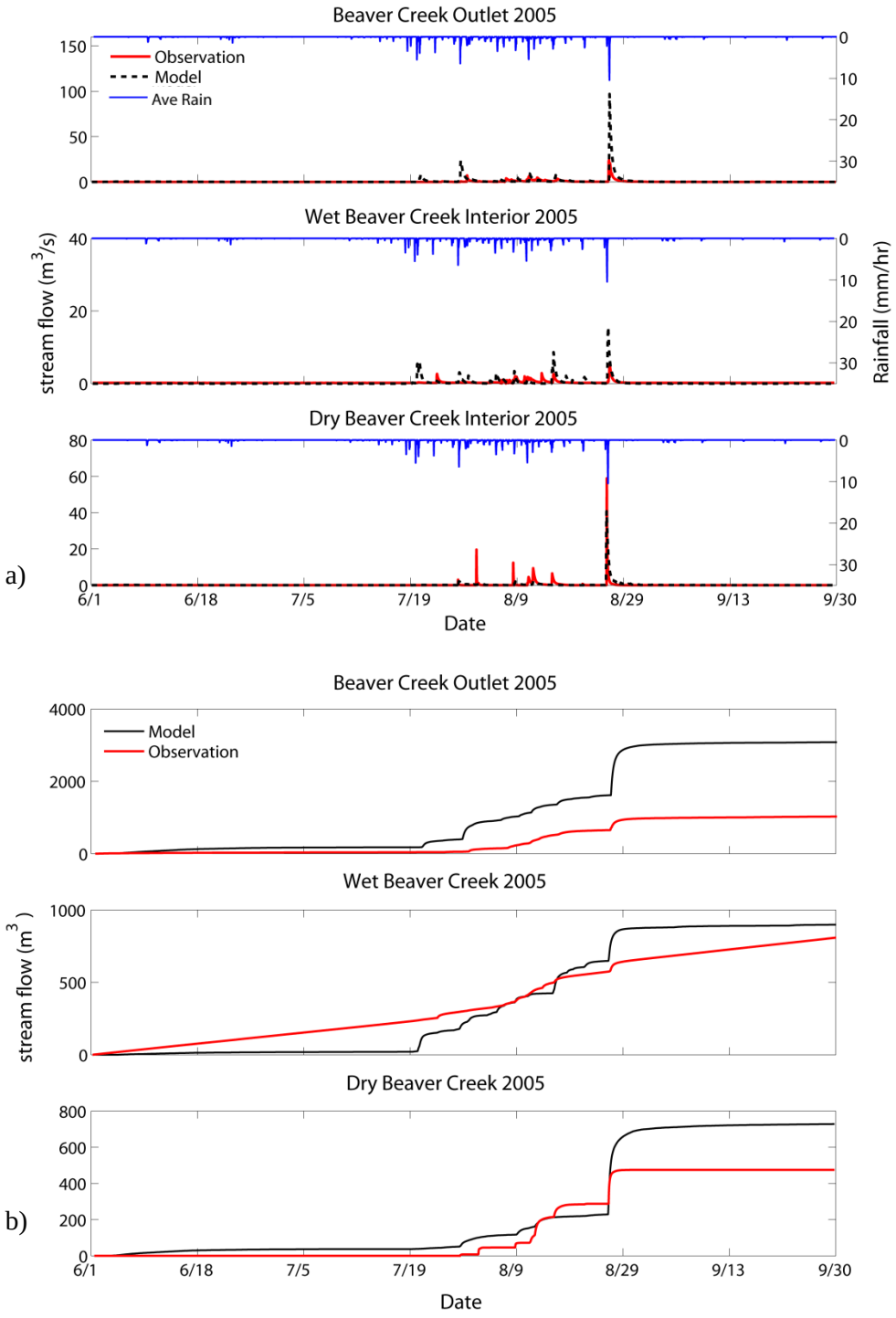

Figure 21: Modeled and observed streamflow for the 2005 summer simulation for a) hourly time series and b) cumulative time series

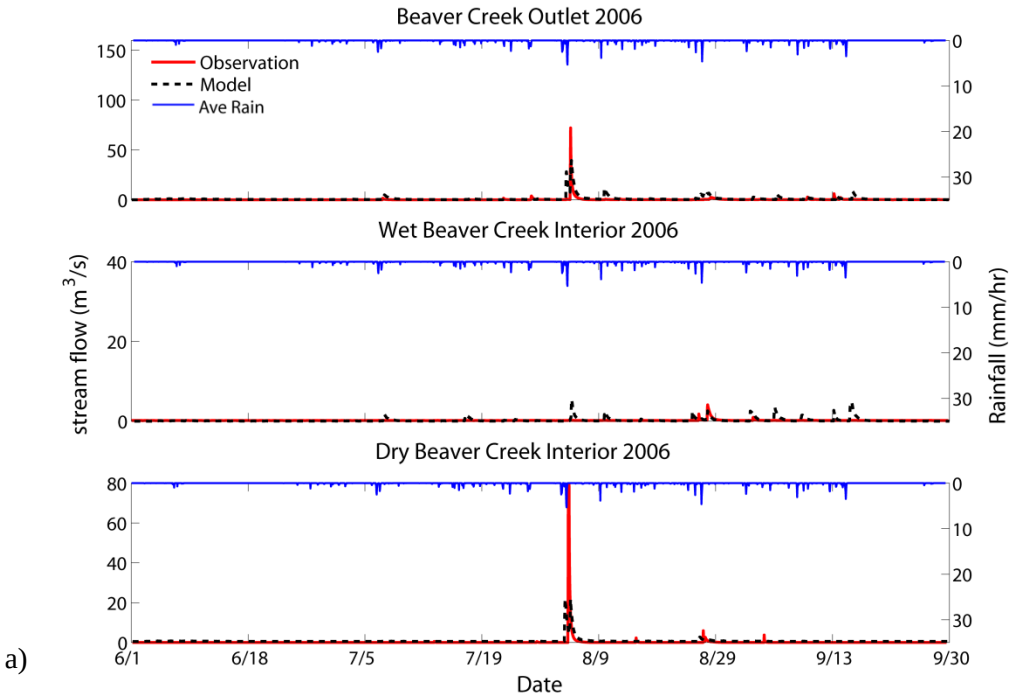

a)

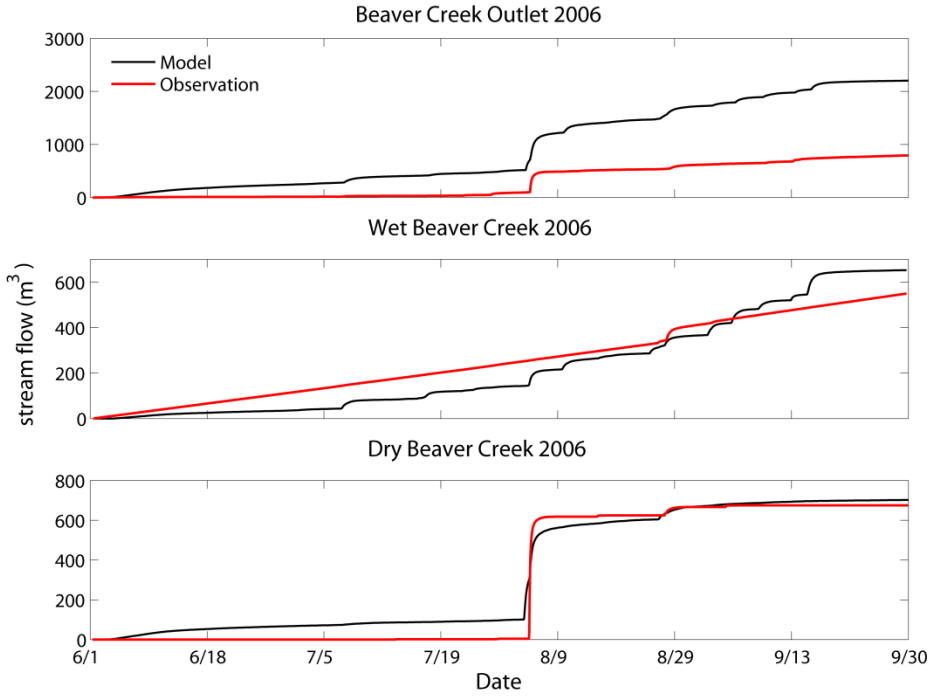

b)

Figure 22: Modeled and observed streamflow for the 2006 summer simulation for a) hourly time series and b) cumulative time series

To evaluate the predictive power of the hydrologic model over the course of the summers, three different metrics are utilized; the Nash-Sutcliff model efficiency coefficient (NSE), Root Mean Square Error (RMSE), and a bias factor. NSE is commonly used to determine the efficiency of a model to predict discharge when compared to observed streamflow:

$$NSE = 1 - \frac{\Sigma(Q_{obs,i} - Q_{model,i})^2}{\Sigma(Q_{obs,i} - ave(Q_{obs}))^2} \qquad \text{Equation 35}$$

In this equation, n is the total of discrete values, Q_{obs} is the observed streamflow, and Q_{model} is the modeled streamflow at time i. NSE ranges from -∞ to 1; a value of 1 expresses a perfect match to observed, while a value of 0 signifies that the model is as accurate as the mean of the observed data, and anything below 0 indicates that the observed mean is a better predictor than the model. RMSE is also another commonly used metric defined as the difference between observed and modeled values. The difference between these values at each time step are called residuals, whereas the RMSE functions to culminate them into a single measure of predictability and is defined in the following equation, all values denoted are the same as described above.

$$RMSE = SQRT\frac{\Sigma(Q_{obs,i} - Q_{model,i})^2}{n} \qquad \text{Equation 36}$$

Finally the percent bias, Bias, was calculated to measure the average tendency of the simulated data to be larger or smaller than their observed counterparts (Gupta & Sorooshian, 1999). A value of 0 indicates that the observed and the predicted values

align, whereas positive values indicate model underestimation and negative values indicate overestimation. Bias is calculated as:

$$Bias = SQRT\frac{\Sigma(Q_{obs,i} - Q_{model,i} * 100)}{\Sigma Q_{obs,i}} \qquad \text{Equation 37}$$

Table 10 outlines the statistical data for the calibration year and Table 11 for the validation summers, 2005 and 2006. Based on the NSE, the outlet streamflow for all summers examined are above predictability of the mean of the observed flow. Whereas Wet Beaver Creek is less than 0 for all summers examined, and from this statistic modeled results shows a less than desirable outcome. An important feature here to note is that the Wet Beaver Creek is a perennial stream and base flow during a summer season fed by upland aquifers are difficult to model. Dry Beaver Creek, like the outlet, shows greater predictability than the average of the observed streamflow. RMSE is in units of discharge and measures the distance, on average, of a data point from the fitted line. The stream discharge must be taken into account in evaluating RMSE, the outlet has the largest discharge rate and thus it is appropriate for it to have a large RMSE. The Bias is negative for all stream values in the calibration summer; thus, the model is over estimating streamflow on average. For 2005 and 2006, the Bias values are positive, which indicates underestimation.

Table 10: Statistical summary for the 2007 calibration simulation

	2007 Calibration		
	NSE (-)	RMSE (m^3/s)	Bias (-)
Outlet	0.35	4.4	-4.1
Wet BC	-1.68	2.8	-1.1
Dry BC	0.01	1.5	-2.5

Table 11: Statistical summary for validation simulations summers 2006 and 2005

	2006 Validation			2005		
	NSE (-)	RMSE (m^3/s)	Bias (-)	NSE (-)	RMSE (m^3/s)	Bias (-)
Outlet	0.42	2.7	5.4	0.38	4.5	6.7
Wet BC	-6.5	0.9	9.4	-2.34	1.32	9.8
Dry BC	0.49	3.4	6.5	0.42	1.86	4.2

Based on the evaluation of the statistical qualifications as outlined in (Moriasi, Arnold, VanLiew, Binger, & Harmel, 2007), the model for calibration and validation summer performs adequately. Higher levels of performance, although desirable, were not obtained.

A point of uncertainty that needs to be considered in calibration efforts is accounting for the precipitation errors; how does the precipitation products interpret data and, in turn effects what happens in the model. The NEXRAD forcing utilized here, like the gauge and NLDAS data, is an hourly rate. An example of what this means, is that a storm that has an intensity of 30 mm/hr for 10 minutes, equates to an hourly forcing to the model of 5mm/hr. Work done by (Assouline, et al. 2007) revealed that temporal averaging of precipitation at the hourly scale caused an underestimation of time to

ponding. Monsoonal precipitation events are characterized by high intensity. Events that occur on the sub-hourly scale would be muted in the NEXRAD forcing for a short burst high intensity event and this would affect the model hydrographs. Forcing averaging over the hour when an event occurs at a higher intensity, for a shorter period of time could explain the failure of the model to capture such a dramatic recession limb for many of the hydrographs.

With the calibrated parameter set at a level that is determined to be adequate, an evaluation was made to continue the look at how the model is affected by the three differing precipitation forcing produces. As shown in Figure 23, all three summers are forced with each of the previous discussed precipitation products to examine the hydrologic response.

The forcing products have varying degrees of agreement with the observed cumulative streamflow. In almost all the cases, with the exception of Dry Beaver Creek during 2005, the rain gauge greatly overstates the basin response to precipitation. For all three summers the NEXRAD is able to capture the cumulative volume for Wet Beaver Creek. This statement is also appropriate for NLDAS; however, this product delivers precipitation amounts over longer time periods when compared to the other products, and therefore could not capture the peaks in the stream hydrographs. This statement is critical, as it tells us that not only is the volume delivered important but the time frame it which it is delivered is just as significant. Both NEXRAD and NLDAS do a comparable job in interpreting volumes rates. Of all the products NEXRAD was able capture the spatial variability without over exaggeration of precipitation events.

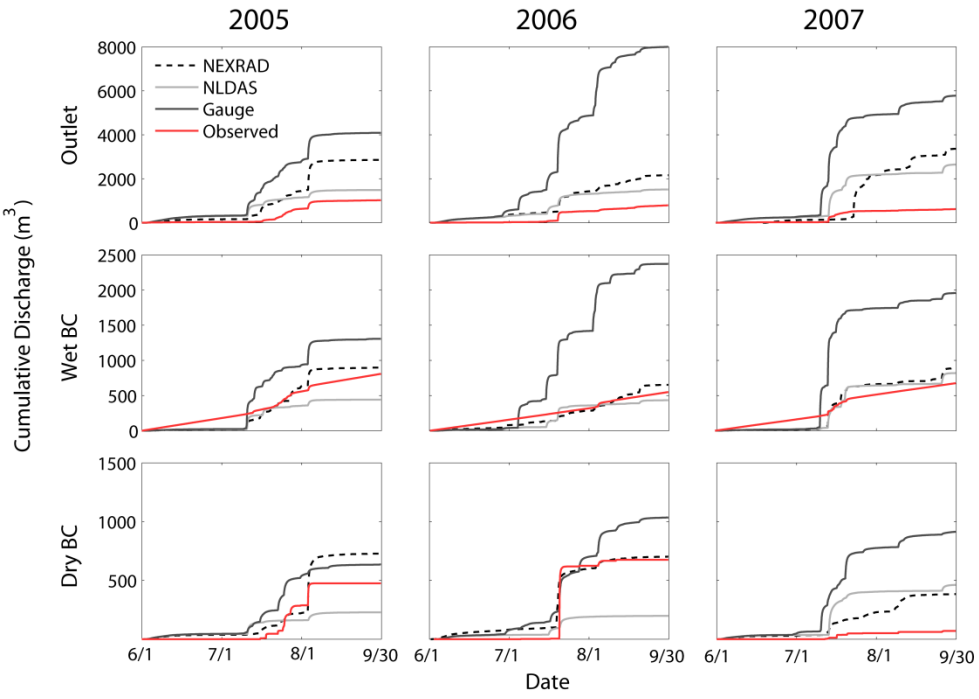

Figure 23: Cumulative streamflow for 2005, 2006, and 2007 using all three precipitation forcing products

When examining the largest event that occurred in 2007 for each precipitation product, it is clear how each product affects the modeled basin response. This event occurred on July 28th, and as seen from Figure 24, the spatial variability differs greatly across each forcing type. The Gauge stations capture the main source of rain in three Thiessen polygons. The NEXRAD displays the main source of the events as how rainfall amounts dissipate from that point. The NLDAS is can almost be considered homogenous across the basin for the precipitation totals for this specific event. The hydrographs in this same figure shows that gauge forcing greatly over estimates the runoff response and NLDAS creates less intense and elongated hydrographs.

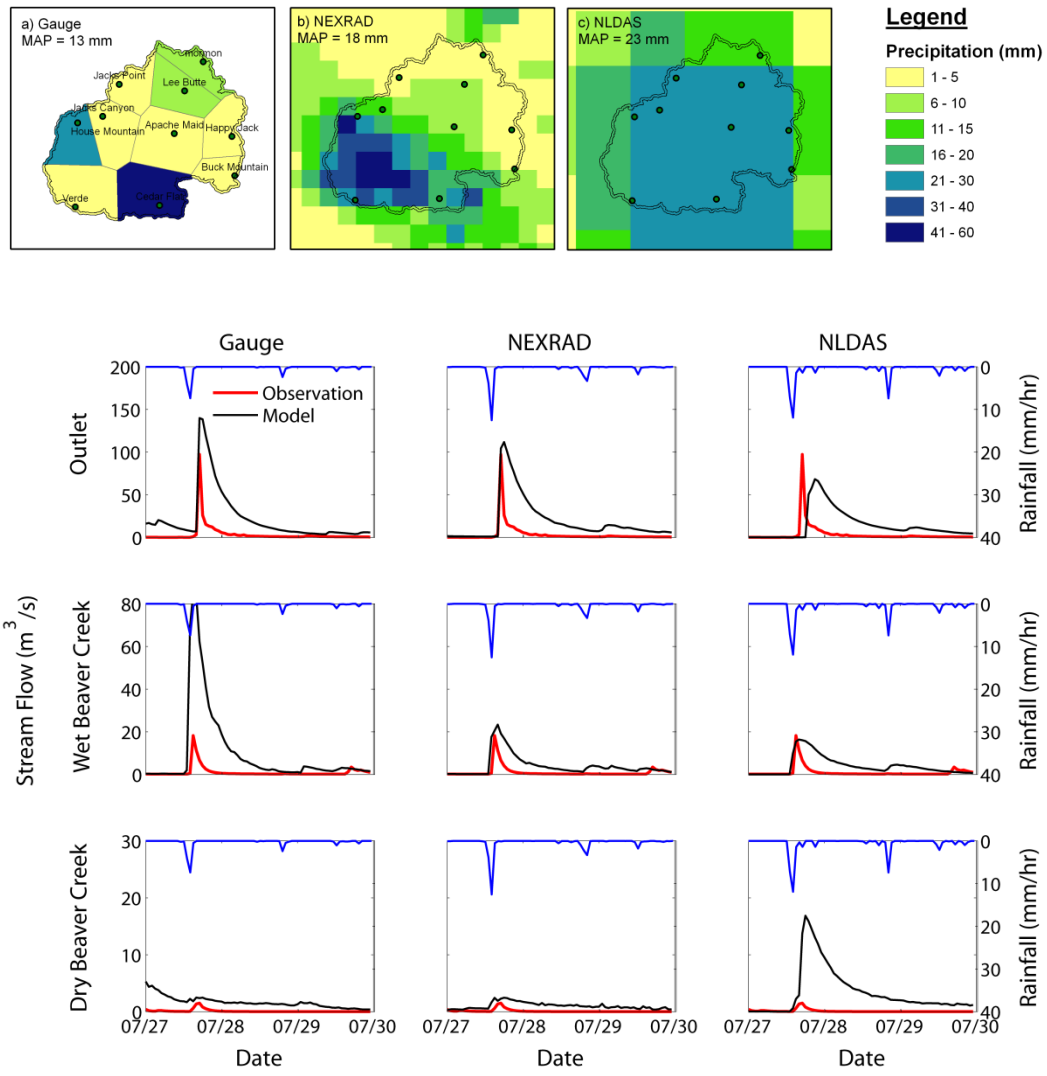

Figure 24: Modeled vs. Observed streamflow utilizing all precipitation forcing products for the event on 7/28/2007.

Calibration of a basin this size and complexity with several gauge station sites is challenging and should account for the fact that the period of chosen examination, the summer monsoonal period, adds layers of complexities as precipitation is highly variable and is characterized as occurring in short intense bursts. This characterization is difficult to capture with precipitation forcing products that are available. A model of this size that

contain 76,624 nodes, lack in some physical data to constrain parameters sets and is challenges to match streamflow for three separate.

3.2 HISTORICAL AND FUTURE CLIMATE SCENARIO

After adequate calibration and validation was performed and the model was deemed sufficient for the purposes of this study, climate change scenarios were applied to the model and evaluated based on a number of variables. This section focuses on evaluation of climate change scenarios when applied to the Beaver Creek model. The simulated response were evaluated on a comparison to climate change scenarios for two time periods; the historical representation that runs from 1990-2000 and the future period from 2031-2040.

To manage a resource system for current populations as well as projected growth, it is common practice to look at historical patterns and experiences to gauge how to plan for water resource needs and its accompanying infrastructure (Army Corps of Engineers, 1992). This practice may no longer be the best viable option if, due to climate change conditions, precipitation patterns do not following historical precedence and therefore expectations are difficult to gauge. Understanding the effects of climate change on a hydrologic system is critical to understanding the future of water resource availability and its potential effects on extreme event occurrences and intensities, among these are the convective events of summer monsoonal rain.

This study utilizes GCMs that have been downscaled regionally to provide a series of climate scenarios for this region of interest. GCMs provide atmospheric circulation on a global scale comprised of atmospheric, land-surface, cryosphere, and biosphere with coupling between components. While GCMs are a good indicator of

global climatic trends, they do not always realistically represent precipitation on a local scale due to their coarse spatial resolution and physical parameters (Dominguez, et al. 2012; Lee, et al. 2007; Paeth, et al. 2007). This statement is especially true in areas of complex terrain. Error in the capacity of GCMs to model regional weather in the southwestern U.S. may be due to inadequate representation of topography (Brazel, et al. 1993). To better capture these atmospheric processes at a finer scale, GCMs are dynamically downscaled by Regional Climate Models (RCM) using their lateral boundaries in order to achieve detailed regional and local atmospheric data (Castro, et al. 2005). RCMs are commonly able to capture mean and extreme precipitation events at the regional scale (Diffenbaugh, et al. 2005).

RMCs are generally a better tool for a study such as this, over GCMs, as they have this higher spatially variable resolution as well as computational expedience. The simulations in this study have been dynamically downscaled to a 10 km resolution using the Weather Research Forecasting (WRF) RCM. The WRF model was driven by the GCM developed by the UK Hadley Center for Climate Prediction and Research and commonly referred to as HadCM3. The model was run under IPCC emissions scenario A2. The IPCC developed 20 different scenarios based on future greenhouse gas pollution as a driving force to atmospheric conditions. Each scenario makes assumptions about the future economic development and global markets and their effects on the environment. The scenarios are classified into 4 groupings; A (economic focus), B (environmental focus), 1 (globalization), and 2 (regionalization). For the purposes of this study, the A2 scenario was chosen as this appears to better follow the actual conditions since the projections were issued. This scenario is characterized by increasing population and

regionally oriented economic development, as well as high forcing of greenhouse gas concentrations.

There have been several GCMs developed; however, not all of them show favorable performance with respect to precipitation patterns in the southwestern U.S. Of those available, the HadCM3 has been reported as having a good capability in capturing the effects of El Nino Southern Oscillation (ENSO) (Sungwook, et al., 2012). Dominguez et al. (2009) showed that HadCM3 captured precipitation, temperature, atmospheric circulation, and ENSO interannual variability realistically in the southwestern U.S.

This study utilizes two decadal periods to evaluate the effects of increased greenhouse gas emissions on the climatic system. The historical period is represented by the decade 1990-2000 and the future scenarios are 2031-2040, each generated by the same RCM model whose difference is in the GCM boundary conditions that show higher greenhouse gases in the future. These high resolution scenarios are then used in the hydrologic model in a consistent way. The RCM was developed to cover most of the state of Arizona in the U.S. and portions of northern Mexico. Figure 25 illustrates the 10 km grid cells that cover Beaver Creek.

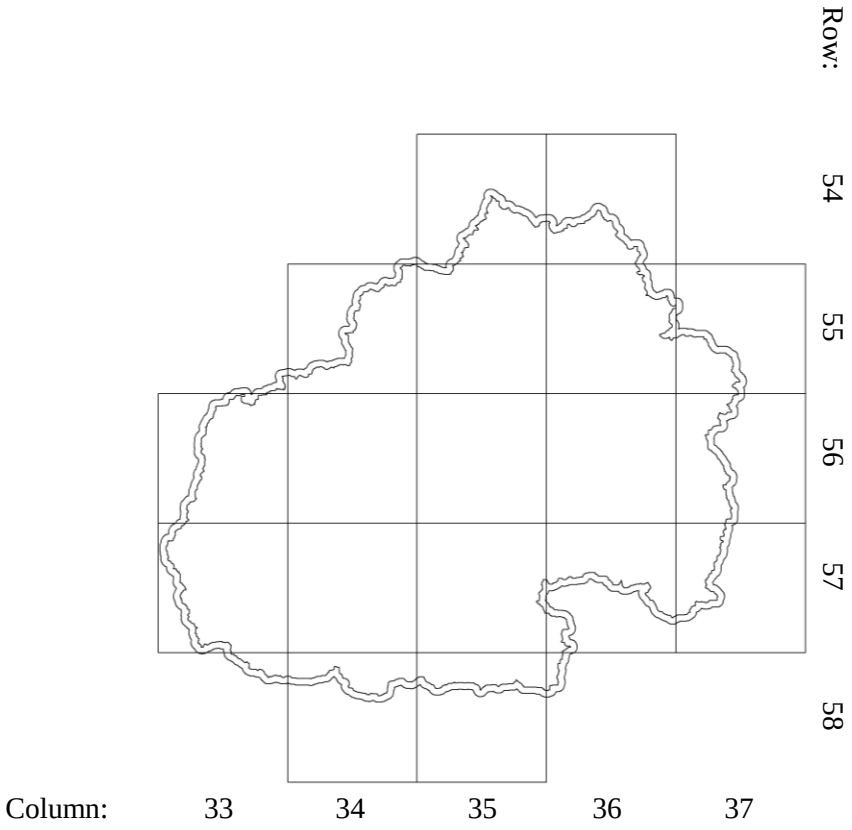

Figure 25: WRF pixel coverage over the Beaver Creek

Summer air temperatures were discerned for each period to evaluate changes in the decadal average. Figure 26 displays the average of summer, increasing steadily over the course of the summer and declining as the season approaches conclusion ends. Average summer temperature for the Beaver Creek watershed increases 1.2ºC over the course of the two time periods. Temperature patterns are slightly different when comparing the historical period to the future. The historical period has temperature that increases up to August, peaks, and declines.

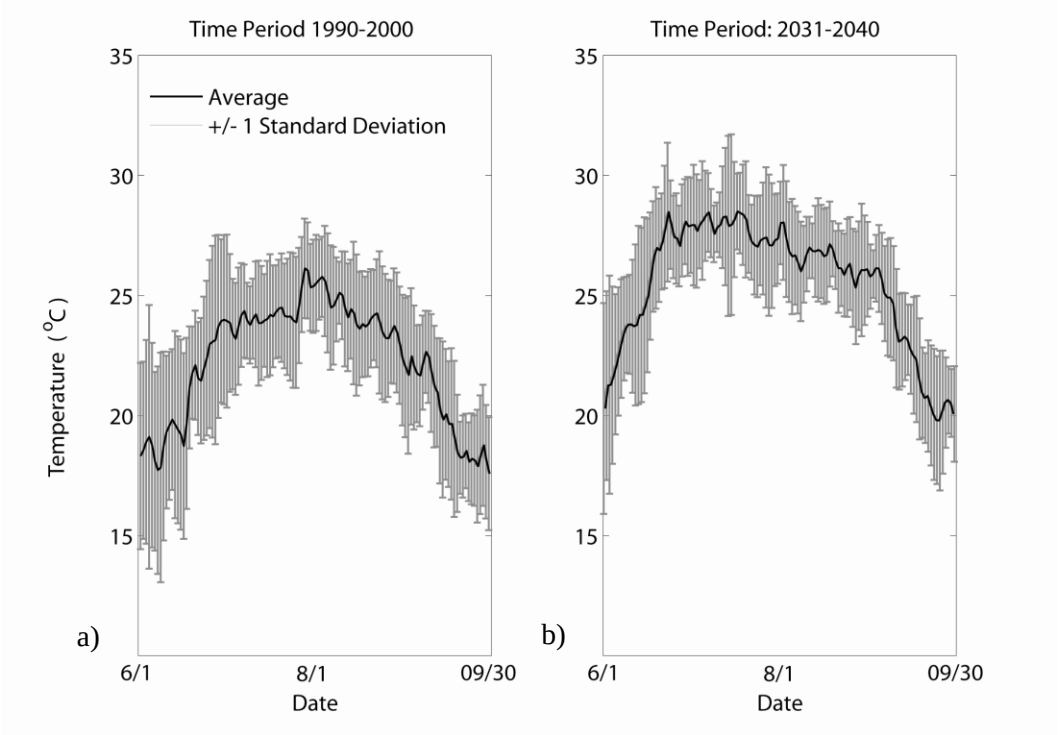

Figure 26: Average decadal summer temperatures for the WRF model's a) historical period and b) future period.

The future period increases during the initial month of summer, temperature increases at a higher rate, peaks earlier in the summer. The pattern for the future scenarios are not as bell shaped as the historical pattern, and display a slight plateau until the end of August.

Although there is much concern over temperature increases for future climate change, there is potential for higher variability and change in precipitation patterns. Precipitation was basin averaged and then averaged again over the two decadal periods, much like temperature. What is seen is a drastic increase in summer monsoonal precipitation totals and variability. Precipitation totals are almost two and a half times greater in the future average when compared to the historical.

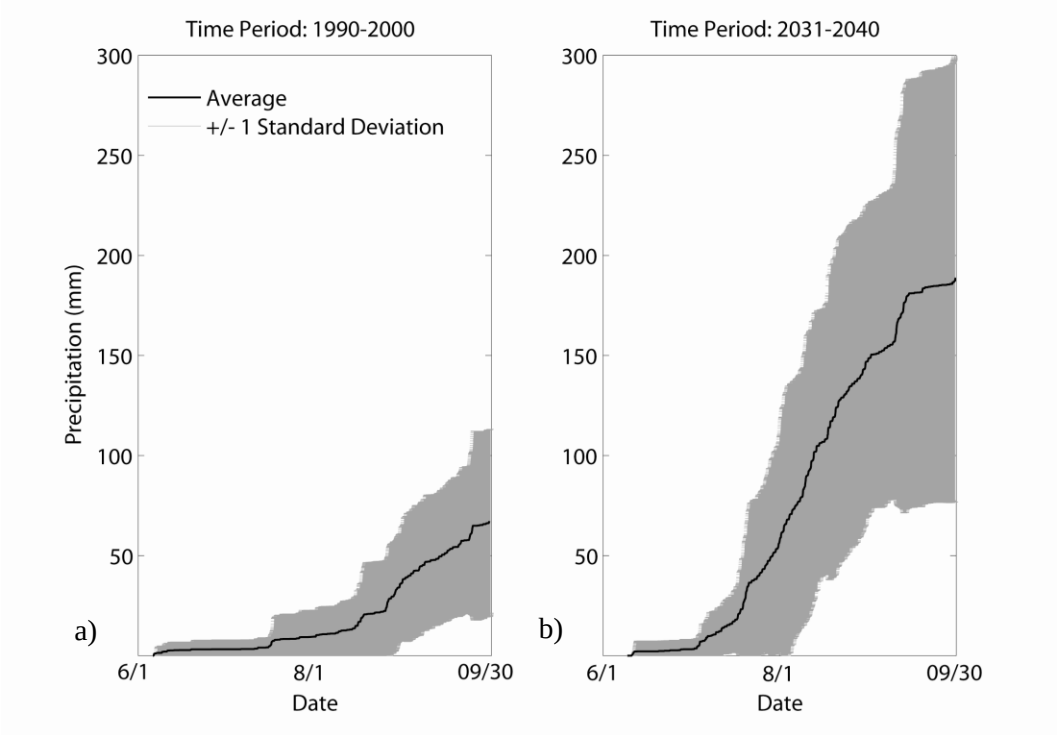

Figure 27: Average decadal cumulative summer precipitation for the climate change simulations for a) historical period and b) future period.

As can be seen from the Figure 27, the variability is also greater in future which match up well to what many GCMs predict as discussed previously.

The cumulative precipitation averages for the two periods are mirrored in the runoff response from the basin. The cumulative streamflow at the outlet of the basin averaged over both decades can be seen in Figure 28. As with the precipitation, the streamflow in the future scenario is much greater than that of the historical. When comparing average across the decades, increases are seen in the future summer streamflow by as much as a factor of three. Variability is also consistent with precipitation patterns as well. Increases in cumulative volume happen earlier in the summer for the future scenarios when compared to historical.

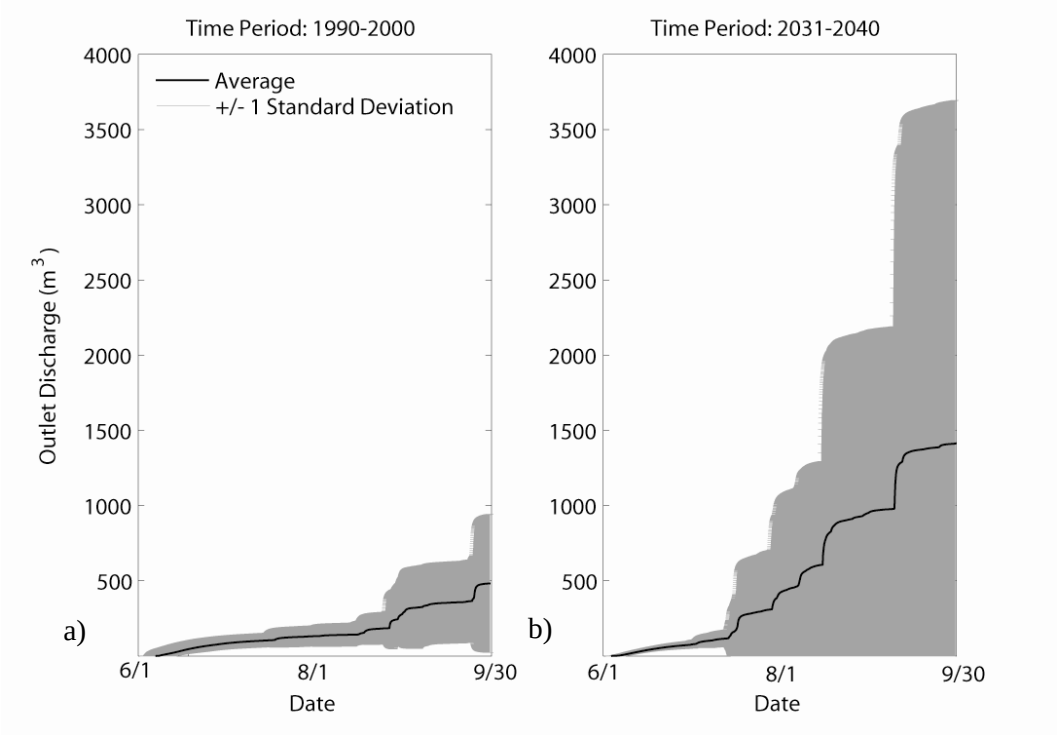

Figure 28: Average decadal cumulative summer runoff discharge for climate change simulations for a) historical period and b) future period.

Large increases in the cumulative average give evidence to a characterization of large streamflow response to certain events. Event intensity results in a quicker basin response. This could account for the how dramatic the runoff is in comparison to the historical period. When comparing precipitation the increase is roughly two and a half; however, streamflow runoff is three times the increase. During summers of heavier rain, precipitation events cause a greater amount of runoff then experienced in the historical period.

In previous studies, air temperature increases are suggested to lead to changes in evapotranspiration. ET has been evaluated, during summer time conditions, to the consequences of climate change as seen in Figure 29. ET is presented as the cumulative hourly amount throughout the summer, as well as daily averages throughout the summer.

As can be seen from both representations of ET, there is not a large distinction when comparing the averages from the historical decade to the future decade. Figure 29a was made with hourly output from the model and variability is represented with the standard deviation, whereas in Figure 29b, the amounts are totaled for the day and variability is calculated from for daily variability.

The cumulative totals for summer volumes are very similar between each time period. The average between decades is not largely affected in the summer time due to climate change. However, evapotranspiration is more variable in the future at the hourly scale, although it does not differ substantially when comparing daily ET. In both periods, ET starts out high, as summer time temperature rise steadily and available soil moisture is being consumed. As shown in Figure 27, as the monsoon period begins and precipitation occurs, ET steadily declines. This trend is, in part, is due to cloud cover occurrence during the precipitation events. With the onset of monsoonal storms the system experiences more cloudiness, this cuts down on incoming solar radiation amounts. Incoming solar radiation amount have a dramatic effect of ET levels (Brown, 2000).

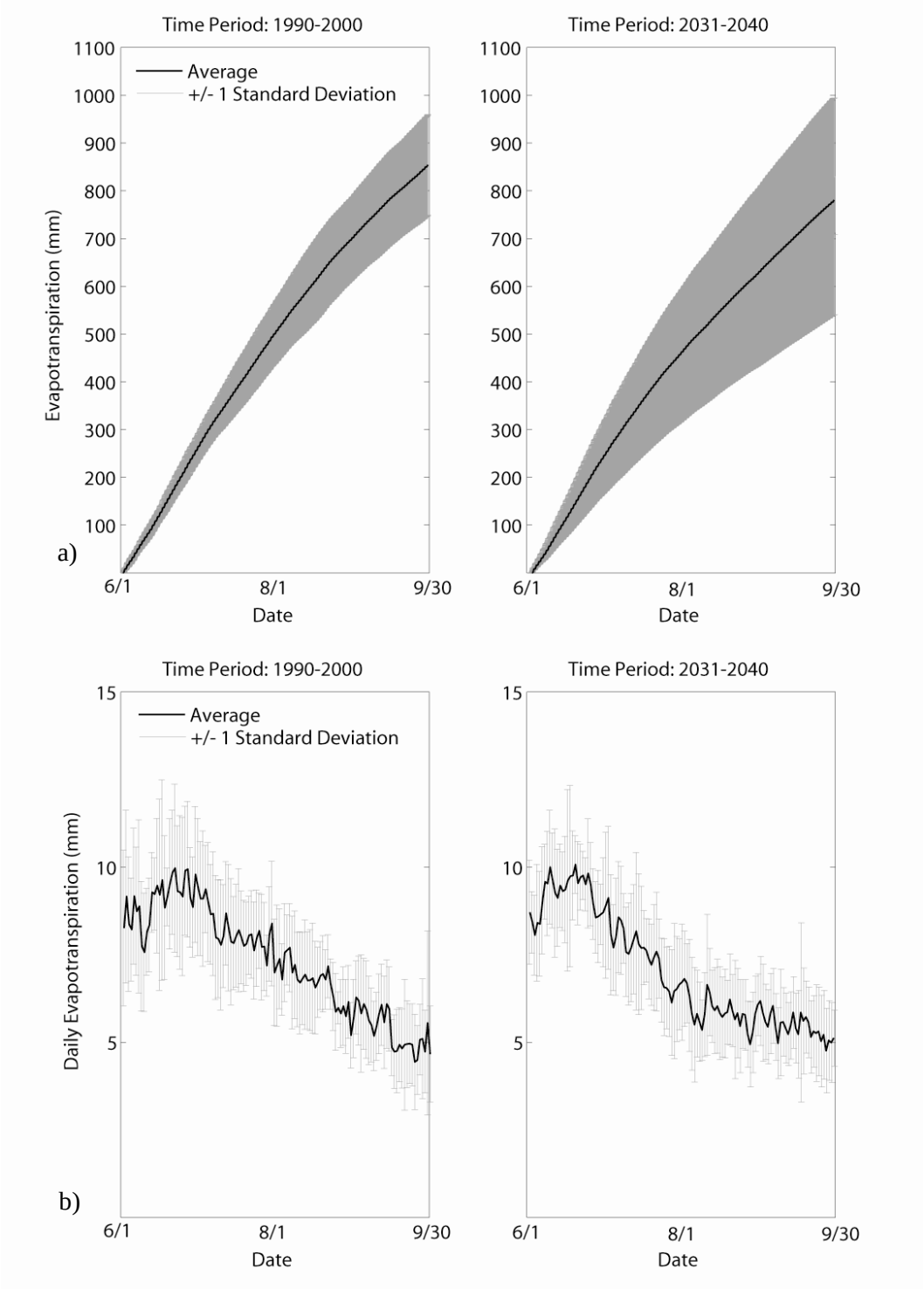

Figure 29: Historical and future a) average cumulative *hourly* ET and b) average *daily* ET.

Table 12 represents the water balance for the two comparative climate change time periods. In this table, the average totals and standard deviation from these totals are presented. This table includes changes in stored soil moisture as well as runoff coefficient. Precipitation is, on average, higher in the future than in the historical period. The summer with the greatest precipitation totals is 405 mm in the future compared to 151 mm in the historical period. The lowest precipitation totals are 51 mm for the future period and 24 mm for the historical period. The future period, on average, has 111 mm more precipitation than the historical period. ET in this table can be seen as not vary much between the two periods, both time periods have an average summer time ET approximately at 850 mm. Soil moisture, taken from stored moisture and the groundwater component of the model, adds to the effects of ET during the summer period. The runoff coefficient is an indicator of the basin response to summer precipitation and in that way is related to ET and its hydrological response to climate. The runoff coefficient is the ratio of runoff to rain:

$$r = \frac{runoff\ (mm)}{rain\ (mm)} \qquad \text{Equation 38}$$

In both periods, *r* is low, and on average around 2%. Rain in apportioned into runoff, ET, and storage (soil moisture), the low runoff ratio is related to a high amount of rainfall being consumed by ET.

Table 12: Water Balance for all years in the historical and future periods

WRF Historical Period						WRF Future Period					
	P (mm)	ET (mm)	Q (mm)	ΔS (mm)	r (-)		P (mm)	ET (mm)	Q (mm)	ΔS (mm)	r (-)
1990	106	649	1.17	-544	0.01						
1991	85	848	1.57	-764	0.02	2031	51	917	0.39	-867	0.01
1992	74	857	2.71	-786	0.04	2032	187	753	1.50	-567	0.01
1993	92	936	2.94	-847	0.03	2033	257	782	3.22	-528	0.01
1994	106	649	1.17	-544	0.01	2034	76	851	0.55	-776	0.01
1995	24	923	0.42	-900	0.02	2035	176	856	2.37	-683	0.01
1996	32	929	0.39	-897	0.01	2036	169	863	1.84	-696	0.01
1997	51	917	0.39	-867	0.01	2037	405	831	25.89	-452	0.06
1998	85	900	0.88	-816	0.01	2038	204	872	4.62	-672	0.02
1999	151	894	5.18	-748	0.03	2039	61	947	0.76	-887	0.01
2000	49	897	0.44	-848	0.01	2040	302	810	7.95	-515	0.03
AVE	**78**	**854**	**1.6**	**-778.3**	**0.02**	**AVE**	**189**	**848**	**4.9**	**-664.3**	**0.02**
STD	**37**	**105**	**1.5**	**126.0**	**0.01**	**STD**	**112**	**58**	**7.7**	**149.0**	**0.02**

To dissect the basin responses between the two periods, two sets of summers that have similar precipitation totals are evaluated to produce time series output of the variables discussed above. The 1992 and 2043 summers have comparable precipitation totals of 74 mm and 76 mm respectively. These summers were chosen due to their closeness in totals and because for the historical period, this is a close representative to mid-range total, for the historical period mid-range is at 64mm. Summers 1999 and 2036 have comparable totals of 151 mm and 169 mm. This sets of comparison summers were chosen, again, due to their closeness in totals and because for the historical period 1999 had the highest precipitation total.

In both sets of comparative summers, air temperature is consistently higher in the future when compared to the historical. ET does not display the same trend. For example, during the earlier part of June and the latter half of August, in the 1992 verses 2034 comparison, the temperature is clearly higher in the future. However, ET daily totals are very similar in both summers. For the summer season, increases in temperature do not necessarily mean higher ET rates. In Figure 30a, during the latter half of August, around the 29th, there is a large precipitation event in the historical summer. This event corresponds to lower temperatures, when compared to the same time from in the future summer. ET during this time frame of the summer is relatively similar between the two comparison summers.

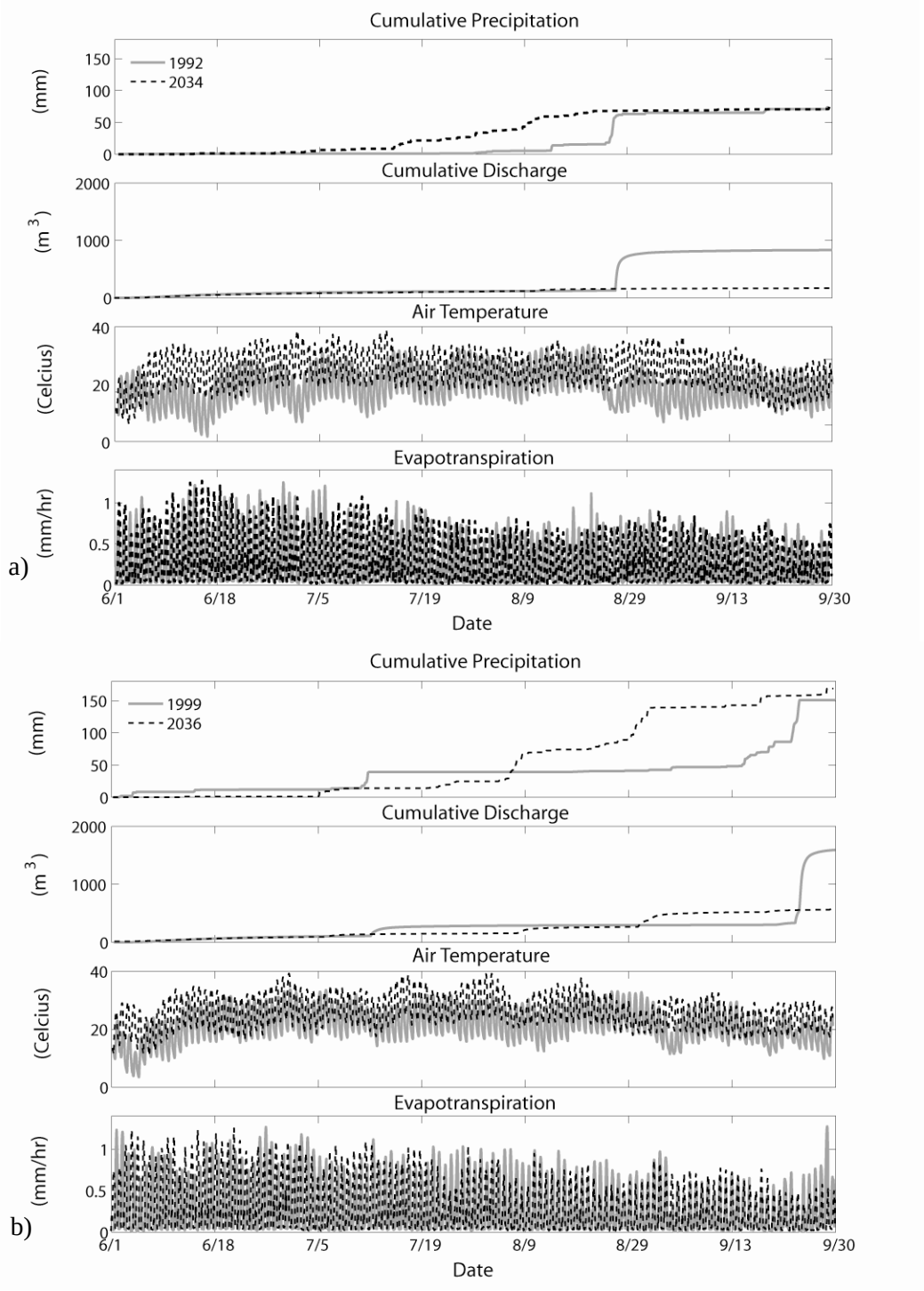

Figure 30: Comparison between similar cumulative precipitation totals for historical and future summers a) 1992 and 2034 and b) 1999 and 2036. Time series includes basin average cumulative precipitation, cumulative outlet discharge, basin average air temperature, and basin average ET.

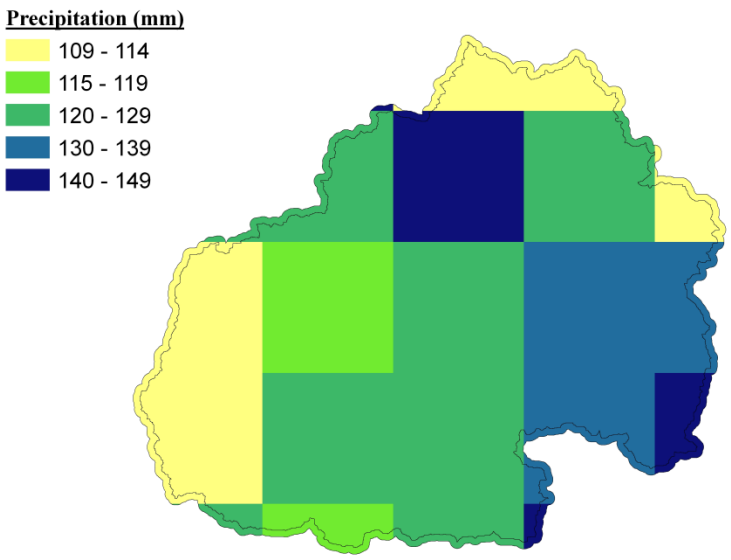

Figure 31: Spatial precipitation difference between the future period and the historical period.

When comparing the historical period with the future period, precipitation, on average, is calculated to increase. This increases is; however, not going to be spatially homogenous, amounts will depend on the location within the basin. Figure 31 is the representation of the precipitation spatial differences between the two time periods. In this figure the largest precipitation increases occurs in the northeastern section of the basin along the Mogollon Rim, with areas of least increase along the flatter low lands near the outlet and the upland areas along the plateau portion of the rim. The Mogollon Rim is the southwestern edge of the Colorado Plateau. This spatial pattern is telling of the RCM's ability to model orographic uplift that is characteristic of monsoon precipitation. This spatial pattern also affects hydrologic elements of the basin.

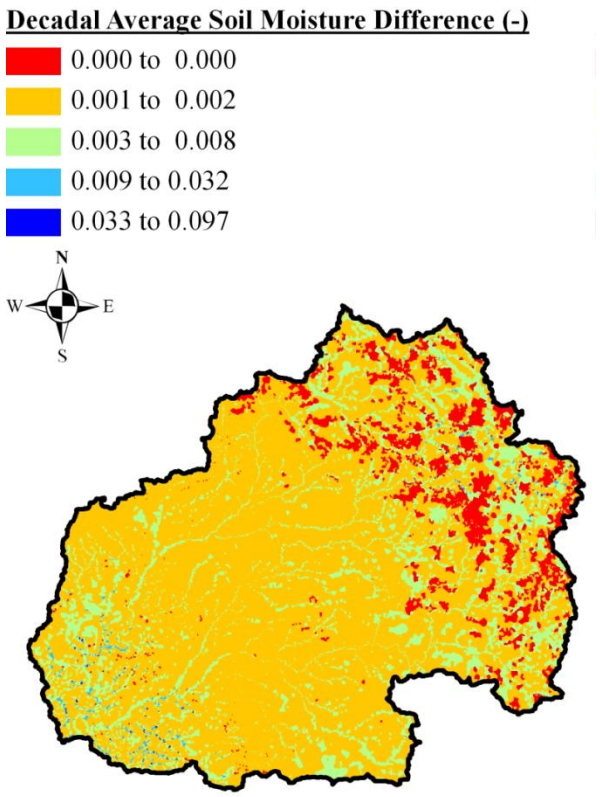

Figure 32: Spatial soil moisture difference between the future period and the historical period.

In Figure 32, the spatial difference of average soil moisture between the two periods of interests is illustrated. Soil moisture, on average, increase only is small amounts. However, from the map the pattern increases from upstream to downstream. In areas along the plateau portion of the Rim there is almost no increase. The slight increase in the direction moving down stream to the outlet display that lateral conductivity plays a role, up gradient to down gradient, in soil moisture patterns and upland areas isolated from upland influence are unchanged.

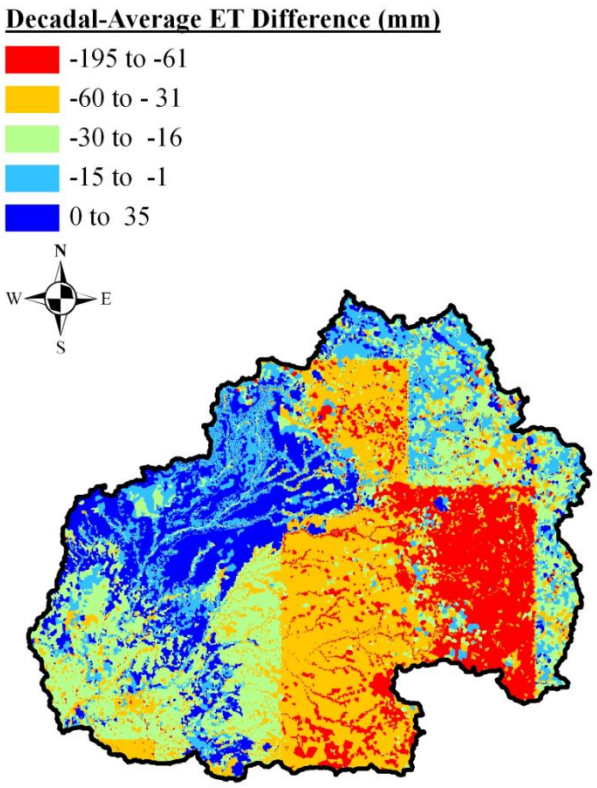

Figure 33: Spatial evapotranspiration difference between the future period and the historical period.

Figure 33 is more complex in its spatial pattern. This figure shows the evapotranspiration difference, on average, between these two time periods ET patterns. The figure illustrates that ET follows soil class patterns as well as precipitation and weather. The precipitation and weather forcing elements can be seen in box outline of the figure. Areas where the box outlines lie, are areas in Figure 31 of highest precipitation differences and areas where soil classes seem to dominate the ET pattern are areas of lowest precipitation increases. Areas of higher precipitation amounts, along the Mogollon Rim, incur higher occurrences of cloud cover and therefore those areas have a slight decrease in ET for the average future period.

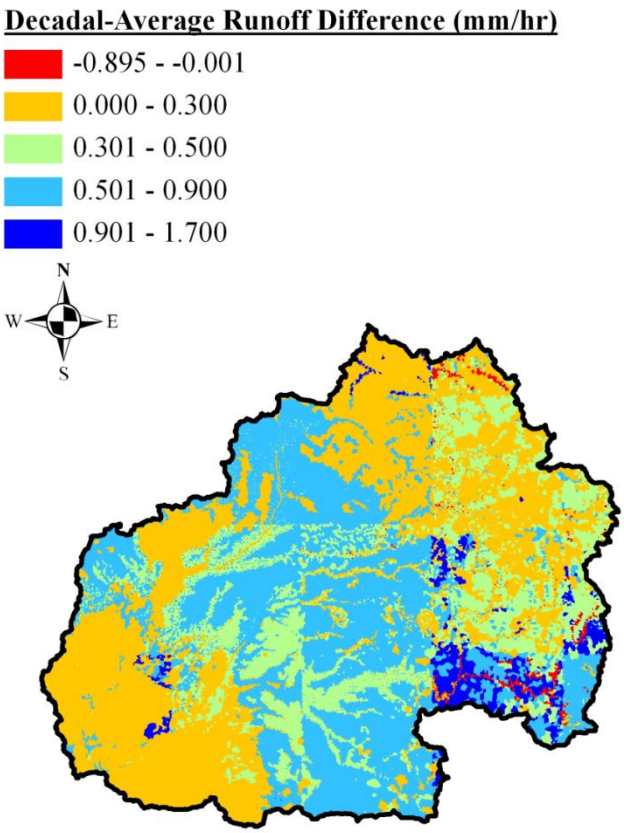

Figure 34: Spatial runoff difference between the future period and historical period.

The middle portion of Dry Beaver Creek has higher ET in the future, as precipitation in this area has a lower increase when compared to other areas. Lower occurrences of precipitation have lower occurrences of cloud cover leaving this portion of the basin ET differential between the periods controlled by soil properties.

The spatial difference of runoff between the historical and future period is illustrated in Figure 34. The clay and exposed bedrock in the center portion of the basin display a high region for increase in runoff production. These soil classifications are of lower in permeability when compared to the other classes in Beaver Creek; as such soil characteristics have a large influence on runoff production.

4 CONCLUSIONS AND FUTURE WORK

The goals of this research project are separated into two portions:

(1) Apply a hydrologic model to Beaver Creek Arizona using the modeling software tRIBS, to a level of reasonable confidence such that it is able to portray three separate observational summers from three individual stream gauge stations.

(2) Utilize this model by applying a scenario from a RCMs to evaluate the hydrologic response during the summer monsoon period for a historical period and for a future period that is characterized by climate change conditions due to increased greenhouse gas emissions.

Results from the calibration exercise for Beaver Creek reveal that tRIBS was able to capture many of the events observed in the calibration and validation summers. The model exhibited a good response to major storm events and the stream hydrograph response matched reasonable well with the observed. The model, however, was unable to replicate the drastically short recession limb of the major event during the calibration summer. Although all of the summers overestimated the seasonal volume of streamflow for the basin outlet, the model was able to capture seasonal volume and for all three summer for both Dry Beaver and Wet Beaver Creekl. Possible reasons the model over exaggerated stream flow at the outlet is that tRIBS is not able to model ground water extraction for urban systems and channel losses between the interior gauging stations and the outlet.

Precipitation is quite variable in this region and is characteristic of monsoon events. Precipitation forcing products play a major role in modeling the basin response

and can have a dramatic effect on parameterization. Three forcing products are presented in this body of work to exemplify how selection of products can affect the outcome of the modeled hydrologic response to the monsoonal seasons. Rain gauge amounts were able to capture event timing, but the resolution was very coarse and tended to cause the basin to overestimate streamflow when compared to observational record. Choosing this precipitation forcing could have led to a calibration with parameters that are not within reasonable range acceptable for the soil or land cover type in this basin. The NLDAS forcing was able to capture rainfall amounts but not timing. NLDAS pixels are also coarse and tend to mute out the intensity of a monsoonal convective storm. Of the three presented, NEXRAD was deemed the best candidate for use as forcing to the distributed hydrologic model. Although NEXRAD has its own systematic errors associated with it, the spatial resolution afforded by the product was able to do the best job in capturing the precipitation variability and streamflow volume.

The dynamically downscaled scenario from WRF of the HadCM3 model made possible by Dr. Francina Dominguez and Erick Rivera Fernandez at the University of Arizona was utilized in forcing the tRIBS Beaver Creek model. An analysis was done comparing a historical decade, 1990-2000, to a future decade, 2031-2040.

The modeled results from the climate change comparison exhibited future air temperatures with increases, on average, of 1.2 ºC in the summer months for this study site. Accompanying this is an increase in precipitation, by almost 2.5 times the historical period amount during the NAM. This was not a broad all-encompassing increase, when comparing precipitation totals across summers, the future period had an increase in variability of as much as 5 times the historical. Increases in precipitation and intensity

were shown that streamflow production will substantially increase from historical expectations. This increase was modeled as much as three-fold in reference to the historical period examined in this study. The standard deviation of summer streamflow totals was calculated to increase by as much as 5 times from the historical period to the future. This statistic indicates that expectation for Beaver Creek streamflows would be have high fluctuations from year to year.

Evapotranspiration summer totals were shown to have no substantial difference, on average, between the historical and the future period. ET totals, showed a slight decreased in the future period, mainly due to increases in average precipitation events and thereby cloud cover. ET decreases occurred in areas of the basin where precipitation totals showed the greatest increase.

Expanding on this study's efforts would be of further interest to the hydrologic community and water resources and policy managers. In this study, the NAM season was examined for the Beaver Creek watershed; further interest would be to examine an entire water year. Beaver Creek, and Arizona at large, is affected by a bimodal precipitation system; the winter snowpack and summer monsoon. Examination of effects of climate change during the summer monsoon (e.g. this study), and on winter snow runoff, would help quantify and validate climate change impacts to future water supply and water related risk assessment. Snow runoff is a major component to water resources of this region, not just Beaver Creek, but the Verde and Salt River watersheds. These watersheds supply the Phoenix metropolitan area with as much as 40% of their water and previous studies have shown that climate change would affect this water supply (Ellis, et al. 2004). By utilizing the Beaver Creek model for a full water year, climate change

effects to the region could be used as verification to previous studies but at a much finer resolution.

As Verde and Salt River are major watershed that effect water resourcese to a broad population, climate change comparison, utilizing this study as a springborad, using tRIBS would be useful. Effets could be examined not only as a outlet streamflow analysis, but also over differeing land cover types and interio stream junctions. tRIBS has an advantage of fine spatial resolution and as such, interior areas could be examined. Examples of this are; which landcover types are most effected by climate change, how can land cover alterations or uraban expansion conterat or accelerate the effects of climate change, and what areas would see the highest increase in runoff. The increases in precipitation and increases in runoff over Beaver Creek would likely happen to the broader Verde and Salt as these basin, specially the Verde, are also effected by climate interaction with the Mogollon Rim.

Higher summer precipitation would have an influence on infrustructure needs of the area and re-examination of planning for high intensity occurances would be a consequance to changing runoff regimes. Infrustructure are designed, many times, using a criteria of past intense precipitation and thereby the intensity of the runoff response. This increases would alter design criteria. Quanifing this response would be of interest to resourse and infrustructure planners.

5 REFERENCES

Adams, D. K., & Comrie, A. C. (1997). The North American Monsoon. *Bulletin of the American Meterological Society*, VOL. 78, 2197-2213.

Aerts, J. J., & Droogers, P. (2004). *Climate change in contrasting river basins: adaptation strategies for water, food, and environment.* Wallingford: CABI Intrnational.

Army Corps of Engineers, U. (1992). *Guidelines for risk and uncertainnty analysis in water resources planning.* Fort Belvoir, Va: Water Resources Support Center Institution for Water Resources.

Arnell, N., & Reynard, N. S. (1996). The effects of climate change due to global warming on river flows in Great Britain. *Journal of Hydrology*, VOL. 183, 397-424.

Assouline, S., Selker, J. S., & Parlange, J. Y. (2007). A simple accurate method to predict time of ponding under variable intensity rainfall. *Water Resources Research*, VOL. 43: doi:10.1029/2006WR005183.

Baker, M. B. (1982). *Hydrologic regime of forested areas in the Beaver Creek watershed.* Fort Collins, Co: Rocky mountain forest and range experiment station, Forest Service, US Dept of Agriculture.

Baker, M. B. (1984). Changes in streamflow in an herbicid-treated pinyon-juniper waterhed in Arizona. *Water Resources Research*, VOL. 20, NO. 11, 1639-1642.

Baker, M. B. (1986). Effects of Ponderosa Pine treatment on water yield in Arizona. *Water Resources Research*, VOL. 22, 67-73.

Baker, M. B. (n.d.). *Description and history of the Beaver Creek experimental watershed*. Retrieved 2011, from http://ag.arizona.edu/OALS/watershed/beaver/history.html

Barontini, S., Grossi, G., Kouwen, N., Maran, S., Scaroni, P., & Ranzi, R. (2009). Impacts of climate change scenarios on runoff regimes in the southern Alps. *Hydrol. Earth System Sciences Discussion*, VOL. 6, 3089-3141.

Bengtsson, L., & Semenov, V. A. (2002). Secular trends in daily precipitation characteristics: greenhouse gas simulation with a coupled AOGCM. *Climate Dynamics*, doi:10.1007/s00382-001-0218-4.

Bergstrom, S., Carlsson, B., Gardelin, M., Lindstrom, G., Pettersson, A., & Rummukainen, M. (2001). Climate change impacts on runoff in Sweden - assessments by global climate models, dynamical downscaling and hydrological modelling. *Climate Research*, VOL. 16, 101-112.

Beven, K. (1985). Distributed Models. In M. G. Anderson, & T. P. Burt, *Hydrologic Forecasting* (pp. 405-435). New York: Wiley.

Beven, K. J. (1984). Infiltration into a class of vertically non-uniform soils. *Hydrology Science Journal*, VOL. 29, 425-434.

Beven, K. J. (2002). Runoff generation in semi-arid areas. In L. J. Bull, & M. J. Kirkby, *Dryland Rivers: Hydrology and Geomorphology of Semi-arid Channels* (pp. 57-105). New York: Wiley and Sons.

Bras, R. L. (1990). *Hydrology: An Indroduction to Hydrologic Science.* Reading, Ma: Addison-Wesley-Longman.

Brazel, A. J., McCabe, G. J., & Verville, H. J. (1993). Incident solar radiation simulated by general circulation models for the southwesten United States. *Climate Research*, VOL. 2, 177-181.

Brooks, R. H., & Corey, A. T. (1964). Hydraulic properties of porous media. *Hydrology paper, 3*. Fort Collins, Co: Colorado State University.

Brown, P. (2000). *Turf Irrigation Management Series:1*. Tucson, Az: The University of Arizona College of Agriculture. Retrieved from ag.arizona.edu/pubs/water/az1194.pdf

Buonomo, E. R. (2007). On the robustness of changes in extreme precipitation over Europe from two high resolution climate change simulation. *Q. J. R. Meterological Society*, VOL. 133, 65-81.

Cabral, M. C., Garrote, R. L., Bras, R. L., & Entekhabi, D. (1992). A kinematic model of infiltration and runoff generation in layered and sloped soils. *Advance Water Resources*, VOL. 15, 311-324.

Cameron, D., Beven, K., & Naden, P. (2000). Flood frequency estimation by continuous simulation under climate change (with uncertainty) . *Hydrology and Earth System Sciences*, VOL. 4, 393-405.

Castro, C. L., Pielke Sr., R. A., & Leoncini, G. (2005). Dynamic downscaling: assessment of value retained and added using the Regional Atmospheric Modeling System (RAMS). *Journal of Geophyscial Research*, doi:10.1029/2004JD004721.

Castro, C. L., Pielke Sr., R. A., Adegoke, J. O., Schubert, S. D., & Pegion, P. J. (2007b). Investigation of the summer climate of the contiguous U.S. and Mexico using the regional atmospheric modeling system (RAMS). *Journal of Climate*, VOL. 20, 3888-3901.

Chiew, F. H., Whetton, P. H., & McMahon, T. A. (1995). Simulation of the impact of climate change on runoff and soil moisture in Australian catchments. *Journal of Hydrology*, doi: 10.1016/0022-1694(94)02649-V.

Childs, E. C., & Bybordi, M. (1969). The vertical movement of water in stratified porous material: 1 infiltration. *Water Resources Research*, Vol. 5, 446-459.

Christensen, N. S., Wood, A. W., Voisin, N., Lettenmaier, D. P., & Palmer, R. N. (2004). The effects of climate change on the hydrology and water resources of the Colorado River basin. *Climate Change*, VOL. 62, 337-363.

Cosgrove, B. A., Lohmann, D., Mitchell, K. E., Houser, P. R., Wood, E. F., Schaake, J., . . . Meng, J. (2003). Real-time and retrospective forcing in the North American Land Data Assimilation System (NLDAS) project. *Journal if Geophyscical Research*, VOL. 108, 8842.

Cubasch, U., Waszkewitz, J., & Hegerl, G. (1995). Regional climate changes as simulated in time-slice experiments. *Climate Change*, VOL. 31, 273-304.

Daly, C., Neilson, R. P., & Phillips, D. L. (1994). A statistical-topographic model for mapping climatology precipitation over mountainous terrain. *Journal of Applied Meterology*, VOL. 33, 140-158.

Deardorff, J. W. (1978). Efficient prediction of ground surface temperature and moisture with inclusion of a layer of vegetation. *Journal of Geophysical Research*, Vol. 82, 1889-1903.

Delrieu, G., Andieu, H., & Creutin, J. D. (2000). Quantification of path integrated attenuation of X- and C- band weather radar systems operating in Mediterranean heavy rainfall. *Journal of Applied Meterology*, VOL. 39, 840-850.

Dessai, S., & Hulme, M. (2007). Assessing the robustness of adaptation decisions to climate change uncertainties: a case study on water resources management in the East of England. *Global Environmental Change*, VOL. 17, 59-72.

Diffenbaugh, N. S., Giorgi, F., & Pal, J. S. (2008). Climate change hotspots in the United States. *Geophysical Research Letters*, doi: 10.1029/2008GL035075.

Diffenbaugh, N. S., Pal, J. S., Trapp, R. J., & Giorgi, F. (2005). Fine-scale processes regulate the response of extreme events to global climate change. *Proceedings of the National Academy of Sciences*, doi: 10.1073/pnas.0506042102.

Dominguez, F., Canon, J., & Valdez, J. (2009). IPCC-AR4 climate simulations for the southwestern US: the importance of future ENSO projections. *Climate Change*, VOL. 99, 499-514.

Dominguez, F., Rivera, E., Lettermaier, D. P., & Castro, C. L. (2012). Changes in winter precipitation extremes for the western United States under a warmer climate as simulated by regional climate models. *Geophysical Research Letters*, doi:10.1029/2011GL050762.

Ellis, A. W., Saffell, E. M., & Hawkins, T. W. (2004). A method for definning monsoon onset and demise in the southwestern USA. *International Journal of Climatology*, VOL. 24, 247-265.

Entekhabi, D. (2002). *Report of a workshop on predictibility and limits to prediction in hydrologic systems.* Committee on Hydrologic Science, National Research Council. National Academy Press.

ESRI. (1995-2011). ArcGIS Resource Center.

Fowler, A. M., & Hennessy, K. J. (1995). Potential impacts of global warming on the frequency and magnitude of heavy precipitation. *Natural Hazards*, doi: 10.1007/BF00613411.

Fowler, H. J., & Kilsby, C. G. (2003b). A regional frequency analysis of United Kingdom extreme rainfall from 1961 to 2000. *International Journal of Climatology*, doi:10.1002/joc.943.

Frich, P., Alexander, L. V., & Della-Marta, P. (2002). Observed coherent changes in climatic extremes during the second half of the twentieth century. *Climate Research*, doi: 10.3354/cr019193.

Garrote, L., & Bras, R. L. (1995). A distibuted model for real-time flood forecasting using digital elevation models. *Journal of Hydrology*, VOL. 167, 279-306.

Garrote, L., & Bras, R. L. (1995). A distributed model for real-time flood forecasting using digital elevation models. *Journal of Hydrology*, VOL. 167, 276-306.

Givi, J., & Prasher, S. O. (2004). Evaluation of pedotransfer functions in predicting the soil water contents at field capacity and wilting point. *Agricultural Water Management*, VOL. 70, 83-96.

Grassotti, C., Hoffman, R. N., Vivoni, E. R., & Entekhabi, D. (2003). Multiple timescale intercomparison of two radar products and rain gauge observations over the Arkansas-Red river basin. *Weather Forecast*, VOL. 18(6), 1207-1229.

Grayson, R., & Bloeschl, G. (2000). Organizations and Spatial Processes. 3-16. (R. Grayson, & G. Bloeschl, Eds.) Cambridge, U. K.: Cambridge Univ. Press.

Guan, H., Vivoni, E. R., & Wilson, J. L. (2005). Effects of atmospheric teleconnections on seasonal precipitation in mountainous regions of the southwestern U.S.: A case study in northern New Mexcio. *Geophyscial Reseearch*, doi: 10.1029/2005GL023759.

Gupta, H. V., & Sorooshian, S. (1999). Status of automatic calibration of hydrologic models: comparison with multilevel expert calibration. *Journal of Hydrologic Engineering*, VOL. 4, 135-143.

Hall, A. W., Whitfield, P. H., & Cannon, A. J. (2006). Recent variations in temperature, precipitation, and streamflow in the Rio Grande and Pecos River basin of New Mexico and Colorado. *Review in Fisheries Science*, VOL. 14, 51.78.

Hidalgo, H. G., & Dracup, J. A. (2009). Detection and attribution of streamflow timing changes to climate change in the western United States. *Journal of Climate Change*, VOL. 22, 3838-3855.

IPCC. (2007). Climate Change 2007: The physical science basis. The contribution of working group I to the fourth assessment report of the intergovernmental panel on climate change. In S. Solomon, M. Qin, M. Manning, Z. Chen, & K. B. Marquis. Cambridge University Press: Cambridge, United Kingdom and New York, NK, USA.

Ivanov, V. R., Vivoni, E. R., Bras, R. L., & Entekhabi, D. (2004a). Catchment hydrologic response with a fully distributed triangulated irregular network model. *Water Resources Research*, VOL. 40 W11102, doi:10.1029/2004WR003218.

Ivanov, V. Y. (2002). *A continuous real-time interactive basin simulator (RIBS).* M.S. thesis, Mass. Inst. of Technol., R. M. Parsons Lab. for Water Resour. and Hydrodyn., Cambridge.

Ivanov, V., Vivoni, .. R., Bras, R. L., & Entekhabi, D. (2004b). Preserving high-resolution surface and rainfall data in operational-scale basin hydrology: a fully-distributed physically-based approach. *Journal of Hydrology*, doi:10.1016/j.jhydrol.2004.03.041.

Jones Jr., M. (2007). The daily cycle of winds at Estacion Obispo, Mexico, durinng the North American Monsoon. *SOARS*.

Kim, J. (2005). A projection of the effects of the climate change induced by increased CO2 on extreme hydrologic events in the western U.S. *Climate Change*, VOL. 68, 153-168.

Kite, G. W. (1993). Application of a land class hydrological model to climate change. *Water Resources Research*, VOL. 29, 2377-2384.

Lee, J. (1991). Comparison of existing methods for building triangular irregular network models of terrain from grid digital elevation models. *International Journal of Geographical Information Systems*, VOL. 5, 267-285.

Lee, M. I., Schubert, S. D., Suarez, I. M., Held, I. M., Kumar, A., Bell, T. L., . . . Yoo, S. H. (2007). Sensitivity to horizonntal resolution on the AGCM simulations of warm season diurnal cycle pf precipitation over the United States and northern Mexico. *Journal of Climate*, VOL. 20, 1862-1881.

Leung, L., & Wigmosta, M. S. (1999). Potential climate chance impacts on mountain watersheds in the Pacific Northwest. *Journal of the American Water Resources Association*, Vol. 35, 1463-1471.

Li, L., Hoa, Z. C., Wang, J. H., Wang, Z. H., & Yu, Z. B. (2008). Impact of future climate change on runoff in the head region of the Yellow River. *Journal of Hydrological Engineering*, VOL. 13, 347-354.

Lin, J. D. (1980). On the force-restore method for prediction of ground surface temperature. *Journal of Geophysical Research*, 3251-3254.

Liu, Y., & Gupta, H. V. (2007). Uncertainty in hydrological modeling: towards an integrated data assimilation framework. *Water resources research,*, doi:10.1029/2006WR005756.

Liuzzo, L., Noto, L. V., Vivoni, E. R., & La Loggia, G. (2010). Basin scale water resources assessment in Oklahoma under synthetic climate change scenarios using a fully distributed hydrologic model. *Journal of Hyrologic Engineering*, VOL. 15, 107-122.

Lu, M. (2011). Effect of temporal resolution of hydrological data on annual canopy evaporation derived from a simple interception model. *Hydrological Processes*, DOI: 10.1002/hyp.8296.

Luo, L., Robock, A., Mitchell, K. E., Houser, P. R., Wood, E. F., Schaake, J. C., . . . Tarpley, D. J. (2003). Validation of the North American Land Data Assimilation System (NLDAS) retrospective forcing over the southern Great Plains. *Journal of Geophysical Research*, VOL. 108, 8843.

Martinez-Mena, M., Albaladejo, J., & Castillo, V. M. (1998). Factors influencing surface runoff generation in a Mediterranean semi-arid environment: Chicamo watershed. *Hydrological Processes*, VOL. 12, 741-754.

Mearns, L. O., Giorgi, F., & McDaniel, L. (1995). Analysis of daily variability of precipitation in a nested regional climate model - comparison with observations and doubled CO2 results. *Global and Planetray Change*, VOL. 10, 55-78.

Milley, P. C., Betancourt, J., Falkenmark, M., Hirsch, R., Kundzewicz, Z., Lettenmaier, D. P., & Stouffer, R. J. (2007). Stationarity Is Dead: Whither Water Management. *Science*, VOL. 319, 573-574.

Milne, B. T., Moore, D. I., Betancourt, J. L., & Parks, J. L. (2003). Multidecadal drought cycles in south-central New Mexico: Pattern and consquences. In D. G. Greenland, R. C. Smith, & D. G. Goodin (Eds.), *Climate variability and ecosystem responces at long-term ecological research site* (pp. 286-307). New York, NY: Oxford University Press.

Molnar, P., & Ramirez, J. A. (2001). Recent trends in precipitation and streamflow in the Rio Puerco basin. *Journal of Climate*, VOL. 14, 2317-2328.

Monteith, J. L. (1965). Evaporation and environment. *Symp. Soc. Exp.*, Biol. 19, 205-224.

Moon, J., Srinivasan, R., & Jacobs, J. H. (2004). Stream flow estimation using spatially distributed rainfall in the Trinity River Basin, Texas. *American Society of Agricultural Engineers*, VOL. 47(5), 1445-1451.

Moriasi, D. N., Arnold, J. G., VanLiew, M. W., Binger, R. L., & Harmel, R. D. (2007). Model evaluation guidelines for systematic quanitification of accuracy in watershed simulation. *Transaction of the ASABE*, VOL. 50, 885-900.

Nan, Z., Wang, S., Liang, X., & Adams, T. E. (2010). Analysis of spatial similarities between NEXRAD and NLDAS precipitation data products. *Journal of Selected Topics in Applied Earth Observations and Remote Sensing*, VOL. 3, 371-385.

Neary, V. S., Habib, E., & Fleming, M. (2004). Hydrologic modeling with NEXRAD precipitation in middle Tennessee. *Journal of Hydrologic Engineering*, doi:10.1061/(ASCE)1084-0699(2004)9:5(339).

Nelson, E. J., Jones, N. L., & Berrett, R. J. (1999). Adaptive tessellation method for creating TINS from GIS data. *Journal of Hydrologic Engineering*, VOL. 4, 2-9.

NRCS. (2010-2011). *USDA Natural Resources Conservation Services*. Retrieved from SNOTEL Data & Products: http://www.wcc.nrcs.usda.gov/nwcc/site?sitenum=969&state=az

NRCS, N. R. (n.d.). Soil Survey Geographic (SSURGO) Database for Beaver Creek, Arizona. Retrieved from http://soildatamart.nrcs.usda.gov

Paeth, H., Scholten, A., Friederichs, P., & Hense, A. (2007). Uncertainty inn climate change prediction: El Nino-Southern Oscillation and monsoons. *Global Planetary Change*, doi:10.1016/j.gloplacha.2007.03.002.

Penman, H. L. (1948). Natural evaporation from open water, bare soil, and grass. *Proceedings of the Royal Society of London. Series A, Mathematical and Physical Sciences*, VOL. 193, 120-145.

Pfister, L., Kwadijk, J., Musy, A., Bronstert, A., & Hoffman, L. (2004). Climate change, Land use change and runoff prediction in the Rhine - Meuse basins. *River Research*, VOL. 20, 229-241.

Pilgrim, D. H., Chapman, T. G., & Doran, D. G. (1988). Problems of rainfall-runoff modelling in arid and semi-arid regions. *Hydrological Sciences Journal*, VOL. 33, 379-400.

Rango, K. T., & Kock, R. W. (1990). Climate change effects on the snowmelt hydrology of western North American mountain basin. *IEEE T. Geoscience and Remote Sensing*, VOL.28, 970-974.

Rawls, W. J., & Brakensiek, D. L. (1983). Green-Ampt infiltration parameters from soil data. *Journal od Hydraulic Engineering*, VOL. 109, 62-70.

Rawls, W. J., Brakensiek, D. L., & Saxton, K. E. (1982). Estimation of soil water properties. *Transactions of the ASAE*, VOL. 25, 1316-1320.

Ray, A. J., Garfin, G. M., Wilder, M., M., V.-L., Lenart, M., & Comrie, A. C. (2007). Application of monsoon research: opportunities to inform desicion-makers and reduce regional vulnerability. *Journal of Climate*, VOL. 20, 1608-1627.

Redmond, K. T., & Koch, R. W. (1991). Surface climate and streamflow variability in the western United States and their relationship to large-scale circulation indices. *Water Resources Research*, VOL. 27, 2381-2399.

Rind, D., Goldburg, R., & Ruedy, R. (1989). Change in climate variability in the 21st-century. *Climate Change*, VOL. 14, 5-37.

Robles-Morua, A., Vivoni, E. R., & Mayer, A. S. (2012). Distibuted hydrologic moleling in northwest Mexico reveals the links between runoff mechanism and evaportranspiration. *Journal of Hydrometerology*, VOL. 13, 785-807.

Rogers, R. R., & Yau, M. K. (1989). *A Short Course in Cloud Physics.* Woburn, Ma: 3rd ed., Butterworth-Heinemann.

Rutter, A. J., Kershaw, A. .., & Robins, P. C. (1975). A predictive model of interception in forests. 2. generation of the model and comparison with observation in a coniferous and hardwood stands. *Journal of Applied Ecology*, VOL. 12, 367-380.

Rutter, A. J., Kershaw, P. C., Robin, P. C., & Morton, A. J. (1971). A predicitive model of rainfall interception in forests, 1. derivation of the model from observations in a plantation of corsican pine. *Agricultural Meterology*, VOL. 9, 367-384.

Saunders, S., & Maxwell, M. (2005). *Less snow, less water: climate disruption in the west.* Loisville, CO: The Rocky Mountain Climate Organization.

Seager, R., Ting, M., Held, I., Kushir, Y., Lu, J., Vecchi, G., . . . Naik, N. (2007). Model projections of an imminent transition to a more arid climate in southwest North America. *Science*, VOL. 36, 1181-1184.

Sheppard, P. R., Comrie, P. R., Packin, A. C., & Angersbach, K. (2002). The climate of the US southwest. *Climate Research*, VOL. 21, 219-238.

Shuttleworth, W. J. (1979). *Evaporation.* Wallingford, U.K.: Institute of Hydrology.

Shuttleworth, W. J. (1992). *Evaporation.* (D. R. Maidmen, Ed.) McGraw-Hill, New York: Handbook of Hydrology.

Strzepek, K. M., & Yates, D. N. (1997). Climate change impacts on the hydrologic resources of Europe: A simplified continental scale analysis. *Climate Change*, VOL. 36, 79-92.

Sungwook, W., Dominquez, F., Durcik, M., Valdez, J., Diaz, H. F., & Castro, C. L. (2012). Climate change projection of snowfall in the Colorado River Basin using dynamical downscaling. *Water Resources Research*, doi:10.1029/2011WR010674.

Tarlock, D. A., Corbridge, J. N., Getches, D. H., & Benson, R. B. (2009). Water law: a response to scarcity. In *Water resource management: a casebook in law and public policy* (pp. 1-57). New York, NY: Foundation Press.

Tucker, G. E., Lancaster, S. T., Gasparini, N. M., & Bras, R. L. (2001a). The Channel-Hillslope Integrated Landscape Development (CHILD) model. In R. S. Harmon, & W. W. Doe (Eds.), *Landscape Erosion and Sedimentation Modeling* (pp. 349-388). Norwell, Mass: Kluwer Academy.

USDA, D. o. (n.d.). Retrieved from www.landfire.gov

USGS. (2011). USGS. Retrieved from http://seamless.usgs.gov

Vazquez, R. F., Feyen, L., & Refsgaard, J. C. (2002). Effect of grid size on effective parameters and model performance. *Hydrological Processes*, VOL. 16, 355-372.

Veihmeyer, F. J., & Hendrickson, A. H. (1931). The moisture equivalent as a measure of the field capacity of soils. *Soil Science*, VOL. 32, 181-193.

Vivoni, E. R., Aragon, C. A., Malczynski, L., & Tidwell, V. C. (2009). Semiarid watershed response in central New Mexico and its sensitivity to climate variability. *Hydrology and Earth System Science*, VOL. 13, 715-733.

Vivoni, E. R., Entekhabi, D., Bras, R. L., & Ivonov, V. Y. (2006). Extending the Predictability of Hydrometeorological Flood Events Using Radar Rainfall Nowcasting. *Journal of Hydrometerology*, VOL. 7, 660-667.

Vivoni, E. R., Ivanov, V. Y., Bras, R. L., & Entekhabi, D. (2004). Generation of triangulated irregular networks based on hydrological similarity. *Journal of Hydrological Engineering*, VOL. 9, 288-302.

Vivoni, E. R., Ivanov, V. Y., Bras, R. L., & Entekhabi, D. (2005). On the effects of triangulated terrain resolution on distributed hydrologic model response. *Hydrological Processes*, VOL. 19, 2101-2122.

Vivoni, E. R., Rodriguez, J. C., & Watts, C. J. (2010). On the spatiotemperal variablility of soil moisture and evapotranspiration in a mountainous basin with the North American Monsoon region. *Water Resources Research*, doi:10.1029/2009WR008240.

Vivoni, E. R., Tai, K., & Gochis, D. J. (2009). Effects of initial soil moisture on rainfall generation and subsequent hydrologic response during the North American Monsoon. *Journal of Hydrometerology*, VOL. 10, 644-664.

Wheater, H. S. (2008). Modelling hydrological processes in arid and semi-arid areas: an introduction to the workshop. In H. Wheater, S. Sorooshian, & K. D. Sharma (Eds.), *Hydrological Modelling in Arid and Semi-arid Areas* (pp. 1-20). Cambridge: Cambridge University Press.

Wigmosta, M. S., Vail, L. W., & Lettenmaier, D. P. (1994). A distributed hydrology-vegetation model for complex terrain. *Water Resources Research*, VOL. 30, 1665-1679.

Worley, D. P. (1965). *The Beaver Creek pilot watershed for evaluating multiple use effects of watershed treatments*. Fort Collins, Co: Rocky Mountain forest and range experiment station, Forest Service, US Dept of Agriculture.

Zwiers, F. W., & Kharin, V. V. (1998). Changes in the extremes of the climate simulated by CCC GCM2 under CO2 doubling. *Journal of Climate*, VOL. 11, 2200-222.

APPENDIX A

RESEARCH MATERIAL DATASETS

This appendix includes description of all data utilized during the course of this study. The datasets laid out here contain the following:

- Model simulation setup
- Weather and precipitation forcing
- GIS repository of maps and their associated raster and shp files
- Relevant spreadsheets and documents made during this study

Table13 is the represented summary of this data as found in the delivered hard drive and a brief description of each folder is as follows.

Table 13: Research datasets organization

Description	Location
Figures made in Arc	F:\Appedix_A\BC
Meshbuilder	F:\Appedix_A\Metis_Meshbuilder
Matlab files	F:\Appedix_A\matlab_code
Rain and weather excel files	F:\Appedix_A\Precipitation_weather_data
Happy Jack Snotel	F:\Appedix_A\Snotel
Soils	F:\Appedix_A\soil
Happy Jack model	F:\Appedix_A\HappyJack
Model and forcing	F:\Appedix_A\Saguaro

Figures made in Arc: This folder contains the figures made in Arc Map (e.g. site map, soils map, and land cover map). The coordinate system for all maps was made in NAD. Layers obtained from the ASU GIS repository for the whole of Arizona are located in the subfolder labeled Beaver Creek. Some shp and raster files are not found in this folder (e.g. the soils map is found F:\soils\New soil file\Join_soil_Clip.shp)

Meshbuilder: This folder contains the appropriate files to use the Meshbuilder program and the model simulation that was ran for Beaver Creek to create the mesh.

Matlab files: This folder contains the matlab codes for figures that were made utilizing Matlab. The file 'summer2007' shows model output and can be used for all years examined, but changing the year within the file. All files the code draws from are similarly named throughout the 2005, 2006, and 2007 year. An example of this is observational stream data. All years file path look similar: F:\Appedix_A\Precipitation_weather_data\2007\2007stream_gauge.txt. The only thing that needs to be changed is the year.

Rain and weather excel files: This folder contains observational weather and rain data for all three years of this study; 2005, 2006, and 2007. In the main folder the *prec.xlsx* file has information on precipitation for all gauge stations for the years beyond the study years. The *forcing_compare.xlsx* file contains forcing totals for the remote sensing products compared to the rain gauge. The *Precipitation gauge organized.ods* file contains weather and stream data on the 2006 that was initially collected. The *Yavapairainguages.xlsx* file contains rain gauge station for the 2006 year. This file's name is the same for the 2005 and 2007 year; and is located in their folders named for their year. The file *Stream and Prec Data.xlsx* contains data on the broader Verde and Salt. Weather data in this folder is drawn from two weather stations; one near Mormon Lake and another near Camp Verde. An example of this is the 2005 year, the file is *2005_weather_data.xlsx*. This file contains all weather variables necessary to run in tRIBS. It also contains the raw stream data for all three stream flow gauges, this raw data comes in 15 minute increments. A Matlab code was developed to average stream flow

for the hour as tRIBS has a difficult time simulating fluctuations in flow of 15 minute intervals. This file also contains the full water year for 2005 as this was the year winter simulations were attempted, but not finished. This data is also available in the run file; the Saguaro folder in this database contains all forcing information for the full water year for 2005 as well.

Happy Jack snotel: This folder contains data for the Happy Jack Snotel station. All years from 2000-2010 have excel sheets with relevant data from this station site.

Soils: This folder contains the soil data based obtained from SSURGO. The database obtained from SSURGO comes in survey areas, the survey area of Beaver Creek is in the folder soil_az641, clipped shp files that have been aggregated are contained in the *New soil file*. Soil data can be found in this folder under *soil parameters.xlsx*. This file has all 73 soil types and information extracted from SSURGO for each soil type. Soil parameter tables and land cover tables are also found in this file.

Happy Jack model: This folder contains the input files use to make a model run for the point scale happy jack model.

Model and forcing: This contains model set up for 2005, 2006, and 2007, this includes *.in files; input folder for points, soil, landcover, and iwt files; and all weather and precipitation forcing. For all years the run file is named run2f.in, this is with NEXRAD forcing. Those files that use the exact same inputs, but different forcing are named gauge.in and nldas.in